DYNAMIC ANALYSIS OF TRACK-WHEEL INTERACTIONS FOR HIGH-SPEED TRAINS THROUGH BOND GRAPHS

Thesis Submitted
In Partial Fulfilment of the Requirement
for the Degree of

DOCTOR OF PHILOSOPHY

in

Mechanical Engineering

by

YAMIKA PATEL

(Roll No.- 2K17/Ph.D./ME/04)

Under the Supervision of

Dr. R. C. Singh
(Professor)
Department of Mechanical Engineering
Delhi Technological University
New Delhi, India

Dr. Wolfgang Borutzky
(Professor)
Department of Computer Science
Bonn-Rhein-Sieg University of Applied Sciences, Sankt Augustin, Germany

DEPARTMENT OF MECHANICAL ENGINEERING
DELHI TECHNOLOGICAL UNIVERSITY
(Formerly Delhi College of Engineering)
Shahabad Daulatpur, Main Bawana Road, Delhi-110042, India

August, 2024

DECLARATION

I, herby declare that the thesis entitled "**Dynamic Analysis of Track-Wheel Interactions for High-Speed Trains Through Bond Graphs**" is an original work carried out by me under the supervision of Dr. R. C. Singh, Professor, Department of Mechanical Engineering, Delhi Technological University, Delhi and Dr. Wolfgang Borutzky, Professor, Bonn-Rhein-Sieg University of Applied Sciences, Germany. This thesis has been prepared in conformity with the rules and regulations of the Delhi Technological University, Delhi. The research work presented and reported in the thesis has not been submitted either in part or full to any other university or institute for the award of any other degree or diploma.

Yamika Patel

Place: New Delhi
Date:

Yamika Patel
(Roll No.: 2K17/Ph.D./ME/04)
Deptt. Of Mechanical Engineering
Delhi Technological University
Delhi

CERTIFICATE

This is to certify that the thesis entitled, **"Dynamic Analysis of Track-Wheel Interactions for High-Speed Trains Through Bond Graphs"** submitted by **Ms. Yamika Patel** to the Delhi Technological University, Delhi for the award of the degree of **Doctor of Philosophy** in **Mechanical Engineering** is a bona fide record of original research work carried out by her in our supervision. Her research work is in accordance with the rules and regulations of the Delhi Technological University, Delhi. The results presented in this thesis have not been submitted in part or full to any University or Institute for the award of any degree or diploma.

Dr. R C Singh
(Professor)
Department of Mechanical Engineering
Delhi Technological University
New Delhi, India

Dr. Wolfgang Borutzky
(Professor)
Department of Computer Science
Bonn-Rhein-Sieg University of Applied Sciences
Sankt Augustin, Germany

ACKNOWLEDGEMENTS

I would like to express my profound gratitude, sincere thanks, and appreciation to my supervisors, Prof. R. C. Singh from the Department of Mechanical Engineering at Delhi Technological University, New Delhi, and Prof. Wolfgang Borutzky, Department of Computer Science, Bonn-Rhein-Sieg University of Applied Sciences, Germany for their invaluable guidance, unwavering inspiration, extensive suggestions, and consistent support during this Ph.D. I am thankful from my heart for all the help and encouragement they generously extended to me. Perseverance, exuberance and positive approach are just some of the traits they have imprinted on my personality. These lines are dedicated to my guides:

"गुरुर्ब्रह्मा गुरुर्विष्णु गुरुर्देवो महेश्वरः

गुरुर्साक्षात परब्रह्म तस्मै श्री गुरुवे नमः"

They steered me through this journey with their invaluable advice, positive criticism, stimulating discussions and consistent encouragement. Their advice on both research as well as on my career have been priceless. I would like to thank them for encouraging my research.

I would like to express, my sincere gratitude to Prof. B.B. Arora, Head, Department of Mechanical Engineering, Delhi Technological University, for his support. I sincerely thank Prof. S.K. Garg for his continued inspiration and support during my entire research journey. I am also thankful to Prof. R. S. Mishra for their procedural guidance.

I would like to express my sincere thanks to the members of the Student Research Committee. I want to thank Prof. Ajeet Kumr, IIT- Delhi, Prof. Md. Suhaib, Jamia Milia Islamia-Delhi, Prof. D.S. Nagesh, DTU-Delhi and Prof. A.S. Rao, DTU-Delhi for their invaluable moral support, constant motivation, and valuable feedback during my research work.

I would like to extend my heartfelt gratitude to Prof. Atul Kumar Agarwal (Chairperson-Departmental Research Committee) for his guidance and encouraging support. I want to thank my seniors Dr. Anuj Sharma and Dr. Aashish Gupta for their motivational support. I also want to thank my fellow lab mates of Design Centre, MED, DTU Mr. Sudeep Jain, Dr. Deepak Kumar, Mr. Aakash D Bansal, Ms. Pooja Rani and Mr.

Gaurav Kumar for helping and encouraging me throughout my research. I also thank my juniors Mr. Sumeet Padhi and Mr. Harsh Kumar for their active support and help.

A special heartfelt thanks to my friends, Mr. Anshul Kumar, Mr. Pranit Singh, Ms. Kiran Chholak, Mr. Abdul K Ansari, and Mr. Sundram Mishra for their valuable time, moral support, and critical comments from their experience that have helped me to complete my thesis. They enlightened me with different approach to tackling the publication process when I was exhausted and stuck.

My sincere thanks to all the faculty of the Department of Mechanical Engineering (DTU), who supported me during my entire course work and research work. I am also grateful to Mr. Narendra Bist for his support during my simulation run in the design center lab.

All my academic pursuits become a perceptible reality just because of my parents Shri Om Prakash Patel and Shrimati Sampurna Patel, my younger brothers Vivek and Vikash, and my sister Bhagyalakshmi. I will always be indebted for their love, affection, and support.

I want to express my deepest gratitude to my supervisor Late. Prof. Vikas Rastogi for his unwavering mental and moral support during the ups and downs of my PhD journey. It was under his guidance that I embarked on this doctoral path. If I would stand proud of my achievements, he was the main creditors undeniably. It was my privilege to be under their tutelage and I dedicate this thesis in his memory.

My heartfelt gratitude to everyone who has supported me, both directly and indirectly, throughout my academic and administrative journey.

At last, I would like to bow to the almighty "ॐ" for providing me health, knowledge, wisdom, and courage, to stand for my whole life. The words of my inspiration during this journey:

"उद्यमेन हि सिध्यन्ति कार्याणि न मनोरथैः

न हि सुप्तस्य सिंहस्य प्रविशन्ति मुखे मृगाः"

Yamika Patel
(Roll No.: 2K17/PhD/ME/04)

ABSTRACT

Over the past few decades, railway industries worldwide have been dedicated to enhancing train speeds and load-carrying capacity. However, as train speeds increase, concerns about wheel-track interaction, safety, and passenger comfort have become paramount. The rise in speed and load capacity leads to heightened vibrations in the vehicle-track system, caused by irregularities on the wheel/rail surface.

In light of these challenges, the present study aims to shed light on various aspects of railway dynamics concerning safety and comfort, employing the bond graph methodology. The interaction between the vehicle and the track is a critical factor influencing the safety and comfort of passengers. To investigate this interaction, a comprehensive bond graph model of an asymmetrical railway vehicle-track system is developed. In this model, the vehicle is represented as a lumped system, while the rail and concrete slab are treated as an Euler Bernoulli beam. To delve deeper into the dynamics, the study involves the development of a 1 Degree of Freedom (DOF) wheel model and a 9 DOF half-car vehicle model using the bond graph approach. These models help examine the impact of wheel flat on vehicle track dynamics. Furthermore, the effects of slab track and ballasted track on vehicle dynamics are also discussed.

The study also focuses on investigating the hunting behaviour of a railway vehicle using a 31 DOF full railway vehicle model as it moves on a curved track. By utilizing the Heuristic nonlinear creep model and Polach theory, the critical hunting speed is determined, and the responses of vehicle components above, at, and below the critical velocity are presented. The authors also examined the derailment behaviour, wheel unloading rate, wheelset lateral forces, and car body acceleration of the developed model due to alignment and cross-level track irregularities.

To assess passenger comfort for high-speed trains, the mean comfort assessment method is utilized. This involves the development of a 50 DOF full-car body model in SIMPACK. The effect of random track irregularities on the passenger ride index with varying vehicle speeds is studied. Also, the study observes the effect of vehicle motion on the passenger ride index.

In conclusion, the study utilizes bond graph methodology to address various aspects of railway dynamics concerning safety and passenger comfort. The comprehensive models developed provide valuable insights into the interactions between the vehicle and track, helping to enhance railway safety and passenger comfort in high-speed trains.

CONTENTS

LIST OF FIGURES

LIST OF TABLES

NOMENCLATURE AND ABBREVIATION

DOF	Degree of Freedom
DIF	Dynamic impact factor
CRC	Concrete Slab
HSR	High Speed Railway
HSRV	High Speed Railway Vehicle
ODE	Ordinary Differential Equation
PDE	Partial differential equation
PSD	Power spectral density
RB	Rail Beam
RMS	Root mean Square

D_f	Amplitude of irregularity
D_f	Amplitude of irregularity
φ_{se}	Angle of Super elevation
A_{slab}	Area of cross-section of slab
μ	Coefficient of Friction
λ	Conicity angle
P_{c1}	Contact force acting at the wheel-rail interface
Z_r	Contact point on the rail
w_c	Cut-off frequency
$R_{foundation}$	Damping coefficient of foundation layer
R_{pad}	Damping coefficient of rail pad
ρ	Density of slab
$\delta(.)$	Dirac Delta Function
Z_{slab}	Displacement of the concrete slab beam
l_s	Distance between the vehicle body and bogie frame mass centre
δ	Flange Clearance
F_{wfc}	Flange contact force
$(EI)_{slab}$	Flexural Rigidity of Concrete slab beam

$(EI)_r$	Flexural Rigidity of Rail
f_{33}	Forward creep coeff.
l_p	Half of the primary lateral suspension arm
l_t	Half of the primary longitudinal and vertical suspension arm
l_c	Half of the secondary lateral suspension arm
d_p	Half-track Gauge
h_g	Height of bogie CG above wheelset CG
h_0	Height of the secondary suspension above bogie CG
h	Height of the vehicle body CG above Wheelset CG
K_h	Hertzian Stiffness
t_{flat}	Instant wheel flat made contacts with rail
$\dot{Y}_{wl}$	Lateral component of velocity of points on left suspension
$\dot{Y}_{wr}$	Lateral component of velocity of points on right suspension
f_{11}	Lateral creep coefficient
ξ_y	Lateral Creepages
K_{ry}	Lateral Stiffness of the rail
f_{12}	Lateral/Spin Creep coefficient
L_f	Length of Irregularity
F_{wl}^L	Linear creep forces on left wheel
F_{wr}^R	Linear creep forces on right wheel
M_{wl}^L	Linear creep moment on left wheel
M_{wr}^R	Linear creep moment on right wheel
x_f	longitudinal coordinate of contact point within the irregularity
x	Longitudinal Coordinate of rail beam
ξ_x	Longitudinal Creepages
M_b	Mass of bogie
M_c	Mass of car body
m_r	Mass of rail per unit length
M_w	Mass of wheelset
N_{mv}	Mean comfort index
$q_j(t)$	Modal amplitude

m_j	Modal Mass
k_j	Modal Stiffness
I_{bx}	Moment of inertia of bogie about X-axis
I_{by}	Moment of inertia of bogie about Y-axis
I_{bz}	Moment of inertia of bogie about Z-axis
I_{cx}	Moment of inertia of car body about X-axis
I_{cy}	Moment of inertia of car body about Y-axis
I_{cz}	Moment of inertia of car body about Z-axis
I_{wx}	Moment of inertia of wheelset about X-axis
I_{wy}	Moment of inertia of wheelset about Y-axis
I_{wz}	Moment of inertia of wheelset about Z-axis
F_{wL}^{n}	Non-linear creep forces at the contact point on left sided wheel-rail
F_{wR}^{n}	Non-linear creep forces at the contact point on right sided wheel-rail
M_w^L	Non-linear moment at the contact point on left sided wheel-rail
M_w^R	Non-linear moment at the contact point on right sided wheel-rail
β_{ij}	Non-linearity factor in Heuristic creep model
N_L	Normal force at the Left wheels
N_R	Normal force at the Right wheels
N_w^L	Normal force component at the contact point on left sided wheel-rail
N_w^R	Normal force component at the contact point on right sided wheel-rail
NR	Number of Discrete support
nm	Number of Modes
v	Poisson's ratio
x_j	Position of j_{th} discrete support
x_w	Position of the wheel
R_r	Radius of the rail profile
R_w	Radius of the wheel profile
R_t	Radius of Track
M_r	Rail mass per unit length
A_l , A_v	Roughness coefficients for a particular line level
α_{ij}	Saturation Constant in Heuristic creep model

$Y_j(x)$	Shape Function
G	Shear Modulus
w	Spatial frequency
f_{22}	Spin creep coeff.
ξ_{sp}	Spin Creepages
P_0	Static Load
$K_{foundation}$	Stiffness of foundation layer
K_{pad}	Stiffness of rail pad
F_{sf}	Suspension Force
F_{sfw}	Suspension forces of wheelset
M_{sc}	Suspension Moment
M_{smw}	Suspension Moment of wheelset
$S(w)$	Track Irregularity in terms of PSD function
V	Velocity of railway vehicle
$\dot{Z}_{wl}$	Vertical component of velocity of points on left suspension
$\dot{Z}_{wr}$	Vertical component of velocity of points on right suspension
F_{rj}	Vertical Force due to discrete support provided by rail pad and fasteners
Z_w	Vertical Wheel motion
r_0	Wheel radius
$\Delta Z(t)$	Wheel-rail overlap

CHAPTER 1

Introduction

In this chapter, an introduction to high-speed railway vehicles (HSRV), their evolution, and the dynamics of vehicle-track interaction models are discussed. Additionally, the chapter delves into the motivation behind conducting research in the railway dynamics.

1.1 Introduction

As a means of transportation, a railway vehicle is of the utmost significance and is among the most intricate and dynamic systems in engineering. In the modern day, railroads have constant difficulties competing with aviation and road transportation networks worldwide. Consequently, there is a concerted global effort to enhance the efficiency of railway vehicles, with particular attention paid to factors like comfort, safety, and speed. Two main criteria, safety and stability, are usually used to assess the performance of rail vehicles. These factors are measured using a wide range of performance indices that focus on specific aspects of vehicle dynamics. There has been a noticeable increase in vibrations inside the vehicle-track system due to trains' steadily increasing speed and load-carrying capacity.

The speed and load-carrying capacity of trains are consistently increasing, resulting in heightened vibrations within the vehicle-track system. Irregularities on the wheels and rail surfaces cause these vibrations, potentially leading to track component deterioration and negatively impacting the safety and comfort of train operations. The nonlinear relationship between the contact between wheels and rails further compounds the system's complexity.

Hence, a thorough understanding of rail vehicle dynamics is crucial to ensuring the safe and cost-effective operation of modern railways. As the demand for faster, safer, and more

comfortable railway vehicles continues to grow, innovative analysis is required for the dynamics involved in rail and vehicles. Rail vehicle dynamics analysis is critical throughout railway operations, encompassing everything from vehicle manufacturing to infrastructure design and maintenance. This entails looking at a variety of factors, including ride comfort, lateral stability, derailment, and track infrastructure.

The dynamic analysis of high-speed railway vehicles is a critical discipline at the forefront of modern transportation engineering. As the demand for rapid and efficient passenger and freight transportation continues to escalate, the design and operation of high-speed trains necessitate meticulous examination and comprehension of their dynamic behavior. High-speed railway vehicles, unlike conventional trains, face unique challenges due to their elevated velocities, intricate interactions with the track, and the imperative to ensure passenger safety and comfort.

The dynamic study of HSRV delves into the intricate dynamics governing the interaction between the train and its environment, encompassing factors such as wheel-rail interaction, aerodynamics, suspension systems, and control mechanisms. The goal is to comprehend and optimise the myriad forces, moments, and oscillations that influence the performance of high-speed trains, ensuring stability and safety across diverse operational conditions.

In dynamic analysis, researchers employ advanced simulation techniques, multibody dynamics models, and real-world testing to unravel the complexities associated with high-speed rail travel. The insights gained from this analysis not only inform the design and engineering of the trains themselves, but they also contribute to the development of robust control systems, maintenance strategies, and emergency response protocols. As we propel into an era where high-speed rail networks play an increasingly pivotal role in global transportation infrastructure, the dynamic analysis of high-speed railway vehicles stands as

an indispensable discipline. It ensures the reliability, efficiency, and safety of this cutting-edge mode of transportation. This introduction sets the stage for a comprehensive exploration of the multifaceted considerations and challenges inherent in the dynamic analysis of high-speed railway vehicles.

The wheel-track interaction of high-speed railway vehicles constitutes a cornerstone in the realm of transportation engineering, wielding significant influence over the performance, safety, and efficiency of these advanced rail systems. As trains hurtle along at remarkable speeds, the intricate interplay between the wheels and the track becomes a focal point of the study, demanding a nuanced understanding to optimise operational dynamics and ensure passenger well-being.

The interaction between the wheels and the track is a multifaceted dance involving mechanical intricacies, material science considerations, and dynamic forces. Wheel-rail contact phenomena, such as rolling, sliding, and adhesion, form the bedrock of this interaction, shaping the vehicle's stability, wear characteristics, and overall efficiency. The high speeds inherent to these systems introduce unique challenges, necessitating a detailed examination of the forces exerted on both the wheels and the track.

This field of study extends beyond the physical contact points, delving into the broader implications for railway infrastructure and vehicle design. It encompasses the impact of wheel and rail profiles, maintenance practices, and environmental conditions on high-speed trains' performance. Furthermore, advancements in wheel materials, lubrication technologies, and monitoring systems play a pivotal role in shaping the wheel-track interaction landscape.

To ensure a long lifespan of rail infrastructure and the security of both passengers and freight, it is essential to thoroughly research and comprehend the dynamic interaction between wheels and rails. This study lays the groundwork for a more comprehensive

investigation of the complexities surrounding wheel-track interaction in high-speed railway vehicles. It delves into the engineering marvels and challenges that characterize this essential aspect of modern rail transportation.

1.2 Motivation

Rail transportation offers several features and advantages over road transportation. It is significantly more energy-efficient and economical compared to road transportation. The social impact in terms of environmental pollution is also significantly lower in the case of rail transportation. Construction expenses for rail networks are approximately four to six times less than those for roads, considering equivalent traffic levels. Additionally, it is the single foremost transport system capable of utilizing any form of primary energy. Undoubtedly, the railway transportation system is a remarkable invention of the 19th century that ushered in a new era for humanity. It has facilitated closer interactions between communities and accelerated the movement of materials and goods. Railways are recognized as one of the most economical, efficient, and environmentally friendly modes of transportation. It plays a very pivotal role in national development and increasingly becoming a key player in worldwide transport policies.

Indian Railways is one of the largest transportation modes in the world. With a modest beginning in India on April 16, 1853, when the first wheels rolled on rails from Bombay to Thane, Indian Railways established itself as the primary mode of transportation for the country's socio-economic development.

Since its inception, the Indian Railways has emerged as a main means of transportation to unite the scattered markets and in so doing pave the way for a recent market economy. It serves to link industrial (manufacturing) centres with markets as well as centres for raw materials and helps industrial development. It further links agricultural

centres with inaccessible markets. It affords rapid, consistent, and cost-effective transport solutions to different industrial sectors such as energy, coal, and petroleum. It connects places, allowing for large-scale, rapid, and low-cost movement of people and goods across the country. In doing so, the Indian Railways establishes itself as a symbol of national unity as well as a strategic tool for improving defense preparedness.

India's rail transport is exclusively managed by Indian Railways, a government department operating under the Ministry of Railways. This state monopoly oversees the world's fourth-largest railway network, with 119,630 kilometers of total track and 92,081 kilometres of running track. As of the end of 2015-16, the network consisted of 66,687 kilometres of routes that served 7,216 stations. Indian Railways stands as one of the largest and busiest rail networks globally, facilitating the daily transportation of twenty-two million passengers and over one billion tons of freight.

Despite having the fourth-largest rail network, Indian Railways does not have any high-speed rail (HSR) lines with operational speeds of more than 200 km/h. The fastest train in India at present is the Gatimaan Express with an operational speed of 160 km/h. Vande Bharat train has been designed to run at a maximum speed of 180 km/h. However, the Government of India is now moving forward with plans to introduce high-speed trains in the country. As a step in this direction, it has established the High-Speed Rail Corporation of India Limited (HSRC) to oversee the development and implementation of high-speed rail projects across India. Not only Indian Railway, but railway companies around the world are under constant pressure to compete with air and road transport systems. Worldwide attention has thus been directed towards improving the efficiency of railway vehicles in terms of speed, safety, and comfort [1].

In recent decades, global railway industries have been striving to enhance the speed and load-carrying capacity of trains. Safety and comfort are paramount concerns,

particularly at high operating speeds. The pursuit of increased speed and load capacity is often accompanied by heightened vibrations in the vehicle-track system, stemming from irregularities on the wheel/rail surface. This heightened vibration raises the risk of damage to track components, adversely impacting both the safety and comfort of train operations. The nonlinear relationship between wheel/rail contact and track components adds complexity to the system, necessitating significant efforts for reliable predictions of wheel/rail interaction forces. This is crucial for identifying the key factors contributing to damage of both vehicle and track components, as well as ensuring improved safety and comfort levels.

A fundamental understanding of rail vehicle dynamics is essential to guarantee the safe and cost-effective operations of modern railways. As demands grow for safer and more comfortable railway vehicles operating at higher speeds with increased loads, innovative methods for rail vehicle dynamics analysis become imperative. The application of such analysis spans the entire spectrum, from rail vehicle manufacturing to various aspects of train operations, including ride comfort, lateral instabilities, derailment potential, track infrastructure design, and maintenance.

Ensuring the safe operation of a train involves designing it to identify and eliminate potential causes of derailment. Simultaneously, achieving comfort for passengers can be realized by effectively controlling unwanted vibrations. Modern trains represent intricate mechanical systems that benefit from advanced modelling and simulation techniques for enhanced analysis and design. The initial step in this process is the development of a detailed model of the railway vehicle system. This model serves as a foundational requirement for studying vehicle performance, refining existing designs, creating new ones, and formulating safety procedures tailored to diverse working and loading conditions. Computer simulations play a significant role in evaluating railway vehicle performance,

assessing safety and comfort, and designing new vehicles [2]. Recent developments in the field of computational mechanics and the computing capability of digital computers pave the way for the dynamic analysis of complex modern trains.

Rail vehicle performance is typically assessed in terms of safety and stability. These aspects, concerning the dynamic performance of the vehicle, are quantified through a set of indices addressing specific facets of dynamic behaviour. The examination of vehicle and train dynamics is generally categorized into two groups: (i) Response, which involves studying the dynamic behaviour in response to external inputs like track irregularities, and (ii) Stability, which focuses on evaluating the system's stability under diverse operating conditions.

To effectively analyze the dynamic performance of rail vehicles and develop a suitable analytical model for such analysis, performance indices must be quantitatively defined. The primary performance indices to be considered are (a) vehicle lateral stability and (b) vehicle ride quality. Both theoretical and experimental perspectives have made numerous attempts to gain a deeper understanding of the dynamics of the railway system. However, in some special scenarios, field experiments on wheel-rail contact mechanics and vehicle dynamics can prove to be challenging due to difficulties in adequately controlling the test conditions and data acquisition [3]. In such cases, modelling and simulation are found to be the best alternatives. Computer simulation allows a designer to focus attention on one or more of the train’s components to predict its dynamic behaviour under specified operating conditions. One can repeat a simulation run with different parameter values and iterate until a satisfactory performance is obtained. This iteration procedure can be much more costly and time-consuming if done through field experiments. Simulation results, however, are useful only as a step in the design procedure, which must necessarily

culminate in hardware and testing. Nevertheless, they can provide insight, reduce costs, and accelerate the design process [4].

A rail vehicle constitutes a complex multibody system. Modelling such a system involves synthesizing various kinematic and dynamic constraints to formulate the equations of motion. The bond graph [5–8], a unified modelling tool across multi-energy domains, is particularly well-suited for modelling multibody systems. The bond graph model serves as a representation of power exchange among various lumped components within a system, facilitated by a power-conservative junction structure. This inherent property enables modellers to construct a bond graph model solely based on kinematic and dynamical relations, automatically adhering to the relevant dynamical and kinematic constraints. The distinctive characteristic of bond graphs inspired the author to employ this formulation in modelling the vehicle-track system, aiming to gain a comprehensive understanding of crucial aspects in the realm of rail vehicle dynamics.

.

CHAPTER 2

Literature Review

The preceding chapter provided an introduction to High-Speed Railway Vehicles (HSRVs) and their dynamics. This chapter presents an in-depth literature survey focusing on rail dynamics, encompassing theoretical modelling of HSRV, lateral dynamics and passenger ride comfort under various operating conditions.

2.1 Review of Literature

In the past few years, substantial research has been conducted on numerous areas of high-speed railway dynamics, with the primary goal of increasing speed, ride quality, safety, comfort, track and wheel maintenance, and so on. To align the scope and goals of current research, the review of literature has been divided into three categories.

1. Theoretical and computational modelling of high-speed railway vehicle and track structure.
2. Lateral dynamics of high-speed railway vehicle.
3. Ride comfort analysis.

2.1.1 Theoretical and Computational Modelling of High-Speed Railway Vehicle and Track Structure

A wide variety of theoretical and analytical models have been presented to study the dynamic behaviour of vehicle track interaction under different running conditions. According to the current literature, there are two unique types of railway tracks: the traditional track system, often known as the ballasted track system, and the ballastless track system, also known as the slab track system. The ballasted track system comprises sleepers

(ties) arranged on top of a layer of ballast, with rails attached to the sleepers through rail pad fasteners. The ballast provides stability, drainage, and support for the sleepers, while the sleepers provide support and stability for the rails. This type of track is designed for trains operating at speeds up to 200 km/h. On the other hand, high-speed tracks are designed for trains that operate at speeds above 250 km/h (155 mph) and are typically used for intercity and high-speed trains. High speed tracks can be ballasted or slab tracks, with the latter being more common. The slab track consists of a continuous concrete slab laid directly on the ground or the concrete supporting layers, with rails embedded in the concrete. Slab tracks are designed to provide a smoother ride and reduction in noise & vibration. The main differences between conventional and high-speed tracks are the design, materials, and construction techniques used to create them. Slab tracks require more precise alignment and levelling, with tighter tolerances for curves and gradients, to ensure the stability and safety of the train at high speeds. They also require more durable materials and construction techniques to withstand the higher stresses and forces generated by high-speed trains. Due to the different properties and operating conditions of the two systems, the modelling of ballasted track and high-speed train track are different.

Over the last few decades, various theoretical and computational models of track structure have been presented by various researchers. Correia et. al [9] presented a ballasted track model using a 2D approach to investigate the dynamic response track structure. Uzzal et al. [10] presented a numerical model of the ballasted track to evaluate the effect of wheel flat at the wheel-rail interface. A two-dimensional model of the ballasted track system has been developed upon consideration of three subsequent layers. Bian et al. [11] used FE analysis (FEA) software package ANSYS to study the rail-wheel impact analysis due to the wheel flat on a ballasted track. Hou et al. [12] developed a two-layer 3D finite element model of ballasted track using finite element method to study the effect of wheel-track

interaction for high-speed range. Kumar et al. [13] employed a bond graph approach to create a two-layer 3D ballasted track construction to investigate the dynamic analysis of vehicle track interaction caused by flat wheels. Bond graphs provide a succinct visual representation of all types of interacting energy domains. As a result, many academics use bond graphs as modelling tools to investigate many elements of rail and road vehicle dynamics. Sayed et al. [14] presented a comprehensive three-dimensional (3D) finite element (FE) model to simulate the dynamic response of ballasted railway tracks subjected to train movement loads, and the critical speed was explored for various train-track-ground system conditions. The commercial software MIDAS-GTS was used to create a four-layer 3D ballasted track model. SIMPACK is used to create a 3D dynamic model of a high-speed train linked with a flexible ballast track in order to compare the dynamic performance obtained from the entire train/track model (TTM) and the single-vehicle/track model (VTM) Ling et al. [15].

Nowadays, slab track superstructure is used widely compared to the ballasted one by dint of its advantages. Initially, a 2D numerical model of vehicle/slab track dynamics has been developed to calculate the dynamic response of railway vehicle and slab track structure [16–18]. A study was conducted to analyse the dynamic response of the slab track when subjected to harmonic moving point pressures. A frequency domain model consisting of two layers of beams was utilized [19, 20]. In the past decade, numerous three-layer slab track variants have been created. Qingsong et al. [21] evaluated the dynamic behaviour of a continuous slab track with rail imperfections in the frequency domain. Zhang et al. [22] also examined the random response of a vertically connected vehicle/discontinuous slab track structure to random excitation in the frequency domain. In their investigation, the researchers used a three-layer model to mimic the track, with a continuous rail layer, an intermittent concrete foundation layer, and an intermittent concrete base layer. Song et al.

[23] and Sadeghi et al. [24] have enhanced the aforementioned model in order to analyse the dynamic interaction between a vehicle and a discontinuous slab track while taking the nonlinear hertz theory into account.

A review of the literature indicates that 2D and 3D slab track models have been only developed to study the track dynamics in detail and track sub-structure characteristics have not been included to study railway vehicle dynamics [25–28]. But from past decades, various 2D and 3D vehicle slab track models have been presented to investigate the effect of track irregularity and track flexibility on stability and safety analysis of railway vehicles. Zhai et al. [29] studied the influence of train speed on a train ride comfort index for high-speed trains running on two layered 3D slab tracks model. Zhao et al. [30] used Multi body dynamics software (SIMPACK/SIMULINK) for modelling and simulation of high-speed railway vehicle and flexible slab track structure. In this study, dynamic responses of high-speed railway car body have been calculated due to wheel polygonalisation. A transient FE model for the wheelset-rail rolling contact was created using ANSYS/Ls-dyna to mimic the high-speed operation of a free wheelset on a slab track.

To better understand the dynamics of the railway system, several attempts have been made from both theoretical and experimental points of view. Computer simulation is found to be the best solution to simulate rail dynamics problems [31, 32]. Simulation allows a designer to focus his attention on one or more of the train's components to predict its dynamic behaviour under the given operating conditions. One can repeat a simulation run with different parameter values and iterate until a satisfactory performance is obtained [33, 34].

2.1.2 Lateral dynamics of high-speed railway vehicle

In the context of high-speed railway vehicles, hunting and derailment are two critical aspects of lateral dynamics. In terms of performance, there is an urgent need to investigate

the lateral stability characteristics of high-speed rail cars. An important issue in this regard is a detailed assessment of a railway vehicle's critical speed when traversing a certain track [35]. This critical speed, a nonlinear function impacted by elements such as the wheel-rail contact profile, adhesion coefficient, bogie suspension dynamics, railway line topology, and others, acts as a direct constraint on the railway vehicle's maximum permitted operating speed. A derailment may result from the wheelset's undamped motion, which is contained by the wheel flange and rail, over a particular forward speed. This motion creates significant lateral creep forces at the wheel-rail contact [36]. As a result, hunting stability analysis and critical speed prediction are crucial steps in the railway vehicle design process [37]. Previous research on hunting instability has focused on the concept of a single or dual wheelset system, studying the influence of the linked parameters on the critical speed of the wheelset [38]. Polach [39] investigated railway vehicle dynamics and critical speeds using linear and nonlinear creep models. Cheng et al. [40] used linear and nonlinear creep models to study the consequence of suspension features on hunting speeds. Lee et al. [41, 42] examined hunting stability using a six-degrees-of-freedom model system that accounted for the vertical and rolling motions of the wheelset and bogie systems. They expanded their analysis by using 8 and 10 DOF models to evaluate the hunting stability of high-speed railway vehicles with different suspension settings. Wang et al. [43] used car models to evaluate derailment ratios, the effect of vehicle speed on derailment quotients for linear and non-linear creep models with varying suspension features has not been investigated. Cheng et al. [44] created a comprehensive 20-DOF model that included lateral displacement and yaw angle for each wheelset, as well as lateral and vertical displacements for the bogie and vehicle body. The model also had roll and yaw angles for the bogie and carbody. However, authors did not consider the roll angle for each wheelset while developing the 20 DOF model. In practice, the roll angle of each wheelset plays an

important role in determining the contact forces among rails and wheels. As a result, the model's failure to include the roll angle for each wheelset may result in inaccurate estimates of dynamic reactions.

With the advent of speed, the safety of a high-speed railway vehicle, particularly its derailment behaviour, is a very important issue. Vehicle designers have always been interested in the issue of high speed with no derailment. In the past few years, many researches have been administered to resolve this issue. During a derailment, the wheel drifts away from the rail and is unable to continue rolling. To analyze this effect, Nadal [45] proposed a derailment ratio, which solely depends on lateral and vertical forces acting on the wheel, flange contact and friction coefficient between wheel & rail. However, Weinstock [46] studied that derailment was associated not only with the derailment coefficient on the flange side but also on the non-contact side of the flange. From the experiment, it is evaluated that above mentioned criteria are valid only for small yaw angle [47]. Under the quasistatic assumption, Barbosa [48] developed a 3D contact model to improve Nadal derailment criteria by considering creep forces. A lot of literature studies have been found on the lateral stability of high-speed railway vehicles which consider the linear and nonlinear creep forces [40, 49]. Wickens [50] provided the curving performance of the asymmetrical truck based on a linear creep model neglecting the creep moments between wheels and rails. Using oblique impact theory, Polach and Wang [39, 51] determine the critical hunting speed for impact derailment.

From the work of Zboinski et al.[52], the creep moments were estimated from the longitudinal and lateral creep forces based on longitudinal, lateral and spin creepages. In some of the research, the nonlinear creep moment was neglected while using the nonlinear creep models [39, 53–55]. Also, the derailment analysis of various vehicle models was carried out by utilizing the linear creep model. Under a practical scenario, the hunting

stability of railway vehicles and their dynamic response are sensitive to the method of calculating creep forces and moments. Cheng et al.[55] developed a 20 DOF railway vehicle model. This model incorporates lateral displacement and yaw angle for each wheelset, along with lateral and vertical displacements for the bogie and vehicle body. Additionally, it considers the roll and yaw angles for both the bogie and car body. Cheng et al. did not take the roll angle for each wheelset into account when developing their 20 DOF model. Nevertheless, in actual situations, the roll angle constitutes a crucial DOF for each wheelset, as it directly impacts the contact forces between rails and wheels. Therefore, neglecting roll angle in the modelling of wheelsets can lead to imprecise calculations of the derailment quotient.

Despite the fact, Wang et al. [43] have estimated the derailment quotient using the complicated railway vehicle models and stated in their research that very few study had been conducted yet so far for evaluating the derailment quotient for both the linear and nonlinear creep models along with the suspension parameters. The geometry of a track plays a vital role in ensuring the safety, stability, and comfort of train transportation. The presence of track irregularities introduces unwanted vibrations that can lead to potential risks in train operations and passenger safety [56]. Track geometry can undergo deviations from its original design due to factors like track settlement, repeated loads, and rail defects. Track irregularities can be categorized as: alignment, track gauge, longitudinal level (track profiles), and cross level. The vertical deviations between consecutive running table levels along the track are referred to as the longitudinal level. Conversely, cross level denotes the vertical distance or elevation distinction between the left and right rails. Horizontal deviations between consecutive positions of the track are referred to as alignment. Finally, the track gauge is calculated by locating the points at which lines intersecting each railhead profile perpendicular to the travelling surface are at the shortest distance. To summarize,

track irregularities consist of deviations in cross-level, track gauges, longitudinal level, and alignment that are brought about by factors such as track settlement, recurrent loads, and rail defects. These irregularities affect the geometry of the track and require routine inspection and upkeep to guarantee maximum efficiency and safety [57].

Early research on this subject was reported by Wickens [58] which addresses the dynamic stability of railway vehicle wheelsets and bogies. Fei et al. [56] examined the intricate interaction between vehicles and tracks, taking into account a range of complex irregularities. Additionally, safety indicators such as the derailment coefficient, wheel unloading rate, and wheelset lateral force are determined for both a C70 freight train track and a 25-ton passenger train. Karis et al. [59, 60] and Choi et al. [57] investigated the association between track irregularity and vehicle reaction, using a combination of numerical modelling and empirical data. Cantero et al. [61] proposed a method for detecting track abnormalities produced by infrastructural problems using the vehicle's vertical acceleration and the wavelet transform. Sadeghi et al. [62] used a thorough parameter analytic approach to investigate the impact of track irregularities on driving ease, and they discovered that short-wave track irregularities have a considerable influence on driving comfort. Liu et al. [63] investigated the combined effects of vehicle speed and track imperfections on vehicle vibration, discovering that vertical abnormalities had the greatest impact on vibration unpleasantness at all speeds. Youcef et al. [64] used a modal principle of the superposition method to examine the dynamic response of cars with casual and non-random track irregularities, revealing how track abnormalities affect the vehicle's vertical acceleration. The interconnectivity of track irregularity, vehicle vibration, bridge vibration, and vehicle speed were examined by Hung et al. [65] using a 3D finite element transient dynamic analysis. Hou et al. [66] developed a train-track-bridge-model (TTBM) in ANSYS to analyse the dynamic responses of the high-speed train used as the safety and stability

evaluation indexes under measured track irregularity. Kumar et al. [67] used the bond graph approach to investigate the hunting and stability analysis of medium and high-speed trains. The influence of track irregularities on the running behaviour of high-speed trains has been studied by choi et al. [57]. Track irregularities with various wavelengths and amplitudes were developed to observe the running behaviour of high-speed trains. Derailment coefficients, lateral loads, bogie acceleration and body acceleration of Korean train express were calculated to observe the effect of track irregularity using the VAMPIRE program.

2.1.3 Ride comfort analysis

With the advancement in technology, railway vehicles are not only achieving new heights but can now run at very high speeds and attain a great extent of comfort. Previous studies exhibit those vibrations are the main source of passenger discomfort. Hence to improve the ride quality, it is required to reduce the vibration. Track irregularities (due to sudden braking of trains, irregular track maintenance, irregular running speed), geometric irregularities (improper design, wear), and material non-linearities are reasons for vibration generation in railway vehicles.

These vibrations are transferred to various components (wheelsets, bogie, car body) of railway vehicles during operations. Vibration responses from the car body are further transferred to the human body through supporting components like the car floor and seats. Once the frequency of two systems becomes nearly equal, a resonance phenomenon arises, which causes a high amplitude of vibration, further resulting in higher discomfort to passengers [63]. These vibration responses are recorded in terms of acceleration signals. Experimental results show that the human body is more susceptible to vertical acceleration response near 5Hz and less susceptible below the 2Hz frequency range [68, 69]. It is crucial to determine the modes of vibration of the car body near the natural frequency of the human

body so that necessary steps can be taken to eradicate that mode. Earlier research shows that rigid car body mode transpired in the frequency range of 0.3 Hz to 8 Hz, and flexible modes take place from 7 Hz to 20 Hz [70]. Passenger comfort while riding a train depends on the intensity of vibrations, direction, frequency and exposure time. These vibrations can prevent passengers from performing any sitting activity and also affect passengers' health. Train vibrations are considered a prime factor in passengers' ride comfort [71, 72]. It becomes necessary to develop a method which assesses a passenger's ride comfort while riding a railway vehicle [73, 74]. However, it becomes impossible to develop a general method acceptable to all the countries and their rail standards as every country has different vibrational characteristics [75]. In the mid-20th century, a researcher named “Sperling” proposed an advanced method called the ride Index method (W_z) to determine the ride comfort of a passenger [76–78]. Ride comfort requirements for railway cars have been set in accordance with ISO 2631 standards by the International Union of Railways (UIC), the European Committee of Standardization (CEN), and the International Standard Organization (ISO) [79, 80]. These standards are identified as the UIC 513R leaflet [81], EN 12299 [82] and ISO 10056 [83], respectively.

Suzuki [84] discussed about several different ways to measure ride comfort and related Japanese studies that had been done. Gangadharan et al. [85] did an experimental and analytical study of a train coach's ride comfort. They also did a parametric study to find ways to improve the design for a better ride index. Above mentioned ride comfort evaluation method used different articulation techniques to evaluate the acceleration signal. As a result, establishing an unmediated link between various evaluation methodologies is challenging.

However, various researchers tried to establish a correlation between these methods. Kim et al.[86] determined the ride comfort indices using Sperling's method, ISO 2631 and

UIC 513 recommended method and tried to establish the relationship between them. Similarly, many researchers compared the ride comfort indices using Sperling's method, EN12299 continuous comfort and mean comfort method. The comfort index at sitting and standing positions is also calculated and examined by Munawir et al. [87]. Dumitriu et al. [88] evaluated passenger comfort using the mean comfort method and Sperling's method and found that different assessment methods will show different results under identical boundary conditions. Furthermore, Kumar et al. [89] developed a biodynamic model to calculate passenger ride comfort using Sperling's index. Jiang et al. [90] explore the merits and demerits of EN12299 and Sperling's method. Further, experimental data was recorded by Haladin et al.[91] on the in-service tramway to compare different ride comfort evaluation techniques such as the Sperling's Ride index method, EN12299 comfort method and equivalent level of vibrations methods.

Various numerical simulation tools are designed to predict the dynamic behaviour of the railway vehicle. These numerical tools predict the dynamical performance of a railway vehicle at the designing phase and also examine the issues arising during usage as effectively as possible. Numerical simulations allow the investigation of a railway vehicle's dynamic behaviour under extreme parameters that cannot be noticed during real testing situations [92]. The development of advanced computer systems and Finite-element numerical methods has magnified the search for numerical calculation methods for vehicular vibration. Many researchers have developed a 3D dynamic model of high-speed trains to predict the vibration response and compare the results with those obtained from field monitoring [93–95]. There are different commercially available simulation software like ANSYS, SIMPACK, and LS-DYNA to perform such analysis in various ways.

2.1.4 Bond graph modelling

The modelling of engineering systems using bond graphs is grounded on the power argument between the system's fundamental parts. This method enables the integrated depiction of numerous energy regimes inside the system. Paynter [96] proposed the breakthrough idea of depicting systems in terms of power bonds, integrating physical system elements into so-called junction structures that were representations of restrictions. This power exchange representation of a system is known as a Bond Graph, and it can be oriented towards both power and information. Banerjee et al. [97] created a bond graph model to depict the dynamics of a rail wheelset moving down a curved track, using capsule-like sub-models. A railway truck running on a flexible tangent track has been modelled by Saha et al. [98] through bond graph formulism considering eighteen DOF vehicle with six DOF for each wheelset and the truck unit. Kalker's linear creep model was utilized to calculate rail-wheel contact forces. Simulations were conducted to investigate truck-critical speeds and stability behaviour. A bond graph model of a truck running on a flexible curve track has been created with eighteen degrees of freedom by Banerjee et al. [99]. Simulations were used to investigate the truck's stability and curving behaviour. Banerjee et al. [100] constructed a bond graph model of a free railway wheelset running over a flexible bent track using a module-based technique. The wheelset model was created using subsystem models rather than linearity approximation. Various subsystem models were collected to create a complete whole bond graph model of a wheelset for simulation on a stiff railway track. The bond graph technique was used to articulate and simulate the behaviour of railway vehicle drive systems, closely duplicating real-world railway operating scenarios along a standardized piece of track [101]**.** The method was illustrated using examples from the construction of symmetrical, anti-symmetrical, and mixed three-dimensional motion models of a motor vehicle [5]**.** Margolis et al. [102] demonstrated a four-wheel and

nonlinear vehicle dynamic model with electrically controlled brakes, steering and suspension corners. Controllers were not modelled in fact, but were exhibited through simulation [102]**.** Kumar et al. [103–105] used bond graph methodology to study the vertical lateral dynamics of railway vehicle moving on the ballasted track. A 3 Dimensional, 9 DOF and 31 DOF railway vehicle has been developed through bond graph. The authors also developed a biodynamical human model to study ride comfort through a bond graph approach. Patel et al. [106] investigated the effect of wheel irregularity on the vertical dynamics of wheel-rail interactions. They used a bond graph technique to create a two-layered slab track.

2.1.5 SIMPACK modelling of high-speed railway vehicle

To understand the dynamic behaviour of intricate mechanical systems and the interaction of interconnected rigid or flexible bodies subjected to external forces and constraints, engineers and researchers may use SIMPACK, which is a robust simulation software package built for multi-body system dynamics (MBDS). SIMPACK excels in modelling and simulating the dynamics of interconnected rigid and flexible bodies. This capability allows the researcher to study the vehicle track interactions between different components of a railway vehicle and track structure. Wu et al. [107] have used SIMPACK software to study the impact of a flexible wheelset on the dynamic responses of a high-speed railway car in the presence of a wheel flat. Jelila et al. [108] have used a multibody dynamic simulation approach to investigate wheel-rail contact behaviour at turnout. Du G et al. [109] have studied the structural dynamics of railway tracks in order to increase the track quality at a higher speed range through SIMPACK and ABAQUS. Vehicle ride quality has also been evaluated in their research work. An integrated numerical method for assessing the dynamic performance of longer trains Bosso et al. [110] have used SIMPACK code to

improve the braking strategy and mass distribution throughout the train Long train simulators in particular have been designed to evaluate the longitudinal forces during the braking operations.

2.1.6 Research gaps

It has been observed from the previous section that, a wide variety of experimental and analytical studies have been conducted for the analysis of different aspects of railway vehicle dynamics**.** Most of the research was carried out by considering the rail-wheel model to study vehicle track dynamics. A more realistic approach for studying the dynamic analysis of vehicle track interaction is by using slab track models.

Limited research has been available which considers the effect of track irregularities on the lateral dynamics of high-speed railway vehicles. Very limited studies have been carried out to determine ride quality and comfort for high-speed trains under irregular track conditions. Again, very limited research has been carried out to model the high-speed trains through bond graphs. Limited research work has been done for studying the vehicle/rail problem using SIMPACK.

2.2 Scope and Objectives of Research Work

The primary objective of this dissertation research is to construct comprehensive models of railway vehicle/track systems, taking into account track nonlinearity and car-body flexibility. The dissertation will establish the following goals, which are also anticipated to be its most significant contributions:

1. To develop a theoretical model of conventional track and high-speed track which may incorporate the dynamic interaction between the track and wheel for high-speed train range.

2. To develop a computational framework for rail vehicle on high-speed tracks using bond graphs.
3. To investigate lateral dynamics of high-speed trains on irregular track.
4. To determine the train ride quality and influence of various vibration and motion components on ride comfort

2.3 Expected Outcomes of Research Domain

The thesis contributes to the following areas of railway dynamics.

Wheel/Rail interaction analysis: A comprehensive general-purpose model of the railway vehicle track system is developed to study interaction dynamics in symmetrical as well as asymmetrical cases. For this, a railway vehicle (RV) and track model are first constructed separately, and then integrated at the wheel rail interface through nonlinear hertz contact. A two-layer slab-track model has been considered. Such a model is required as the forces developed at the interface due to high frequency vehicle-track interaction have a great impact on track deterioration and maintenance.

Lateral dynamics of HSRV: Stability analysis of 31 DOF of high-speed railway vehicle has been investigated for the heuristic nonlinear creep model and Polach model. The effect of short-wave track irregularity on lateral dynamics of HSRV has been investigated when the vehicle is moving on the transition track.

Ride comfort: Comfort analysis of as high-speed railway vehicle has been presented. The proposed 50 DOF high-speed rigid rail model has been developed in SIMPACK. The effect of random track irregularities on vehicle ride comfort has been studied. Also, simulation has been carried out to study the influence of different vibration and motion components on ride comfort.

2.4 Organization of the Thesis

The thesis has been organized into seven chapters. The first chapter is “Introduction” which gives introductory knowledge of railway dynamics and parameter affecting the railway dynamics. Second chapter is a literature survey. It gives a review of earlier work in this field. The exhaustive literature study have been carried to find the literature gaps. On the basis of these research gaps objective and methodology of present research work has been achieved. Third chapter is “theoretical modelling of conventional track and high-speed track”, which may incorporate the dynamic interaction between the track and wheel for high-speed train range. Fourth chapter gives the detailed idea about “computational framework of railway vehicle model”, which include the development of a single degree of freedom of wheel/slab track interaction model and a multi degree of freedom of complete vehicle model through bond graph. Wheel impact assessment results have been compared for both models. The slab track is modelled as an Euler-Bernoulli beam. The bond graph is used for modelling and simulation by using SYMBOLS SONATA® [111]. The fifth chapter presents “the lateral dynamic behaviour of HSRV model”. The influence of track irregularity on the running behaviour of high-speed train moving on the transition track has been explored. A 31 DOF vehicle model has been developed using bond graph methodology. The sixth chapter represents the “ride comfort assessment of high-speed railway vehicles” under the influence of various track excitation. This study provides a deeper understanding of passenger ride comfort at six car-floor positions, and other components of railway vehicles under various track conditions. Finally, the seventh chapter presents the conclusions and scope for future work.

CHAPTER 3

Theoretical Modelling of Conventional Track and High-Speed Track

In the previous chapter, an extensive literature survey of high-speed railway dynamics has been presented. This chapter presents the theoretical formulation of conventional track (ballasted track), high-speed track (slab track) and wheel/track interaction model. A three-layer ballasted track and two-layer slab track have been modelled considering rail as a Bernoulli beam through the bond graph method. The contact model at the wheel-rail interface has also been discussed in detail.

3.1 Introduction

Theoretical modelling is a powerful tool for understanding and predicting the behaviour of the train-wheel-track system. A range of modelling approaches has been developed over the years, including analytical, numerical, and experimental methods. These models can be used to investigate various aspects of railway dynamics, including the vertical and lateral forces acting on the track, the rail deflection and stress, and the response of the train to track irregularities.

In the case of a conventional railway track, the dynamic interaction between the train wheel and the track is primarily governed by the properties of the track, such as stiffness, damping, and geometry. The track is typically modelled as a series of discrete elements, and the interaction between the train and the track is analyzed using multi-body dynamics

methods. The modelling of the wheel-rail system involves a detailed description of the mechanical properties of the wheels, including their mass, moment of inertia, and contact patch geometry [112].

The dynamics of high-speed train track system is more complex due to the higher speeds and interaction forces involved. The track should be designed to reduce the dynamic forces acting on the train, and its geometry and stiffness should be improved for high-speed operation. For high-speed operation, the train-wheel system should be designed with lightweight wheels and improved suspension systems. The modelling of the train-wheel-track system for high-speed operation requires more advanced techniques, such as finite element analysis, multi body dynamics and advanced control systems. To summarize, the interplay between train wheels and the track is an essential component of railway engineering, and theoretical modelling plays a vital role in comprehending and forecasting the system's behaviour. Several factors, such as track and wheel properties, train speed and load, and environmental conditions, influence the modelling of the train-wheel-track system. However, it is important to note that the modelling techniques for conventional railway tracks and high-speed train tracks differ due to their distinct characteristics and operational requirements [113].

In recent decades, global railway industries have been dedicated to enhancing the speed and load-bearing capabilities of trains. The paramount considerations at elevated train operating speeds involve ensuring safety and comfort. The augmentation of both train speed and load-carrying capacity inevitably introduces heightened vibrations within the vehicle–track system, primarily stemming from irregularities on the wheel-rail surface. This elevation in vibrations raises the risk of track component damage, consequently impacting the safety and comfort of train operations. Compounding the complexity of the system is the nonlinear relationship between wheel-rail contact and the track components [114].

Consequently, there is a pressing need for substantial efforts to accurately predict wheel-rail interaction forces, aiming to identify the key factors contributing to vehicle and track component damage.

Based on existing literature, there are two distinct track systems. The initial one is recognized as the traditional track system, commonly referred to as the ballasted track system, while the second one is the ballastless track system, also known as the slab track system. The ballast track system consists of a series of sleepers (ties) laid on top of a layer of ballast, with rails attached to the sleepers through rail pad fasteners. The ballast provides stability, drainage, and support for the sleepers, and the sleepers provide support and stability for the rails. It is preferably designed for the lower operating speed of railway vehicles. In contrast, high-speed tracks are designed for trains that operate at speeds above 250 km/h (155 mph) and are typically used for intercity and high-speed trains. High-speed tracks can be either ballasted or slab tracks, with the latter being more common. Slab track consists of a continuous concrete slab that is laid directly on the ground or the concrete supporting layers, with rails embedded in the concrete. High-speed tracks are designed to provide a smoother ride, reduce noise and vibration, and accommodate trains that require tighter curves and steeper gradients than conventional trains. The main differences between conventional and high-speed tracks are the design, materials, and construction techniques used to create them. High-speed tracks require more precise alignment and levelling, with tighter tolerances for curves and gradients, to ensure the stability and safety of the train at high speeds [115]. They also require more durable materials and construction techniques to withstand the higher stresses and forces generated by high-speed trains. The modelling of a ballasted railway track and a high-speed train track are different due to the different properties and operating conditions of the two systems. In the later sections, the system of railway tracks is discussed in detail.

3.2 Modelling of Track Structure

3.2.1 Assumptions in modelling of railway track system

The following are the fundamental assumptions made while modelling a railway track system [105]:

- The track is assumed to be symmetric along the longitudinal direction.
- Sleepers are assumed to be rigid.
- Zero deflections and bending moments are presumed at the beam-hinged ends.
- The deflection of subgrade/foundation has been neglected in the analysis.
- The cross-sectional properties of the slab track are independent of its length.
- Elastic properties of slab tracks are considered to be homogeneous and isotropic.

3.2.2 Modelling of ballasted track

Currently, the traditional track system, known as the ballasted track system, comprises various elements such as rails, rail pad/fastener, ballast, and the subgrade (roadbed), as depicted in Figure 3.1.

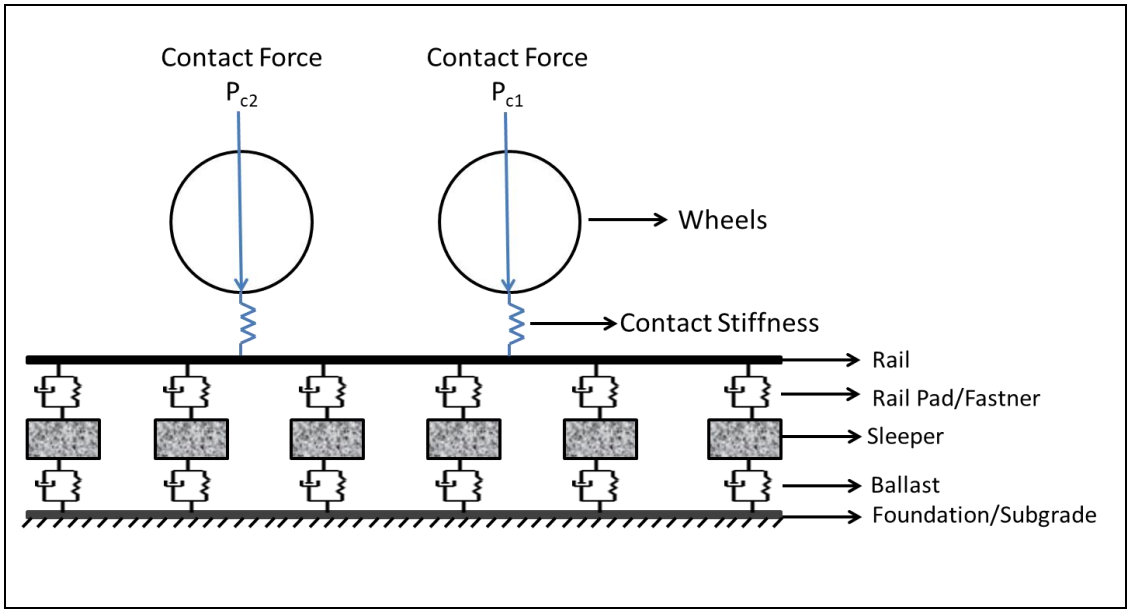

Figure 3.1: Schematic diagram of ballasted track

3.2.2.1 Modelling of rail

Rail is considered as a concatenation of beams of finite length between fasteners on both ends and hinged to them on both ends resting on the ballasted track. In this work, the rail is modelled as the Euler-Bernoulli beam. The rail pad and fasteners, used to connect the rail to the sleeper, are modelled as a massless spring-damper element.

The modal bond graph model of the rail beam termed RB is shown in Figure 3.2. Through 0 junction, a relation between the actual velocity and modal velocity is established, such that the incoming actual velocity is the summation of the product of modal velocity and mode shapes. The transformer acts as a power conservator which transforms the actual

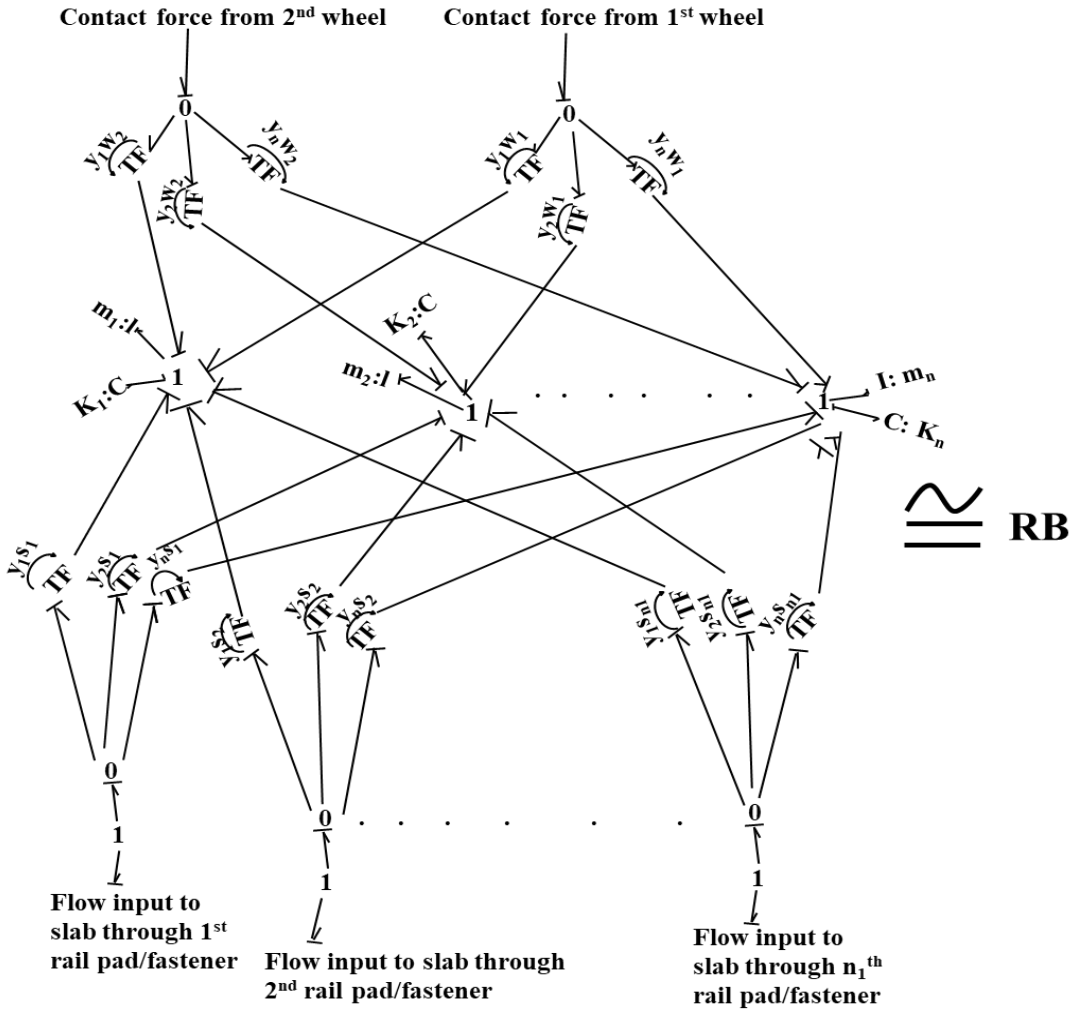

Figure 3.2: Bond graph model of rail beam (RB)

force into the modal forces and these modal forces further act as an input to the dynamic equation. Forces acting at the wheel-rail interface emanate from the 0-junction to the rail structure. The two-port transformer element transforms the forces and provides input modal forces to each mode. These modes are shown by the I and C elements connected to 1 junction. The I element represents the modal mass and the C element represents the mode stiffness. The vertical deflection along the rail-wheel interface is determined by both the longitudinal position of the beam relative to the left side of the rail, denoted as the variable x, and time, represented as t. The entire function is expressed as Z (x, t). The governing partial differential equation (PDE) for the rail beam describes the vertical deflection of the rail under the influence of a dynamic vertical contact force at the wheel-rail interface, as defined in Eq. (3.1).

$$(EI)_r \frac{\partial^4 Z(x,t)}{\partial x^4} + m_r \frac{\partial^2 Z(x,t)}{\partial t^2} = P_{c1}(t)\delta(x - x_{w1}) + P_{c2}(t)\delta(x - x_{w2}) - \sum_{j=1}^{NR} F_{rj}\delta(x - x_j) \tag{3.1}$$

Where $(EI)_r$ is flexural rigidity of rail, m_r is the mass of rail per unit length, P_{c1} and P_{c2} is the contact force acting at the wheel-rail interface, $\delta(.)$ is Dirac delta function, x represents the longitudinal coordinate of rail beam regarding one end, x_w defines the position of the wheel, F_{rj} is the vertical force due to discrete support provided by rail pad and fasteners, NR is the no of discrete support, x_j represents the position of j_{th} discrete support.

A modal superposition technique is utilized to convert a PDE into an ordinary differential equation (ODE) [8, 116–118]. The variable separation method provides the solution to the ODE. The result derived through the variable separation technique encompasses an infinite summation involving the multiplication of the shape function $Y_j(x)$

and the modal amplitude $q_j(t)$. In the ongoing examination, the rail modal model incorporates a total of twenty modes, while the concrete slab modal model involves ten modes. The displacement of the rail beam is expressed by Eq. (3.2).

$$Z_r(x,t) = \sum_{j=1}^{nm} Y_j(x) q_j(t) \tag{3.2}$$

Where *nm* is the number of modes.

The sub-model RB involves every equation of flexible modes. The mode shape function resulting from Eq. (3.3) acts as a transformer moduli in the Bond graph models shown in Table 3.1.

Table 3.1: List of transformer moduli

Transformer moduli	**Moduli**
y_1w_1	$\sin(1*PI*w_1/L_r)$
y_nw_1	$\sin(n*PI*w_1/L_r)$
y_1s_1	$\sin(1*PI*s_1/L_r)$
y_ns_m	$\sin(n*PI*s_1/L_r)$

It is assumed that the ends of the rail beam are hinged. Therefore, the deflection and bending moment at the rail beam ends have zero values. By using the above-mentioned assumption, shape function and natural frequencies obtained, are obtained by Eq. (3.3) and Eq. (3.4).

$$Y_j(x) = sin\ sin\left(\frac{j\pi x}{L}\right) \tag{3.3}$$

$$\omega_j = \left(\frac{j\pi}{L}\right)^2 \sqrt{\left(\frac{EI}{\rho A}\right)} \tag{3.4}$$

By using Eq. (3.2) in Eq. (3.3) and after solving the resultant equation with the help of an orthogonal properties of shape functions, the results come out to be as follows in Eq. (3.5).

$$m_j\ddot{q}_j + k_j q_j = P_{c1}(t)j(x_{w1}) + P_{c2}(t)j\delta(x - x_{w2}) - \sum_{j=1}^{NR} F_{rj}\delta(x - x_j) \tag{3.5}$$

where m_j signifies the modal mass and k_j signifies the mode stiffness at the j^{th} place.

$$m_j = \frac{\rho AL}{2} \qquad j = 1,2 \ldots . . NM \tag{3.6}$$

$$k_j = m_j\left(\omega_j\right)^2 \qquad j = 1,2 \ldots \ldots \ldots NM \tag{3.7}$$

Defining the momentum as

$$p_j = m_j\dot{q}_j \tag{3.8}$$

Eq. (3.5) and (3.6) can be written as

$$\frac{dp_j}{dt} = -k_j q_j + P_{c1}(t)Y_j(x_{w1}) + P_{c2}(t)\delta(x - x_{w2}) - \sum_{j=1}^{NR} F_{rj}\delta(x - x_j) \tag{3.9}$$

and

$$\frac{dq_j}{dt} = \frac{p_j}{m_j} \tag{3.10}$$

The Eqs. (3.9-3.10) represent the reduced 1^{st} order equation of j^{th} modal Eq. (3.5) in terms of bond graph variable p_j and q_j [119].

3.2.2.2 Modelling of rail pad and fastener

Fasteners play a crucial role in linking the rails to sleepers, ensuring a secure connection and maintaining the track gauge stability during operation. Meanwhile, rail pads are responsible for evenly distributing the loads on the rail seat across the sleepers. In the conceptual framework, both rail pads and fasteners are represented as massless spring and damper elements strategically placed between the rail and sleepers. For the sake of simplicity, many research studies typically adopt the assumption of linear pad stiffness. In the bond graph, the stiffness and damping properties of the rail pad and fastener are represented by C and R elements respectively. By introducing C-elements into the model, integral causality is ensured, meaning that the output of the system depends on the integral

or accumulation of the input signal over time. In bond graph modelling, R-elements are used to represent energy storage elements or inertial components. They contribute to increasing the order of the mathematical model by introducing additional dynamic states or variables that capture the system's behaviour more accurately. By incorporating C-elements to enforce integral causality and R-elements to capture energy exchange, the bond graph model becomes more comprehensive and captures the system's dynamics more accurately. This increased fidelity allows for a more detailed analysis and simulation of complex dynamic systems, such as those encountered in engineering applications like mechanical systems, electrical circuits, and biological systems.

3.2.2.3 Modelling of sleeper

The sleepers play a crucial role in maintaining the stability and proper alignment of the railway track. They offer support to the rails, ensuring the preservation of gauge, level, and alignment. Additionally, these sleepers facilitate the transmission of vertical, lateral, and longitudinal forces from the rail to the ballast bed [120]. In this representation, the sleepers are conceptualized as discrete masses, supported individually on the ballast. The schematic of the sleeper is shown in Figure 3.3.

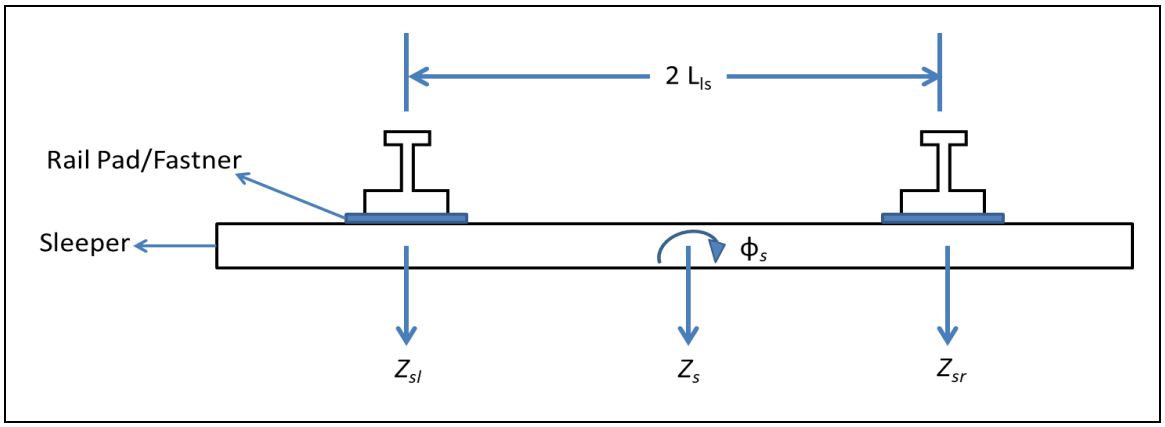

Figure 3.3: Sleeper model

The kinematic relationship is given by Eqs. **(**3.11-3.12) are applied in the bond graph shown in Figure 3.4 as 0-junction. This model is termed as SL.

$$\dot{Z}_{sl} = \dot{Z}_s - \dot{\phi}_s L_{ls} \tag{3.11}$$

$$\dot{Z}_{sr} = \dot{Z}_s + \dot{\phi}_s L_{ls} \tag{3.12}$$

where, $\dot{Z}_s$, $\dot{Z}_{sr}$ and $\dot{Z}_{sl}$ represents the displacement of the sleeper in a vertical direction at CG, right and left end pad location, respectively. $\dot{\phi}_s$ is the roll velocity of the sleeper.

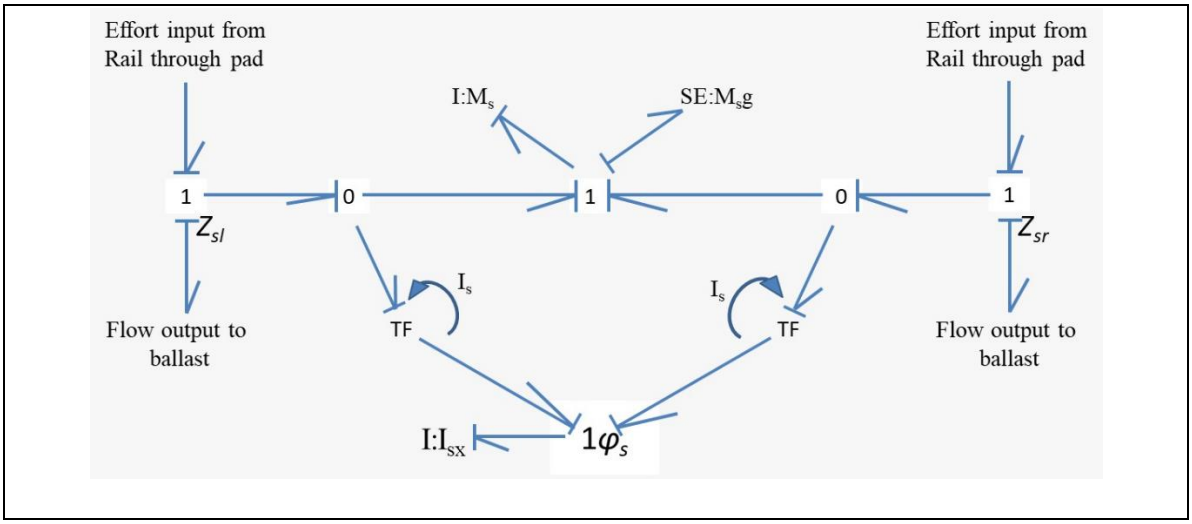

Figure 3.4: Bond graph sub-model of sleeper **(**SL**)**

3.2.2.4 Modelling of ballast

Ballast serves as a foundation made up of crushed stone, effectively distributing forces uniformly to the subgrade, either by direct contact or through the intermediary sub-ballast layer. Positioned just beneath the ballast, the sub-ballast layer consists of finer particles and undertakes similar functions as the ballast layer. The primary function of the subgrade is to endure traffic loads while providing sufficient attenuation. The subgrade's structural classification is determined by crucial characteristics such as the modulus of elasticity and carrying capacity [121]. The ballasts are represented in the model as spring and damper elements without mass, strategically placed between each sleeper and the subgrade. The subgrade, in this context, is treated as a firm and unyielding support. The comprehensive representation of the ballasted track structure can be observed in Figure 3.5.

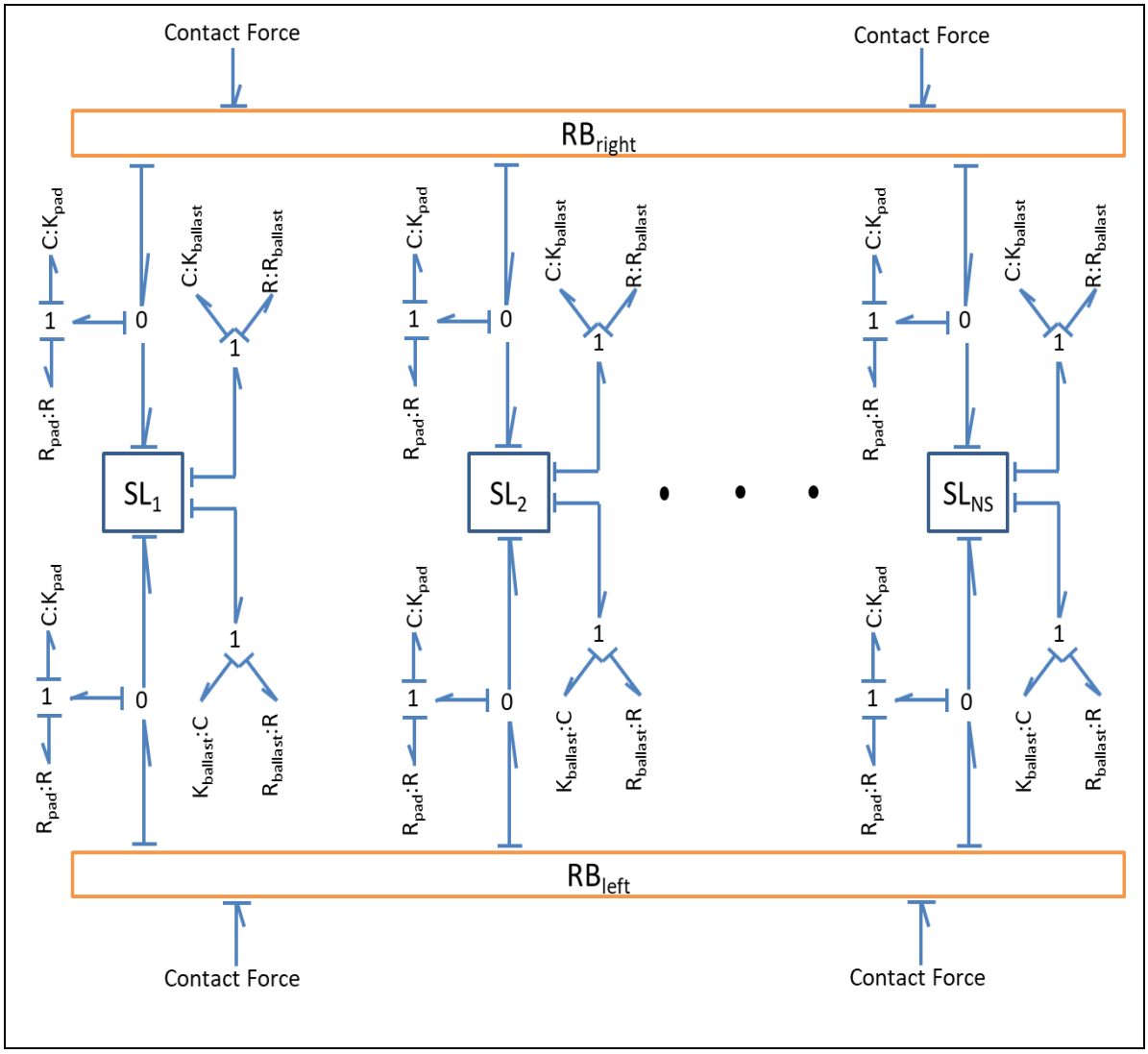

Figure 3.5: Integrated modelling of ballasted track structure

3.2.3 Modelling of slab track

To comprehend the dynamics of wheel/vehicle interactions with slab tracks, one can analyze the slab track using various models, such as the single continuous elastic beam model, two-layer elastic beam model, and three-layer elastic beam model illustrated in Figure 3.6.

In the single-layer continuous elastic beam model depicted in Figure 3.6(a), the rail is represented as a beam resting on an equivalent elastic foundation. The corresponding vibration differential equation is expressed as Eq. 3.13.

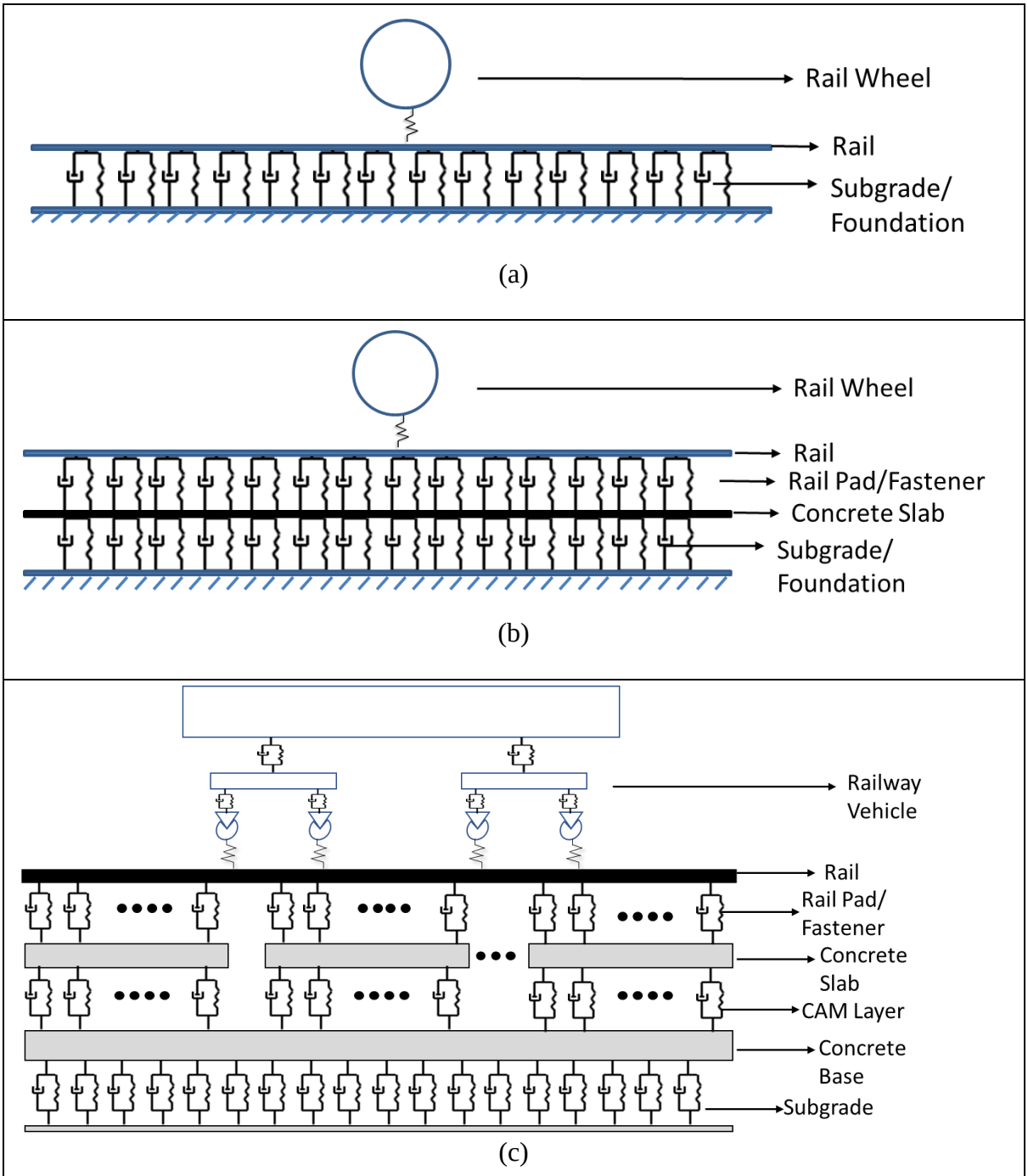

Figure 3.6: Slab track element Model (a) Single-layer continuous elastic beam model of track structure (b) Double-layer continuous elastic beam model of track structure (c)Three-layer slab track element

$$E_r I_r \frac{\partial^4 w}{\partial x^4} + m_r \frac{\partial^2 w}{\partial t^2} + c_r \frac{\partial w}{\partial t} + k_s w = -\sum_{l=1}^{n} F_l \delta(x - Vt - a_l) \qquad (3.13)$$

In double layer elastic beam model, Rail and slab have been modelled as continuous beams resting on a rail pad and elastic foundation respectively. A concrete slab structure is an

elastic beam resting on the foundation, used to support a rail structure. Force interaction at the concrete slab is shown in Figure 3.7. The PDE of the concrete slab beam is represented by Eq. (3.14) [122, 123].

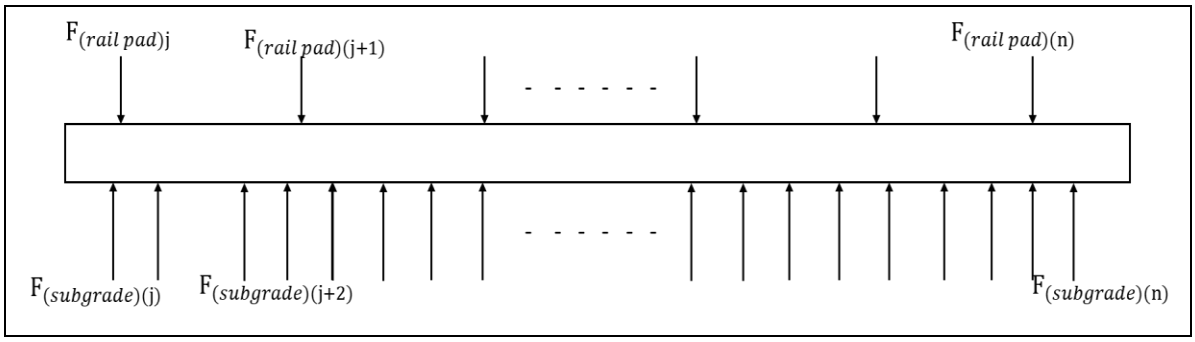

Figure 3.7: Vibration analysis model of slab track

$$(EI)_{slab}\frac{\partial^4 Zslab(x,t)}{\partial x^4} + (\rho A)_{slab}\frac{\partial^2 Zslab(x,t)}{\partial t^2} = \sum_{j=1}^{Np} F_{(rail\ pad)j}\delta(x - x_{pj}) - \sum_{j=1}^{Ns} F_{(subgrade)j}\delta(x - x_{sj}) \quad (3.14)$$

$$Z_{slab} = \sum_{j=1}^{nm} Y_j(x)q_j(t) \quad (3.15)$$

Where $(EI)_{slab}$ is the flexural rigidity of the concrete slab beam and Z_{slab} displacement of the concrete slab beam. Concerning the foundation, it was established through a configuration of springs connected in parallel with dashpots, evenly dispersed without any longitudinal interaction. Utilizing vibration theory and the segregation variable method, the displacements of the slab track are conceptualized as a linear combination of modal coordinates $(q_j(t))$ and mode shape functions $(Y_j(x))$, as depicted in Equation (3.15) [123].

The modal bond graph model of rail and the concrete slab are considered sub-models and are termed as RB sub-model and CRC sub-model respectively. Modal bond graph models of RB and CRC are shown in Figures 3.7 and 3.8 respectively. The sub-model RB involves every equation of flexible modes.

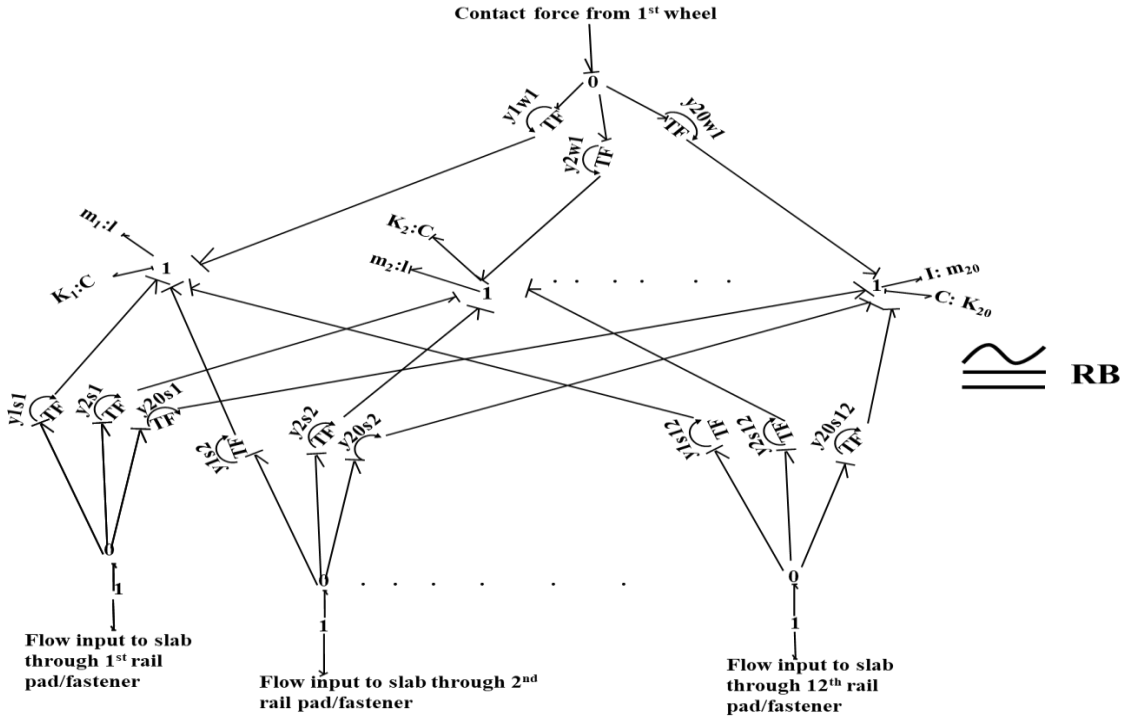

Figure 3.8: Modal bond graph model of concrete Rail Beam (RB) with twenty modes connected to rail with pad and fastener

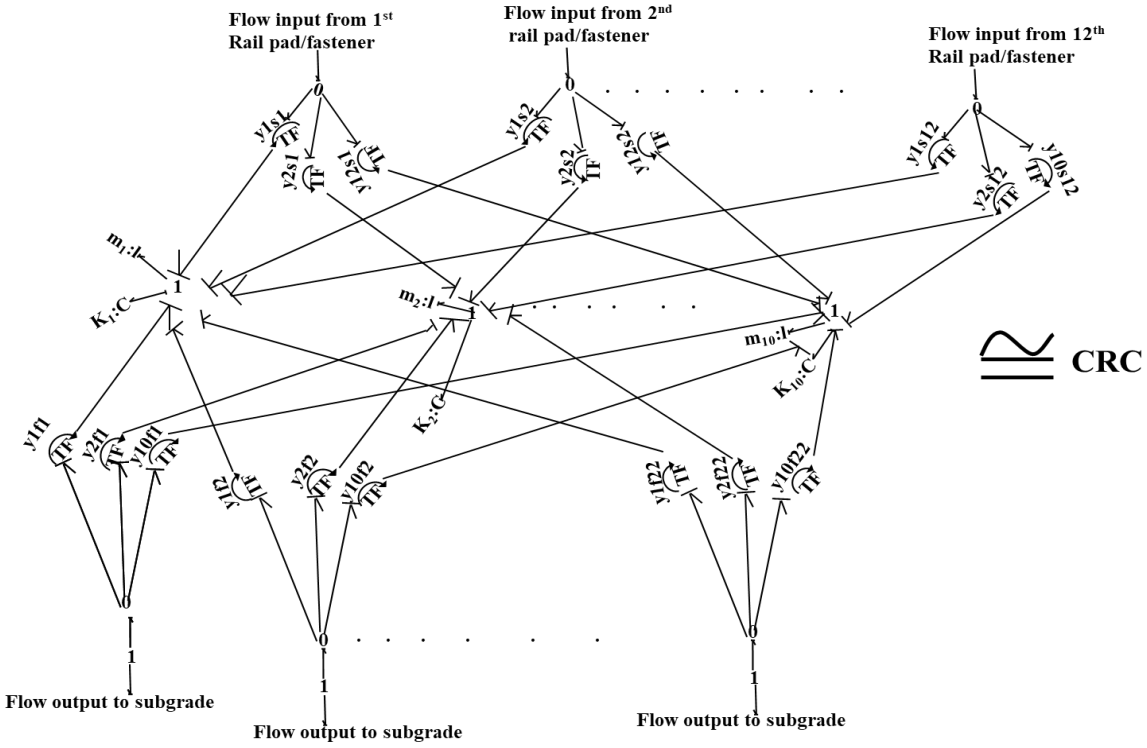

Figure 3.9: Modal bond graph model of concrete slab track (CRC) with ten modes connected to rail with pad and fastener

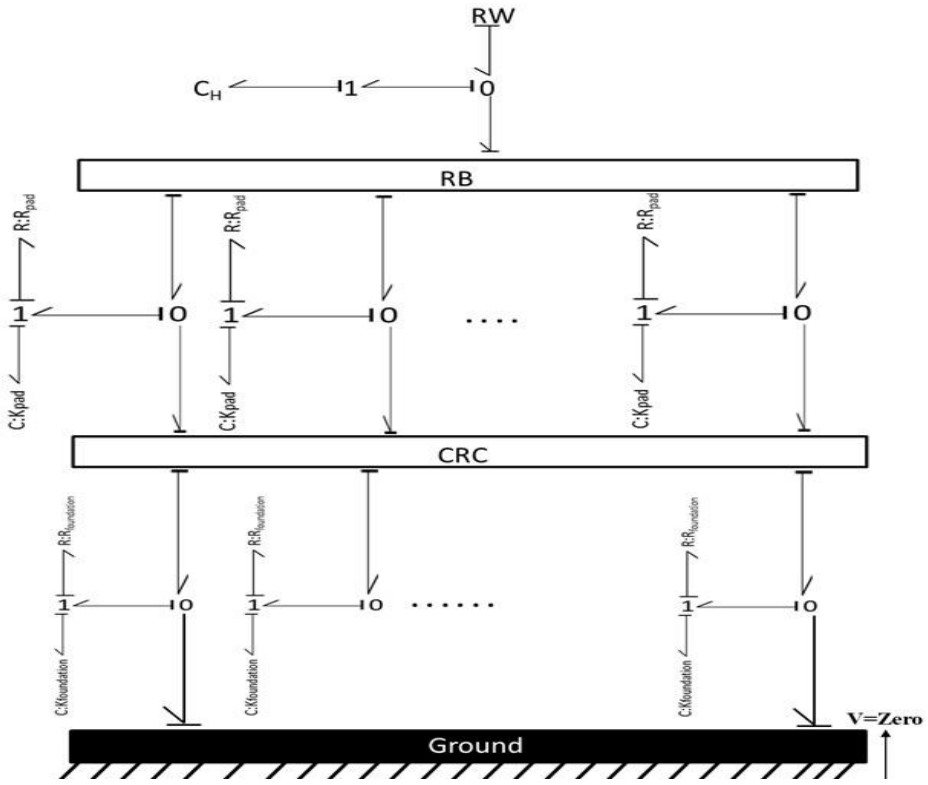

Figure 3.10: Integrated bond graph modelling of slab track

3.3 Wheel Rail Dynamic Interaction Theory

The heightened dynamic forces not only result in elevated levels of noise and vibration but also contribute to potential damage or failure in both the track structure and the vehicle, posing a risk to the safety of railway operations. The root cause of these challenges lies in the dynamic interplay between the wheel and the rail. Consequently, various models elucidating wheel-rail interaction have been developed in the past, employing either the time domain or the frequency domain. These models aim to tackle the aforementioned issues and others associated with railway dynamics [124].

When a railway wheel traverses a straight rail devoid of significant geometric or stiffness irregularities, it is possible to analytically model the wheel-rail contact. The coupling between the wheel and track models is facilitated through the wheel-rail contact model, which takes into account the forces generated during the interaction between the

wheels of the wheel-rail system and the track [125]. The examination of wheel-rail contact encompasses three distinct yet interconnected problems, summarized as follows [126]:

a) The contact geometry problem involves determining the location of the contact point on the profiled surfaces of the bodies.

b) Contact kinematics addresses the systematic definition of creepages, or normalized relative velocities, at the contact point.

c) Contact mechanics focuses on determining the contact forces based on three-dimensional rolling contact theories.

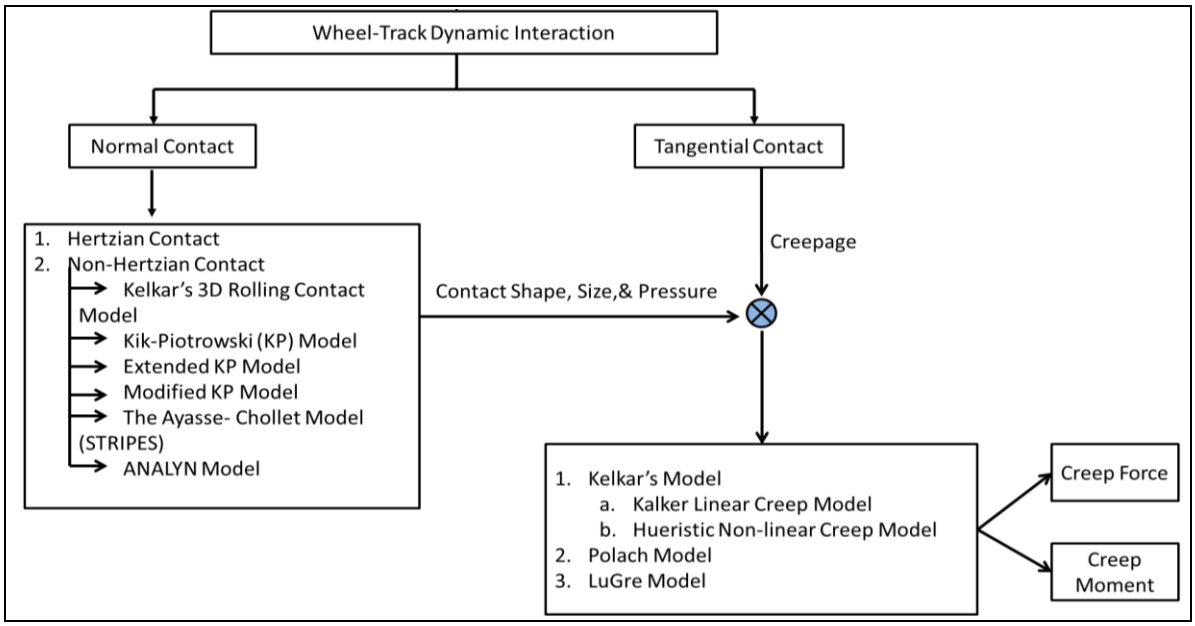

Figure 3.11: Classification of Contact modelling

To address the problem (a), numerous rigid and elastic contact search algorithms [127] are documented in the existing literature. Presently, methods that account for the three-dimensional geometric problem and local contact flexibility are favoured. In the context of the normal contact problem, the Hertz theory [128] holds widespread acceptance in railway engineering due to its efficiency and analytical form. For problems (b) and (c), non-Hertzian contact theory, incorporating creepage theory, has been extensively applied by

many researchers. A visual representation of the wheel-rail contact modelling process is presented in Figure 3.11.

3.3.1 Hertz contact theory

The Hertzian theory is employed to analyze elliptical contact areas and semi-ellipsoid contact pressure distributions within the contact region. This theory, renowned for its efficiency and simplicity, finds widespread application based on the following assumptions [9]:

- In the proximity of the contact, it is assumed that the body behaves like half-spaces.
- The strain at the interface between the rail and wheel is presumed to be negligibly small.
- At a considerable distance from the contact area, any stress developed at the rail-wheel interface vanishes.
- The contact between elastic bodies is treated as frictionless.
- The bodies involved in the analysis are regarded as elastic.

The Hertzian contact theory [9, 129–133] states the relationship between contact force and rail wheel deflection, which is non-linear and is represented as

$$P_c = K_h(\Delta Z(t))^{\frac{3}{2}} \tag{3.16}$$

where K_h signifies the Hertzian stiffness and its value given by the Johnson Eq. [134]as

$$K_h = \frac{4G_{\sqrt{R_e}}}{3(1-\nu)} \tag{3.17}$$

Where G represents the shear modulus of the material and ν represents the Poisson's ratio.

$$R_e = \sqrt{rR} \tag{3.18}$$

$$R = \frac{R_w R_r}{(R_w - r)} \tag{3.19}$$

In the above equations, the *r* variable represents the rolling variable of the train wheel, R_w represents the radius of the wheel profile, and R_r represents the radius of the rail profile. The value of Hertzian stiffness K_h, at a given value of R_w and R_r, is obtained from the work of Newton and Clark [135] and Uzzal [136].

Over the last twenty years, several non-Hertzian contact models for wheel-rail interactions, utilizing the virtual penetration method, have been devised. These models encompass the Linder method [137], the Kik–Piotrowski (KP) model, the Extended Kik–Piotrowski (EKP) model the Modified Kik–Piotrowski (MKP) model [138, 139], the Ayasse-Chollet model (STRIPES) and the ANALYN model [140].

3.3.2 Kalker's 3D rolling contact theory

Kalker, a researcher hailing from the Netherlands, introduced a meticulous 3D rolling contact theory [141] grounded in the complementary virtual work principle. This theoretical framework integrates concepts from elasticity theory and the half-space hypothesis, making several key assumptions: the contact object comprises linear elastic isotropic materials, the contact patches are significantly smaller than the object, the stress induced by surface load diminishes with increasing distance from the contact region, and stresses far from the contact point can be neglected. Through the application of Kalker's 3D contact theory, a numerical program named CONTACT was formulated, facilitating precise simulation of rolling contact interactions between the wheel and rail [142]. Nevertheless, the program's extended computational duration renders it unsuitable for predicting vehicle dynamics and rail damages. As a result, the outcomes derived from

CONTACT are commonly employed to evaluate the accuracy of other engineering approximation models.

3.3.3 Normal contact modelling in the wheel-rail interaction:

The utilization of the multibody formulation in analyzing the forces at the wheel-rail contact provides a precise computation of the normal force exerted at the contact point. Within this framework, the determination of normal contact forces involves considering factors such as the extent of penetration, the relative velocity between contact points, and the material properties inherent to both the wheel and the rail.

3.3.4 Tangential contact modelling using the Kalker linear theory:

The Kalker linear creep theory is a mathematical model used to analyze the interaction between the wheel and rail in railway dynamics, specifically focusing on the phenomenon of creep. Creep refers to the relative sliding and rolling between the wheel and rail surfaces, which is crucial to understanding wheel-rail interaction, especially during braking or traction.

The Kalker linear creep theory was developed by J.J. Kalker and is an extension of his more comprehensive Kalker's FASTSIM algorithm[143]. The linear creep theory simplifies the analysis by assuming a linear relationship between the creep force and the creepage (the relative sliding velocity between the wheel and the rail). This linear relationship is represented by a constant parameter known as the creep coefficient. The creepages are defined mathematically in terms of velocity difference and are given by Eqs. (3.20-3.22).

$$\xi_x = \frac{v_x - v_x^*}{v_x^*} \tag{3.20}$$

$$\xi_y = \frac{v_y - v_y^*}{v_x^*} \tag{3.21}$$

$$\xi_{sp} = \frac{\omega_w - \omega_r}{v_x^*} \tag{3.22}$$

where, ξ_x, ξ_y represents dimensionless longitudinal and lateral creepages respectively whereas ξ_{sp} denotes the spin creepage with the dimension of L^{-1}. Creep forces and moments are generated by these creepages. Creep forces (moment) at the contact surface are given by Eq. (3.23).

$$Creep\ force\ (moment) = Creep\ coefficient\ \times Creepages \tag{3.23}$$

The longitudinal creep force generally acts in the wheelset's forward direction of motion and lateral creep force acts perpendicularly to it in the lateral creep direction, whereas spin creep moment acts in the normal load direction, orthogonal to the creep force components and hence to the plane of contact region. The longitudinal creep force, lateral creep force and spin creep moment at contact are given by Kalker's linear creep theory as presented in Eq. (3.42-3.44) [4].

Longitudinal creep force, $$F_{1x} = f_{33}\,\xi_x \tag{3.24}$$

Lateral creep force, $$F_{3y} = f_{11}\,\xi_y + f_{12}\,\xi_{sp} \tag{3.25}$$

Longitudinal creep force, $$M_{2s} = -f_{12}\,\xi_y + f_{22}\,\xi_{sp} \tag{3.26}$$

where, ξ_x, ξ_y and ξ_{sp} are the longitudinal, lateral and spin creepages given by Eqs. (3.20-3.22) respectively and f_{ija} are creep coefficients. In the bond graph, creep forces are modelled by the R- element by simply attaching the R element to 1 junction.

3.3.5 Tangential contact using the Heuristic nonlinear creep force model

A heuristic nonlinear creep model is developed to define the tangential contact at the wheel-rail interface. The heuristic non-linear creep model is a combination of Kalker's linear creep theory and creep force saturation. The nonlinear creep forces and nonlinear creep

moments result by multiplying saturation factor α_i to the corresponding linear creep force and linear creep moment as shown in Eqs. (3.27-3.32).

$$F_{wLx}^{n} = \alpha_{ij} F_{wlx}^{L} \tag{3.27}$$

$$F_{wRx}^{n} = \alpha_{ij} F_{wrx}^{R} \tag{3.28}$$

$$F_{wLy}^{n} = \alpha_{ij} F_{wly}^{L} \tag{3.29}$$

$$F_{wRy}^{n} = \alpha_{ij} F_{wry}^{R} \tag{3.30}$$

$$M_{wLz}^{n} = \alpha_{ij} M_{wlz}^{L} \tag{3.31}$$

$$M_{wRz}^{n} = \alpha_{ij} M_{wrz}^{R} \tag{3.32}$$

Where F_{wlx}^{L}, F_{wly}^{L}, M_{wlz}^{L}, F_{wrx}^{R}, F_{wry}^{R}, M_{wrz}^{R} are linear creep forces and moments on the left and right wheels in respective directions. Equations of linear creep forces and moments are taken from Kim et.al [144]. α_{ij} represent the saturation constant in the heuristic creep model obtained from Johnson's approach [145] as given in Eqs (3.33).

$$\alpha_{ij} = \begin{cases} \frac{1}{\beta_{ij}}\left(\beta_{ij} - \frac{1}{3}\beta_{ij}^{2} + \frac{1}{27}\beta_{ij}^{3}\right) => \beta_{ij} \leq 3 \\ \frac{1}{\beta_{ij}} => \beta_{ij} \geq 3 \end{cases} \tag{3.33}$$

Where β_{ij} is the non-linearity factor in the heuristic creep model and it is calculated for vehicles under quasi-static motion over the curved track [144].

3.3.6 Tangential contact using the Polach creep force model

The Polach formulation, as outlined in [54, 146], represents the third option for modelling creep forces and is integrated into the computer algorithm. According to the Polach approach, the longitudinal and lateral components of creep forces emerging in the wheel-rail contact area are defined by Eqs. (3.34-3.35).

$$F_{\xi} = F\frac{\upsilon_{\xi}}{\upsilon_{C}} \tag{3.34}$$

$$F_{\eta} = F\frac{\upsilon_{\eta}}{\upsilon_{C}} + F_{\eta S}\frac{\phi}{\upsilon_{C}} \tag{3.35}$$

In Eq. 3.35, F denotes the tangential contact force resulting from longitudinal and lateral creepages, υ_c represents the modified translational creepage (considering the impact of spin creepage), and $F_{\eta S}$ signifies the lateral tangential force arising from spin creepage. Where υ_ξ, υ_η, and φ represent the lateral longitudinal and spin creepage respectively. The model incorporates considerations for creepages, normal contact force, semi-axes of the contact ellipse, modulus of rigidity for wheel and rail materials, friction coefficient, and Kalker creepage and spin coefficients. Similar to the Heuristic method, the Polach formulation disregards the spin creep moment.

The Polach algorithm proves to be a suitable tool for investigating tangential contact forces within the wheel-rail interface. This method enables the computation of complete nonlinear creep forces, accounting for spin. Given its efficiency in computation time, the Polach algorithm can be employed in place of simpler formulations to enhance accuracy or serve as an alternative to more intricate theories, offering computational time savings.

3.4 Remarks

This chapter has focused on the development of a theoretical model for both conventional and high-speed railway tracks, with a particular emphasis on the dynamic interaction between the track and wheel, especially in the context of high-speed train operations.

Theoretical modelling, encompassing analytical, numerical, and experimental approaches, is a powerful tool for comprehending and predicting the behavior of the train-wheel-track system. The chapter highlighted that the dynamic interaction in conventional tracks is primarily influenced by track properties, while high-speed tracks require more sophisticated modelling techniques due to increased speeds and forces.

The discussion differentiated between conventional ballasted tracks and high-speed slab tracks, emphasizing their distinct designs, materials, and construction techniques. The

modelling assumptions for both track systems were outlined, providing a foundation for subsequent analyses. Detailed modelling of various track components, including the rail, rail pad and fastener, sleeper, ballast, and subgrade, was presented. The chapter delved into the modelling of slab tracks, introducing single-layer, double-layer, and three-layer elastic beam models.

Furthermore, the chapter discussed the critical aspect of wheel-rail dynamic interaction theory. The complexity of this interaction, influenced by factors such as contact geometry, kinematics, and mechanics, necessitates various modelling approaches. The Hertz contact theory, Kalker's 3D rolling contact theory, and different models for normal and tangential contact were explored. The presentation of the Kalker linear creep theory, heuristic nonlinear creep force model, and Polach nonlinear creep force model added depth to the discussion on tangential contact modelling. These models offer insights into the creepages and forces acting at the wheel-rail interface, essential for understanding the safety and performance of railway systems.

Summary of the chapter underscores the significance of theoretical modelling in railway engineering, providing a comprehensive overview of the diverse components and interactions within the train-wheel-track system. This research provides a foundation for further analyses and simulations, aiding in the advancement of design, safety, and efficiency for both conventional as well as high-speed railway tracks.

CHAPTER 4

Computational Modelling for Rail Vehicle on High-Speed Tracks using Bond Graphs

The previous chapter gives a detailed description of the theoretical modelling of ballasted track, slab track and wheel-track interaction. This chapter introduces the mathematical and computational framework for a rail vehicle operating on high-speed rail tracks, specifically slab track and ballasted track. Using a bond graph approach, 1 DOF wheel and 9 DOF High-Speed Rail Vehicle (HSRV) have been developed. The vehicle modelled in this context comprises a half car body and a bogie, consisting of two wheelsets. The slab track model is structured with a two-layer design, representing the rail and slab as Euler-Bernoulli beams. In parallel, a three-layer model for the ballasted track incorporates the rail, sleeper, and ballast bed has been developed. The integrated bond graph model is subsequently simulated, incorporating wheel irregularities affecting a single wheel. This simulation offers insights into the dynamics of the interaction between the wheel and rail.

4.1 Introduction

The development of a computational framework for rail vehicles operating on high-speed tracks utilizing bond graph theory represents a sophisticated and innovative approach to the analysis and simulation of dynamic systems. Bond graph theory, a powerful modelling technique in engineering, provides a systematic and unified representation of interconnected physical components and their energy interactions. In the context of rail

vehicle dynamics on high-speed tracks, this computational framework leverages bond graph theory to model and simulate the intricate relationships between various components such as the car body, wheel-rail interaction, suspension systems, and other relevant subsystems.

By integrating bond graph theory into the computational framework, engineers and researchers gain a comprehensive toolset for understanding the complex dynamics of high-speed rail systems. The approach facilitates the modelling of mechanical aspects of the rail vehicle, capturing the interplay of forces, energies, and constraints that influence its performance. This not only allows for a more accurate representation of the system but also enables the exploration of various design configurations and control strategies to enhance the overall performance of the high-speed rail vehicle.

Moreover, the computational framework provides a platform for conducting virtual experiments, allowing researchers to assess the impact of different parameters, environmental conditions, and operational scenarios on the rail vehicle's behaviour. This approach not only accelerates the design and development process but also contributes to the enhancement of safety, efficiency, and reliability in high-speed rail transportation.

The dynamics model of vehicle-track interaction constitutes a complex dynamical system typically decomposed into three subsystems: the vehicle, the track, and the wheel-rail contact, which establishes the connection between the two aforementioned subsystems. This interconnection holds great significance in modelling the interaction between the vehicle and track, and it is influenced by the presence of irregularities in the wheel and rail. Therefore, another crucial factor influencing the dynamics of wheel-rail interaction is the model representing irregularities in the wheel and rail. In the present study, a single wheel and 9 DOF quarter car model, ballasted track model and slab track model have been developed to investigate the effect of variation of the amplitude of wheel irregularity on the

wheel track dynamics at a high train speed range. From the available literature, it has been found that the researchers have used the finite element method approach to analyse the dynamics of the wheel-rail interaction for high-speed railway tracks. In the current research, the authors have used the bond graph approach to analyse the high-speed track model, consisting of two layers of Euler Bernoulli beam connected through a rail pad and fasteners. The bond graph technique is employed to model both the wheel and the slab track structure. Additionally, the modal superposition method is utilized to calculate the dynamic response of the wheel-track system. This dynamic response is characterized by parameters such as wheel-rail overlap, wheel acceleration, and the dynamic induced contact forces at the wheel-rail interface. A comparison has been made between the dynamic response at the wheel-rail interface when the vehicle runs on both slab track and ballasted track, considering the impact of wheel irregularities. To achieve this, a 9 DOF half car model has been constructed using bond graph methodology.

4.2 Modelling of Rail Vehicle and Track Structure

Different vehicle models have been utilized in this research work to examine the wheel-track interaction. It is advisable to opt for a model that is both straightforward and reliable while effectively capturing the required dynamics. To explore the dynamics at the interface between a railway vehicle and the track, a subsystem of the railway vehicle, specifically the 1 DOF and 9 DOF models, along with the track, is regarded as an integrated system interconnected through a wheel-rail interface. A model of wheel-track interaction is formulated by considering the coupling dynamics, as illustrated in Figure 4.1.

4.2.1 Fundamental assumption in modelling HSRV

During the development of the coupled wheel-track system model, the following assumptions are made:

i. The vehicle travels on a tangential track with a constant velocity in the longitudinal direction.

ii. The model is solely subjected to vertical dynamic load.

iii. The deflection of both beams hinged ends and the foundation are zero.

iv. At the wheel-rail contact interface, non-linear Hertzian contact theory is employed.

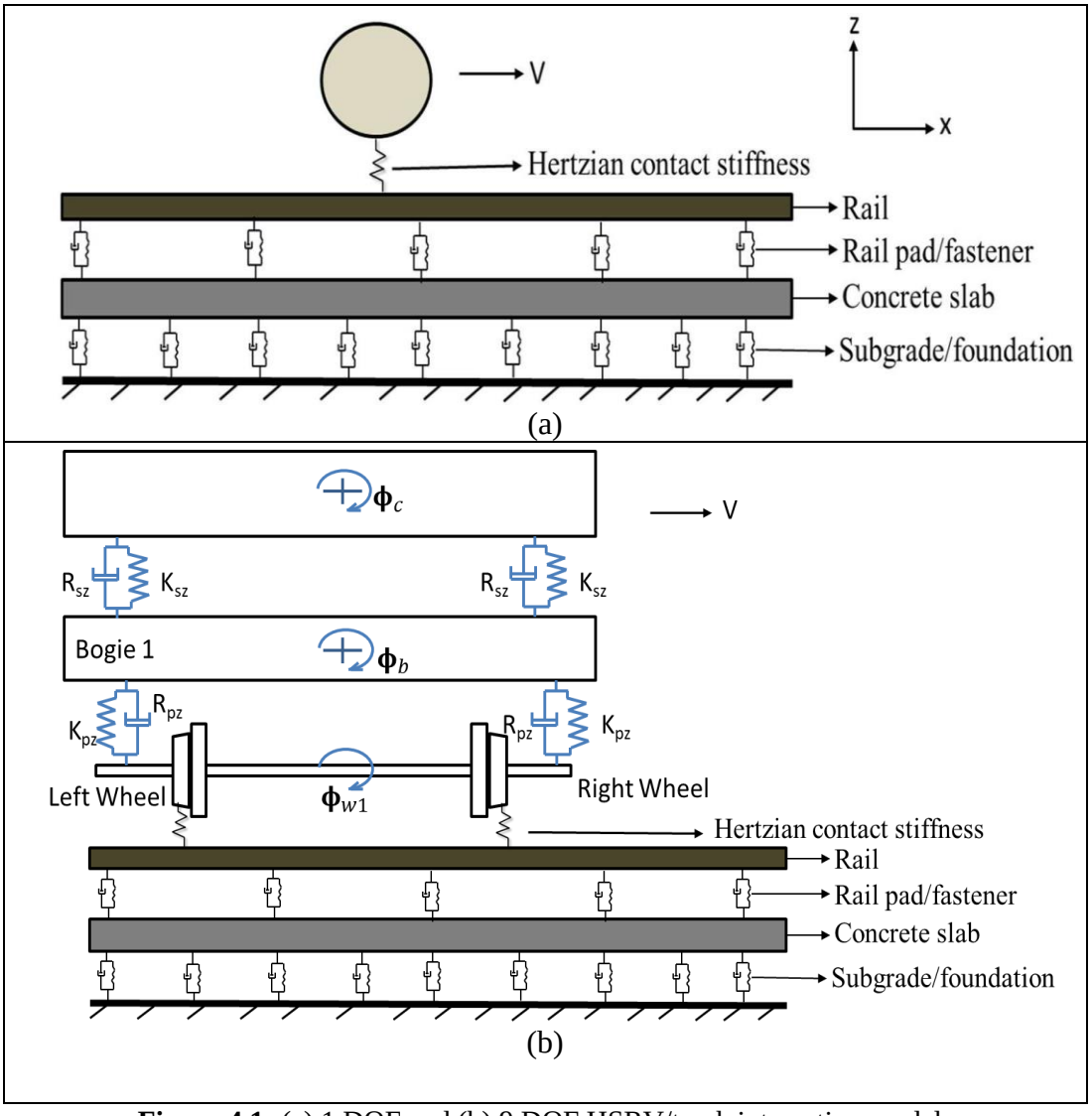

Figure 4.1: (a) 1 DOF and (b) 9 DOF HSRV/track interaction model

4.2.2 1-DOF of a wheel model

A single DOF bond graph model of the wheel is shown in Figure 4.2. The model was subjected to static load P_0. The elements C and f in the bond graph model represent the

displacement calculation and flow direction, respectively. The bond graph model of a single wheel is termed as the RW sub-model and is utilized to create the integrated model later on.

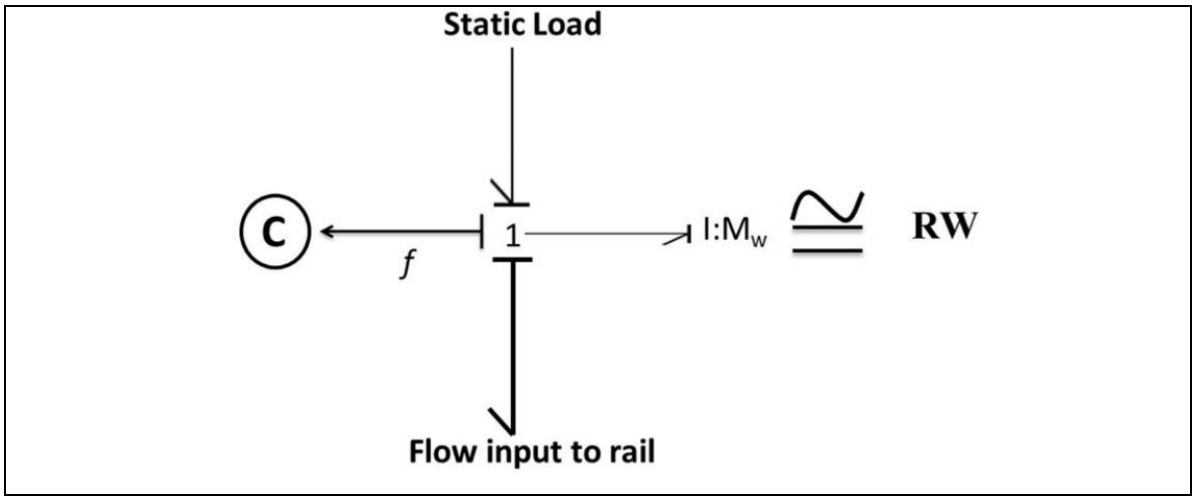

Figure 4.2: Bond graph model of wheel and its sub-model (RW) representation

4.2.3 9-DOF of vehicle model

In Figure 4.3, a realistic representation of a railway vehicle is depicted, featuring 2 wheelsets, a bogie, and a half car body with 9 DOF. The car body is defined with 2 DOF, representing rolling motion and vertical displacement. The bogie is characterized by 3 DOF, encompassing rolling motion, pitching motion, and vertical displacement. Each wheelset is attributed with 2 DOF, representing rolling motion and vertical displacement. The connection between the bogie and the wheelset involves primary suspension elements, while the car body is linked to the bogie through secondary suspension elements.

The elements of the suspension system are represented as an ordered sequence of linear springs and viscous damper. The symbol K_{pz} and C_{pz} represents the spring stiffness and damping coefficient, respectively of the primary suspension system. Likewise, the symbols K_{sz} and C_{sz} represent the spring stiffness and damping coefficient respectively of the secondary suspension system. Displacements of various vehicle components are described

concerning the equilibrium position. Subsequent subsections will provide detailed insights into the bond graph modelling of different railway vehicle components.

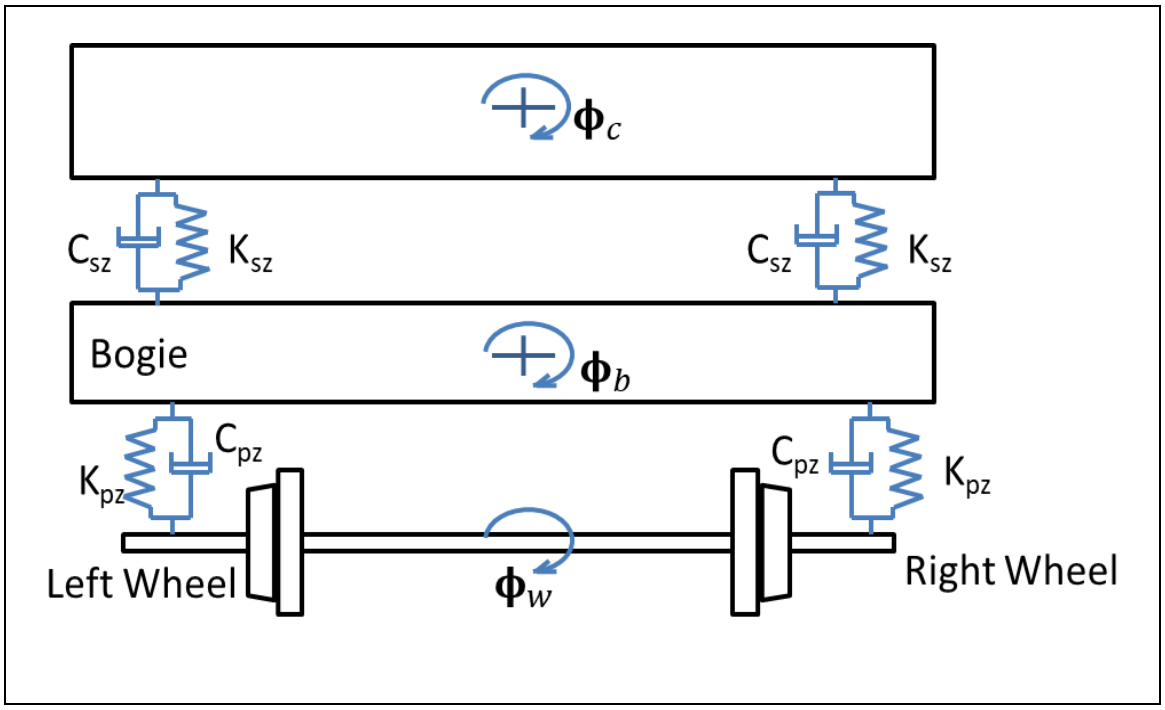

Figure 4.3: Schematic diagram of 9 DOF of HSRV

4.2.3.1 Bond graph model of car body

The car body is considered a lumped mass (M_c) and is connected to the bogie frame through a secondary suspension system, which directly supports it. The car body possesses characteristics defined by the velocity and angular velocity of its centre of mass.

A bond graph model for the car body is established by linking mass and the moment of inertia (I_{cx}) to a 1-junction. The car body's weight (M_{cg}) is applied as an external force and is represented as a Source of Effort element (SE), connected to the 1-junction, specifying the velocity of the car body's centre of mass. It is crucial to accurately impose kinematic constraints for constructing a precise model. Kinematic constraints represent relationships among flow variables, and their correct enforcement involves using 0- and 1-junctions. A transformer is employed to convert angular velocity into a linear velocity component.

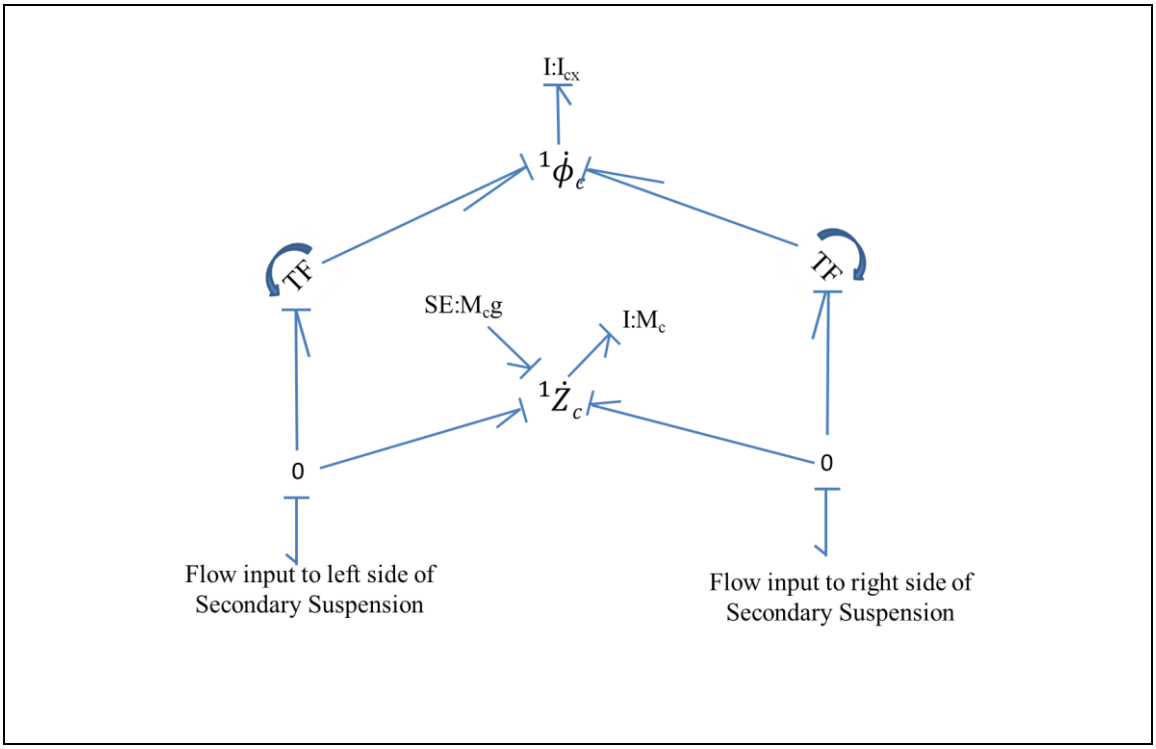

Figure 4.4: Bond graph sub model of a car body **(**CB**)**

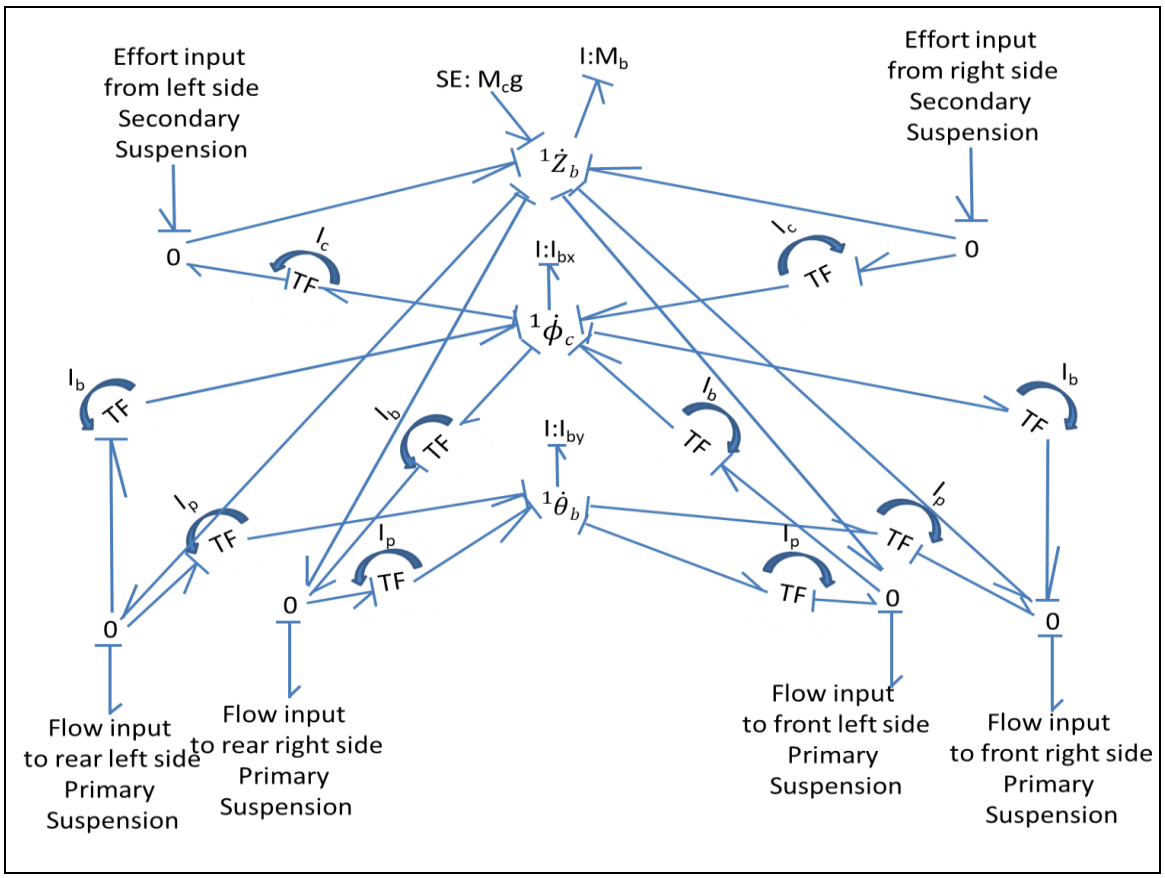

Figure 4.5: Bond graph sub-model of a car body **(**IB**)**

The railway vehicle's bond graph section, illustrated in Figure 4.4, functions as a sub-model representing the car body, identified as CB. The sub-bond graph model of the car body incorporates a 0-junction to enforce the kinematic relations among flow variables outlined in Eqs. (4.1-4.2).

$$\dot{Z}_{cl} = \dot{Z}_c - \dot{\phi}_c l_c \tag{4.1}$$

$$\dot{Z}_{cr} = \dot{Z}_c + \dot{\phi}_c l_c \tag{4.2}$$

Where Z_{cl} and Z_{cr} symbolize the vertical velocities at the points where the left and right secondary suspensions connect to the car body. Z_c denotes the vertical velocity of the centre of mass, while $\boldsymbol{\phi}_C$ represents the angular velocity of the car body.

4.2.3.2 Bond graph model of bogie

The bond graph model of bogie is illustrated in Figure 4.5 and denoted as IB. This model encompasses the vertical, roll, and pitch motion of the bogie. The gravitational force is incorporated into the bond graph using the SE element. Additionally, elements representing the mass (M_b) and moments of inertia (I_{bx} and I_{by}) are connected to the corresponding 1-junctions, representing the velocity of the centre of mass and the angular velocity of the bogie.

The movement of the centre of mass and the angular velocities of the bogie play a vital role in the vertical component of the velocity, as indicated by the right-hand side of Eqs. (4.3-4.8), and this is depicted by the 0-junction.

$$\dot{Z}_{bl} = \dot{Z}_b - \dot{\phi}_b l_c \tag{4.3}$$

$$\dot{Z}_{br} = \dot{Z}_b + \dot{\phi}_b l_c \tag{4.4}$$

$$\dot{Z}_{brl} = \dot{Z}_b - \dot{\phi}_b l_b - \dot{\theta}_b l_p \tag{4.5}$$

$$\dot{Z}_{brr} = \dot{Z}_b + \dot{\phi}_b l_b - \dot{\theta}_b l_p \tag{4.6}$$

$$\dot{Z}_{bfl} = \dot{Z}_b - \dot{\phi}_b l_b + \dot{\theta}_b l_p \tag{4.7}$$

$$\dot{Z}_{bfr} = \dot{Z}_b + \dot{\phi}_b l_b + \dot{\theta}_b l_p \tag{4.8}$$

Where, Z_{bl} and Z_{br} depict the vertical velocity observed at the locations where the left and right secondary suspensions link to a bogie, correspondingly. Likewise, Z_{brl} and Z_{brr} indicate the vertical velocity at the positions where the rear left and right primary suspensions attach to the bogie, respectively. Furthermore, Z_{bfl} and Z_{bfr} represent the vertical velocity at the points where the front left and right primary suspensions connect to a bogie, respectively.

4.2.3.3 Bond graph model of a wheelset

A wheelset refers to the assembly of a wheel and axle in a railway vehicle. The addition of angular motion contributions to the vertical velocity of the left and right contact points is accomplished using Eqs. (4.9-4.10). The bond graph of the wheelset is depicted in Figure 4.6 and is denoted as RW. Similarly, models for other wheelsets are also developed.

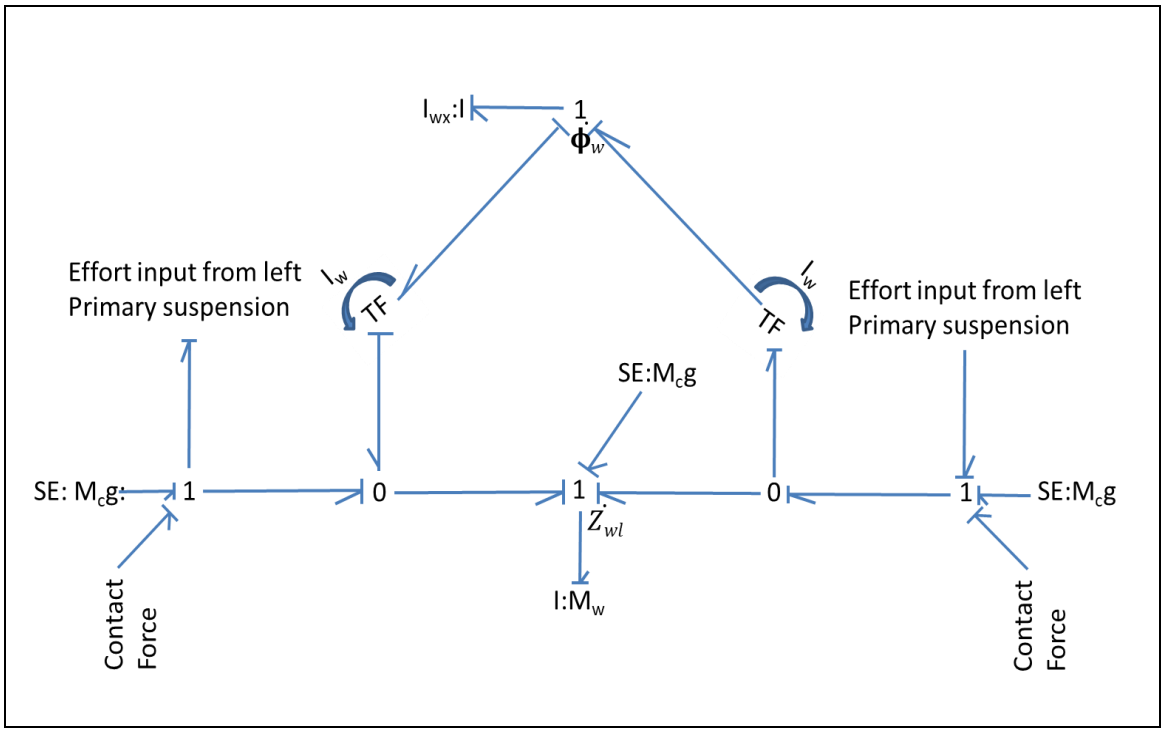

Figure 4.6: Bond graph model of a wheelset **(**IW**)**

$$\dot{Z}_{wl} = \dot{Z}_w - \dot{\phi}_w l_w \quad (4.9)$$

$$\dot{Z}_{wr} = \dot{Z}_w + \dot{\phi}_w l_w \quad (4.10)$$

where, $\dot{Z}_{wl}$ and $\dot{Z}_{wr}$ are vertical velocity components of the left and right wheels connected to the primary suspension.

4.2.3.4 Complete 9 DOF vehicle bond graph model

The complete bond graph representation of the railway vehicle system with nine degrees of freedom (DOF) is formulated through the amalgamation of previously discussed sub-models, encompassing the car body (CB), bogie (IB), and wheelset (RW). The detailed depiction of this integrated model can be found in Figure 4.7, identified as HSRV.

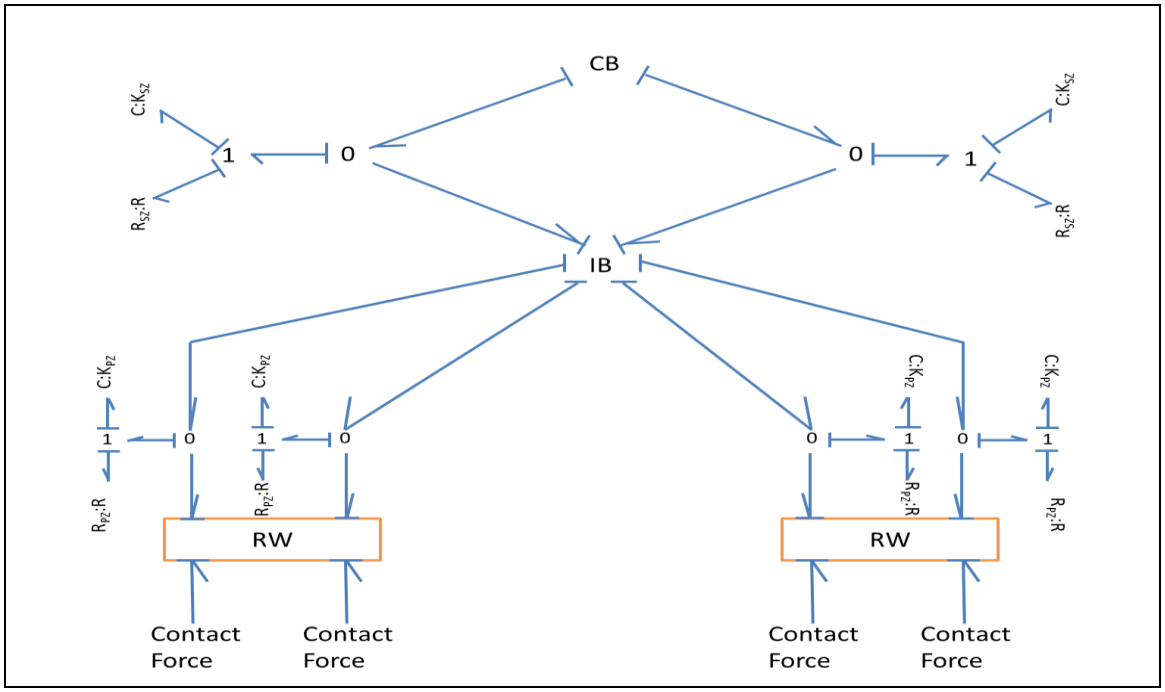

Figure 4.7: Integrated bond graph model of 9 DOF HSRV

4.3 Track Structure Model

4.3.1 Ballasted track

The railway track constitutes a structure composed of parallel lines of rails equipped with fasteners, pads, sleepers (ties), ballast, sub-ballast, and the subgrade. The primary objective

of the railway track is to safely and economically guide trains along its path. For purposes of analysis, the track is considered symmetric relative to its centerline. Notably, the model of the track system is simplified to characterize its dynamic motions exclusively in the vertical plane. The detailed bond graph modelling of the ballasted track structure is discussed in Chapter 3 in subheading 3.2.2.

4.3.2 High speed slab track

A high-speed railway track structure consists of rail, rail pad/fasteners, concrete slab, and foundation. The present study considers a two-layer beam: rail and concrete slab. Twelve rail pads and fasteners are utilized to interconnect both the beams, which are shown by the spring and damper element and the concrete slab is being held in brief by the foundation. The rail pads are placed equidistant to each other by a distance of 0.65 m. The mathematical expression and bond graph modelling of slab track are discussed in detail in chapter 3 under subheading 3.2.3.

4.3.3 Wheel irregularity

The presence of irregularities on the wheel/rail interface induces sharp peak responses in the vehicle-rail system. Some irregularities lead to periodic excitation, while others cause non-periodic or localized excitation. Examples of periodic irregularities encompass rail corrugations, out-of-round wheels or wheel flats, while non-periodic irregularities include indentations on the railhead, welded joint defects, and dipped joints. Periodic irregularities are mathematically represented by cosine functions.

A prevalent irregularity encountered in railway vehicles is the wheel flat. As vehicles may operate with wheel flats before replacement, it becomes imperative to investigate their impact on both vehicle and track components. Wheel flats generate abnormally high forces in the track and vehicle components. Depending on the geometry and size of the flat, these

forces can surpass the static load several times, potentially leading to fatigue cracks, permanent failure, or even vehicle derailment.

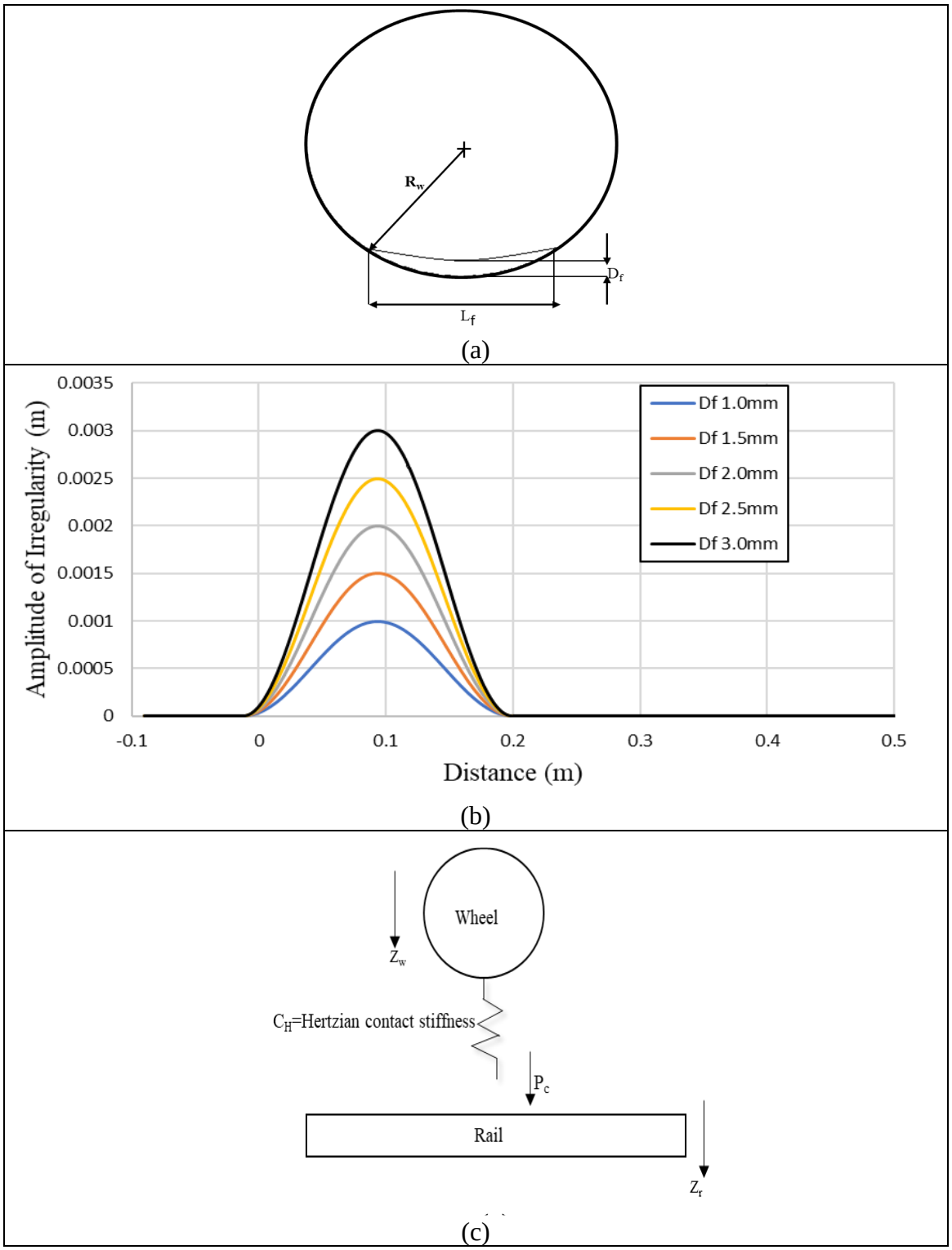

Figure 4.8: (a) Irregularity in the wheel (b) Variation of amplitude of irregularity (c) Wheel-rail interface

Table 4.1: Type of wheel irregularities

Severity	Amplitude (mm)
smooth	0.05
moderate	2
severe	4

Severe wheel flats pose a serious threat to vehicle safety, while smaller ones contribute to track deterioration, consequently increasing maintenance costs. Beyond safety and maintenance concerns, wheel flats also result in reduced passenger comfort. The issue of elevated wheel/rail impact force due to the presence of wheel flats becomes a significant threat for railway industries, especially at increased speeds. Therefore, a quantitative definition of impact load and dynamic stresses is crucial for predicting the safe and effective operation of railway vehicles.

In this research work, a sinusoidal form of wheel irregularity has been considered and expressed in terms of amplitude and wavelength incorporated in the wheel shown in Figure 4.8(a) given by Eqs. 4.11 [10, 24, 136, 147]. Variations of the amplitude of irregularity have been shown in Figure 4.8(b).

$$Z_{irr} = \frac{1}{2} D_f \left[1 - cos\left(2\pi x_f / L_f\right)\right] \tag{4.11}$$

The variables in the given context are defined as follows: L_f represents the length of the irregularity, x_f denotes the longitudinal coordinate of the contact point within the irregularity, and D_f indicates the amplitude of the irregularity. Wheel irregularities with a wavelength of 150 mm, ranging from smooth to severe types, are employed to investigate their impact on the occurrence of the jumping wheel phenomenon. The amplitudes of these wheel irregularities at various severity levels are detailed in Table 4.1 [148]. In this study, the amplitude/depth of the irregularities varies from 0.5mm to 3mm (with a step of 0.5mm),

while keeping the length of the irregularity constant. The parameters for the high-speed wheel-track system can be found in Table 4.2.

Table 4.2: Parameters of the wheel-track mode [149]

S.No.	Parameter	Symbol	Values
1	Amplitude of irregularity	D_f	1.0, 1.5, 2.0, 2.5, 3.0 mm
2	Static Load	P_0	77 kN
3	Flexural rigidity of rail	EI_r	6.625 x 10^6 Nm^2
4	Wavelength of irregularity	L_f	150mm
5	Rail mass per unit length	M_r	60.64 kg/m
6	Instant wheel flat made contacts with rail	t_{flat}	0.001 s
7	Velocity of railway vehicle	v	55, 70, 90 m/s
8	Stiffness of the foundation layer	$K_{foundation}$	60 x 10^6 N/m
9	Damping coefficient of foundation layer	$R_{foundation}$	90 x 10^3 N.s/m
10	Flexural rigidity of slab	EI_{slab}	33.356x10^6 Nm^2
11	Area of cross-section of slab	A_{slab}	0.255m^2
12	Density of slab	ρ	2500 kg/m^3
13	Stiffness of rail pad	K_{pad}	60 x 10^6 N/m
14	Damping coefficient of rail pad	R_{pad}	47.7 x 10^3 N.s/m

4.4 Vehicle track interaction

According to Hertzian contact theory [134–139, 150–152] the relationship between contact force and rail wheel deflection is represented as:

$$P_c = K_h(\Delta Z(t))^{\frac{3}{2}} \tag{4.12}$$

where K_h signifies the Hertzian stiffness and its value given by Johnson [153]. The term $\Delta Z(t)$ represents the wheel-rail overlap, the value of which is determined by the vertical wheel motion Z_w with reference to the contact point on the rail Z_r. If a wheel defect is present on the wheel, its geometry should be considered along with the relative motion

between the wheel and the rail (Figure 4.8(c)) for determining the wheel-rail overlap by using the following Eq. 4.13 [154]

$$\Delta Z(t) = Z_w - Z_{r-}Z_{irr} \tag{4.13}$$

In the situation, when the contact between the wheel and rail disappears *i.e.*

$$\Delta Z \leqslant 0 \tag{4.14}$$

4.5 Simulations study

In this work, the conjugated train wheel-slab track dynamic model is employed to investigate the dynamic behaviour of a high-speed train at different running speeds along with varying sizes of irregularities on the wheel. The simulator (SYMBOL SONATA) [111] used a total number of 1024 steps for the processing of the module with the order of error being 5.0 x 10^{-4}. The simulation was carried out for 11ms. Also, for solving a differential equation, a numerical iterative method, known as the Runge-Kutta method of 5^{th} order, is used. First, the effect of variation of the amplitude of irregularity on the dynamic induced contact force is estimated by varying the amplitude from 0.5 mm to 3 mm. The speed of the wheel is also varied from 180 km/h to 398 km/h to compute the effect on the dynamically induced contact forces at the wheel-rail interface.

4.6 Results and Discussions

4.6.1 Model validation

The reliability of the proposed wheel track model is validated by the results of the Fermer and Nielsen [116] field experiment under the low-speed range and SIMPACK simulation results of Wu and Rakheja [107] under the low to high-speed range as shown in Figure 4.9. The simulation results are obtained for the wheel track model by accounting for the same parameter used in the field experiment (static axle load 117.72 kN, wheel flat length, L_f 40 mm) [116] while introducing the sinusoidal irregularities in the wheel. The deviations of

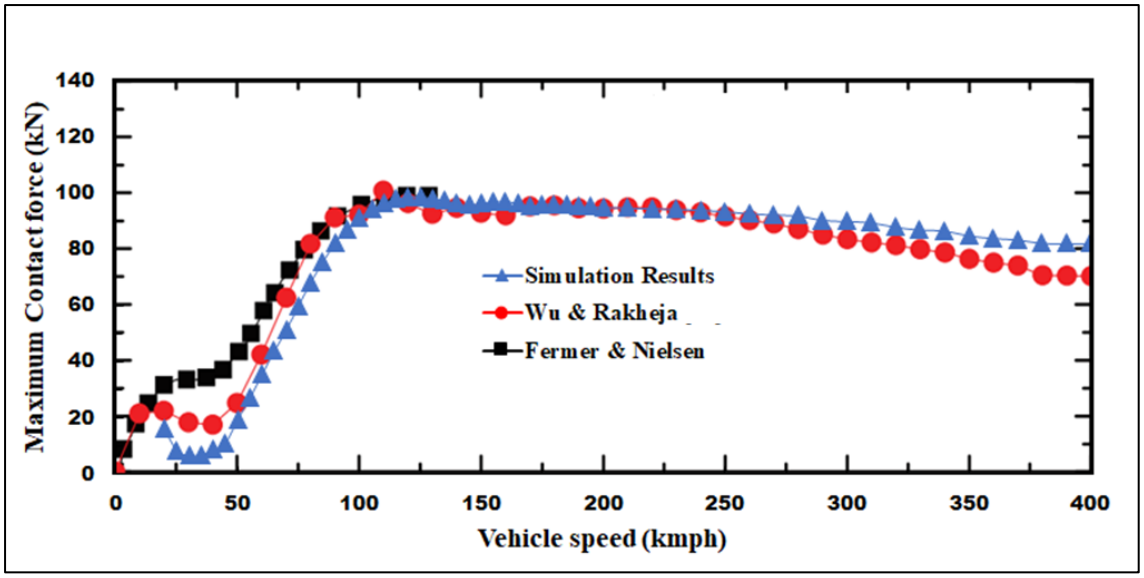

Figure 4.9: Comparison of deviation of maximum contact force with the equivalent static axle load with vehicle speed

maximum wheel-rail contact force from the equivalent static load is evaluated with the testified measured data in the speed range of 0–140 km/h has been compared. It is observed that simulation results match well with predictions by Wu and Rakheja [107] model for the speed range of 10 to 50 km/h, though a massive difference has been observed from the Fermer and Nielsen model [116].

In the speed range of 50 to 140 km/h, the deviation of the peak value of the wheel-rail contact force increases as the vehicle speed goes up to 140 km/h. The simulation results presented here exhibit a strong agreement with both experimental data and SIMPACK analysis within the speed range of 50 km/h to 140 km/h. Both the simulation and experimental observations highlight that the peak saturation force is evident within the speed range of 100–130 km/h. As the train speed exceeds 130 km/h, there appears to be a decrease in the peak contact force. However, SIMPACK simulation results suggest that the peak contact force starts decreasing beyond 120 km/h, while in the current simulation, the peak contact force appears to decrease beyond 135 km/h. This reduction becomes more

rapid beyond 165 km/h, attributed to the rigid wheel-track model utilized in the proposed model, compared to Wu and Rakheja's flexible wheelset model.

The study delves into the impact of different train speeds (ranging from 180 to 378 km/h) on wheel-rail responses, considering a fixed irregularity length of 150 mm and a static axle load of 77 KN. The static axle load acting on the wheel is derived by converting half of the axle load from the gross mass of the car body, bogie frame, and wheel shaft. The section discusses the variations in dynamic responses, encompassing contact force, wheel acceleration, and wheel-rail overlap at the wheel-rail junction. Additionally, the study observes the variations in velocity responses in both the rail and slab structure. The amplitude of irregularity varies for case 1, case 2, case 3, case 4, case 5, and case 6 as 0.5mm, 1.0 mm, 1.5 mm, 2.0 mm, 2.5 mm, and 3.0 mm respectively, with a fixed length of irregularity in each case.

4.6.2 Effect of train speed on the vertical dynamic contact force induced at the wheel-rail interface

Figures 4.10 (a), (b), and (c) present the time histories of vertical contact forces induced at

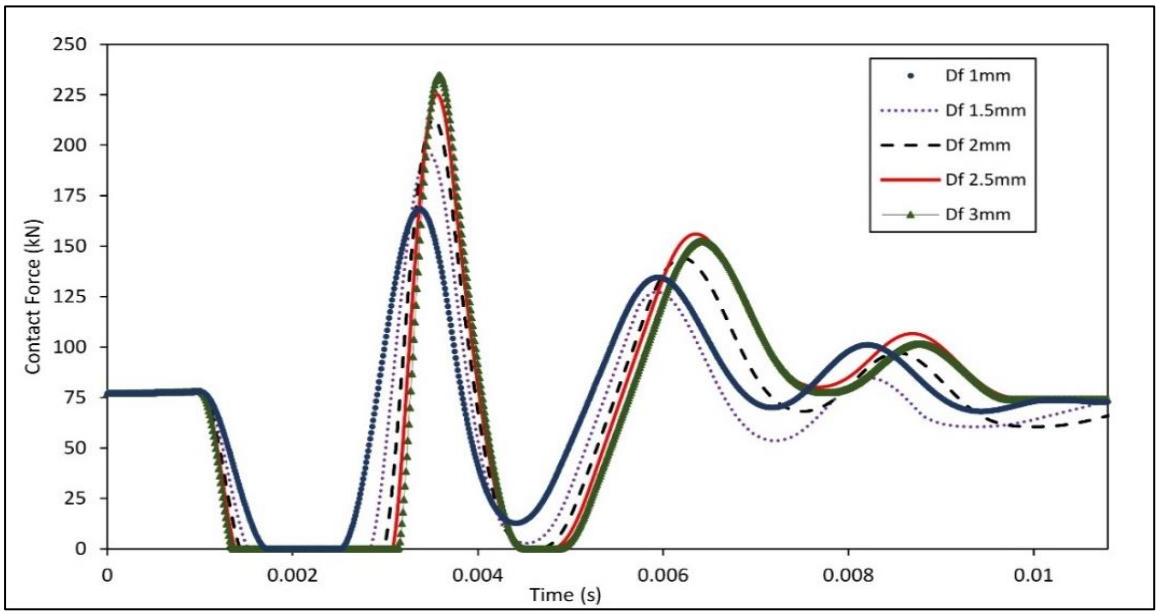

(a)

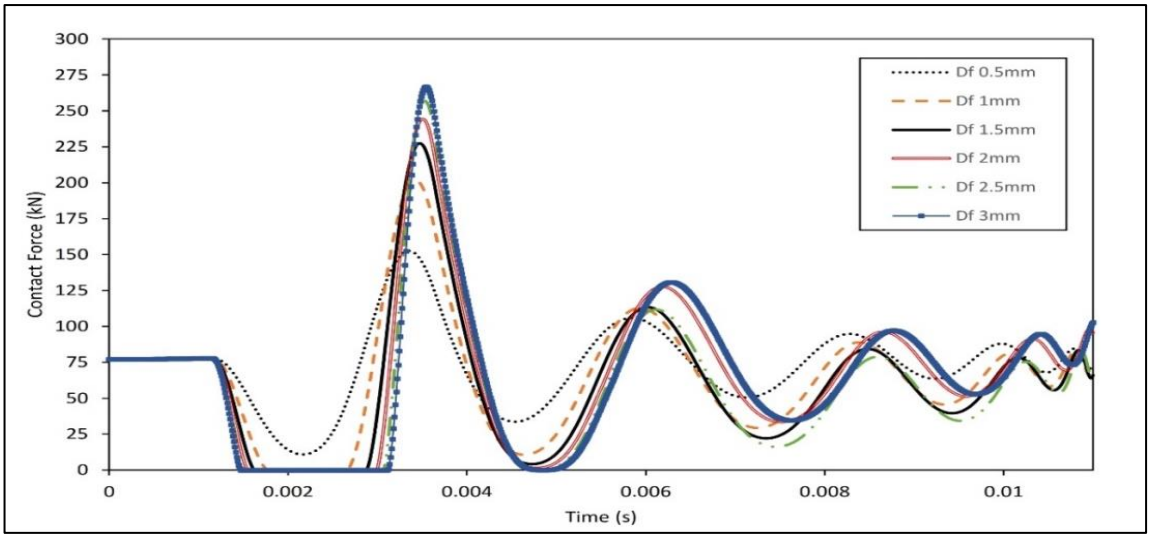

(b)

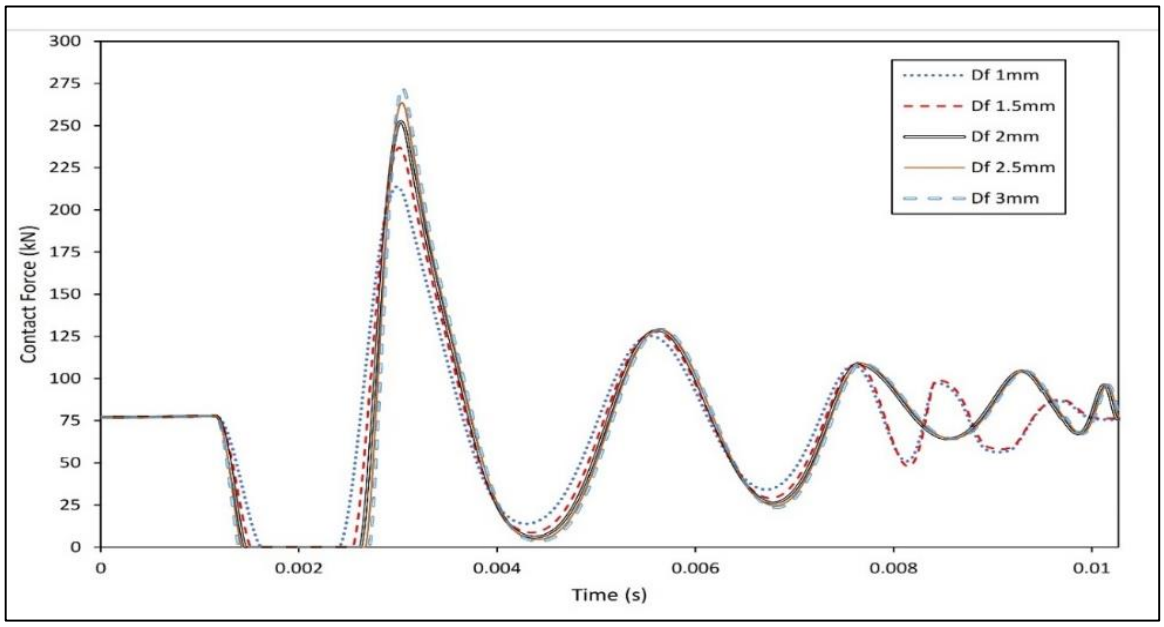

(c)

Figure 4.10: Variation of vertical induced contact force at wheel-rail interface at train speed of (a) 198 km/h (b) 252 km/h (c) 324 km/h

the wheel-rail interface due to wheel irregularities in various cases mentioned above, with wheel speeds of 198, 252, and 324 km/h. The graph illustrates the variation of contact forces over time, depicting a flat line at the simulation's beginning until 0.001 sec, primarily due to the static load acting at the wheel-rail interface. Following this initial period, the trend experiences a sudden dip, attributed to irregularities at the wheel-rail contact point, causing a momentary loss of contact between the rail and wheel.

The static axle load plays a crucial role in maintaining contact between the wheel and rail. Upon the reestablishment of contact, a significant spike in contact force occurs due to the abrupt engagement of the wheel and rail, posing a potential risk of severe damage to the system. Subsequently, the contact forces gradually weaken over simulation time, eventually reducing to the static value of the contact force. This dynamic behaviour underscores the impact of wheel irregularities on the wheel-rail interface and emphasizes the importance of understanding and mitigating the associated risks to ensure the system's integrity and performance.

Figure 4.11(a) displays the variations in peak contact forces in relation to train speed for all cases. Notably, the maximum contact force does not exhibit a consistent increment with the train speed. In the simulation results for case 2, it is observed that impact forces rise from 168 kN to 202 kN for a train speed increase from 198 to 252 km/h, and further from 202 kN to 213 kN for the speed range of 252 m/s to 324 km/h. In case 3, case 4, case 5, and case 6, peak contact force values are recorded as 196 kN, 213 kN, 225 kN, and 234 kN respectively at a train speed of 198 km/h. In the speed range from 180 km/h to 378 km/h, the maximum contact force in case 3, case 4, case 5, and case 6 reaches 236 kN, 252 kN, 264 kN, and 273 kN respectively.

Analyzing the results (by comparing slopes), it is evident that between the speed range of 200 to 250 km/h, there is a rapid increase in maximum contact force. Beyond 250 km/h, the increment becomes more gradual, and after reaching its peak value, the contact force decreases with further increases in wheel speed. The heightened contact force is attributed to the increased momentum at higher speeds. Additionally, at higher speeds, the time of contact between the wheel irregularity and the rail decreases, contributing to the continuous increase in contact force with rising speed. In the range of 200 km/h to 250 km/h, the dominant factor causing increased contact force is the momentum rise, resulting in a faster

pace of increment. However, in the range of 250 km/h to 300 km/h, the influence of momentum weakens due to the reduced time of contact between the wheel irregularity and the rail surface. Consequently, the rate of increase in contact force diminishes at higher speeds, aligning with similar observations in the work of Wu and Rakheja [107].

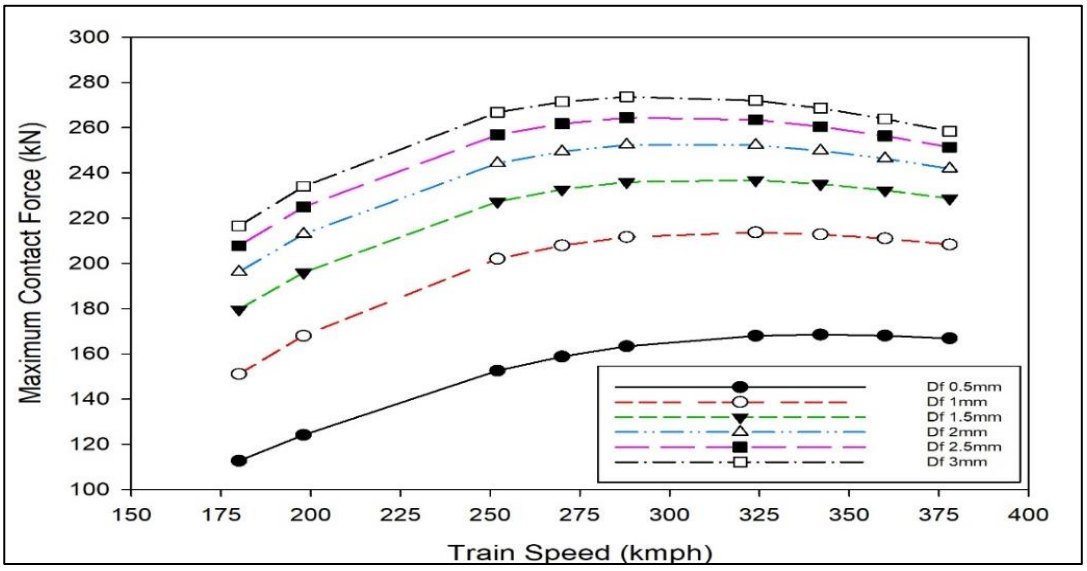

(a)

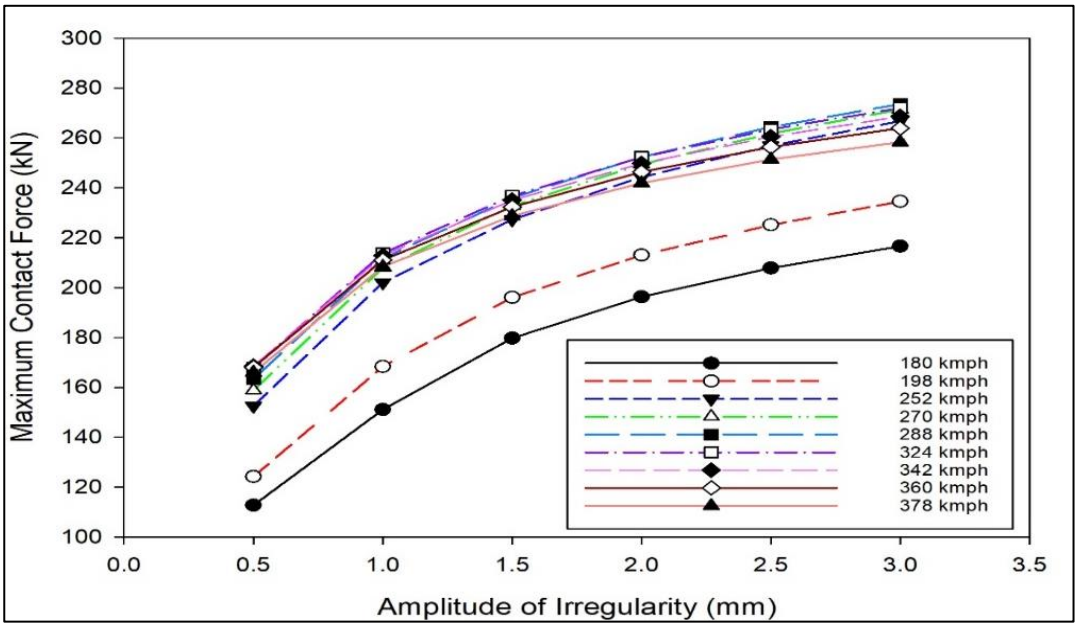

(b)

Figure 4.11: (a) Comparison of maximum contact force as a function of train speed (b) Maximum contact force as a function of amplitude of irregularity

To explore the impact of irregularity amplitude on the maximum induced contact force, six irregularity types with varying amplitudes are examined. Upon comparing the slopes, it is

noted that the maximum contact force experiences a rapid increase when transitioning from a smooth type to a moderate type (i.e., D_f changes from 0.5 mm to 2 mm). Conversely, the increase is more gradual when transitioning from a moderate to a severe type (i.e., D_f changes from 2.5 mm to 3 mm), as indicated in Figure 4.11(b).

The analysis above leads to the inference that the dynamically induced contact forces at the wheel-rail interface, resulting from irregularities in the wheel profile, exhibit a significantly higher maximum value compared to the static axle load. A quantitative relationship is being established between the dynamically induced contact force (F_d), average static axle load (F_s), and wheel irregularities, expressed in terms of the dynamic amplification factor (DAF) [134]. DAF is defined as.

$$DAF = \frac{F_{d,with\ or\ without\ irregularity}}{F_s} \tag{4.15}$$

Upon examining all the cases, it is observed that Dynamic amplification Factors (DAFs) exhibit variations ranging from 1.96 to 3.55 within the speed range of 180 to 398 km/h. Increasing the dynamic amplification factor (D_f) or the static axle load will lead to further increases in DAFs. Elevated values of DAFs have the potential to induce a significant frequency of vibration in the wheel and track system. Hence, it is imperative to undertake regular maintenance of the track structure to ensure its proper functioning.

4.6.3 Influence of amplitude of irregularity in wheel acceleration

Due to the elevated induced contact force at the wheel-rail interface, a notably large acceleration response is observed in the wheel. The evaluation of acceleration response considers amplitudes of 1mm and 3mm irregularities within a speed range of 198 km/h to 324 km/h. At a wheel speed of 198 km/h, the maximum acceleration value increases from

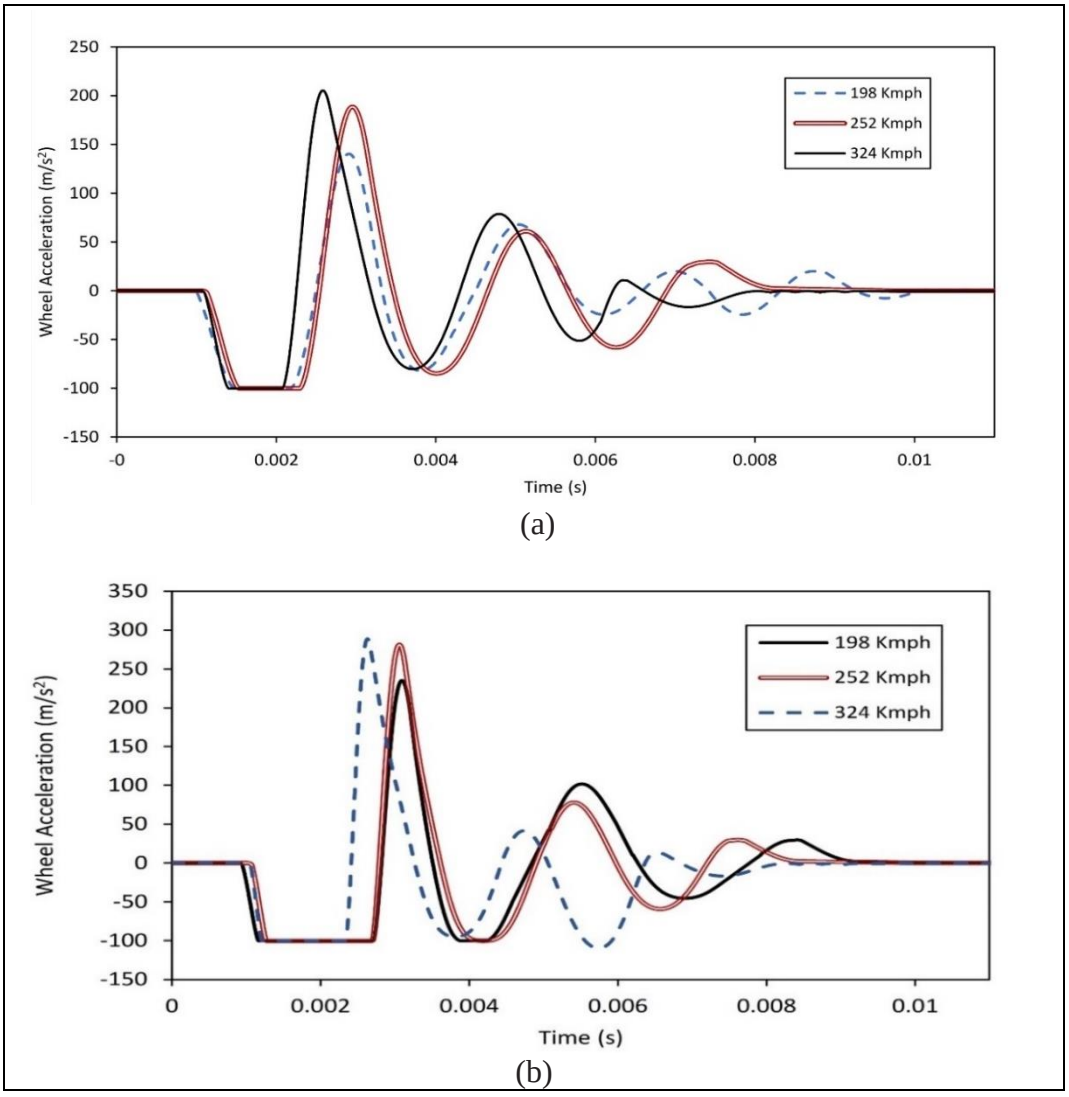

Figure 4.12: Variations of vertical acceleration response of wheel at different wheel speeds at amplitude of irregularity (a) 1 mm (b) 3 mm.

140.269 m/s² to 234.99 m/s² as the irregularity amplitude goes from 1mm to 3mm. Subsequently, at speeds of 252 km/h and 324 km/h, the peak acceleration values rise from 188.469 m/s² to 281 m/s² and from 205.199 m/s² to 288.454 m/s², respectively, with an increase in irregularity amplitude from 1mm to 3 mm. The variation of wheel acceleration response with time history is illustrated in Figures 4.12(a) and (b).

The contact force experiences a rapid increase when transitioning from a smooth irregularity type to a moderate irregularity type, as depicted in Figure 4.11(b). This elevated contact force results in significant vertical motion, recorded as an acceleration response.

According to the findings of this study, the acceleration response exhibits a substantial 81.46% increase as the magnitude of the irregularity (D_f) changes from 0.5 mm to 1 mm. Moreover, the acceleration response sees a further increase of 45.936% and 15.194% as the irregularity type progresses from smooth to moderate and from moderate to severe, respectively, at a speed of 198 km/h.

As the train accelerates from medium to high speed, the wheel's acceleration response undergoes successive increments of 60.64%, 32.13%, and 12.194% with changes in D_f from 0.5 mm to 1 mm, 1 mm to 2 mm, and 2 mm to 3 mm, respectively, at a speed of 252 km/h. The results reveal a continuous rise in acceleration response with increasing speed. Notably, the percentage of increment is more pronounced in smooth and moderate irregularity types compared to severe irregularity at a constant train speed. A similar trend is observed at a train speed of 324 km/h, where the acceleration response increases by 46.67%, 26.31%, and 11.03% for changes in irregularity amplitude in the smooth region, from smooth to moderate type, and from moderate to severe type, respectively.

4.6.4 Displacement at the wheel-rail interface or wheel-rail overlap

The analysis focused on studying the displacement response at the wheel-rail interface within a speed range of 198 km/h to 324 km/h, considering irregular amplitudes ranging from 1.5 mm to 3 mm. The displacement at the wheel-rail interface represents the net vertical displacement of the contact point between the wheel and rail, commonly referred to as wheel-rail overlap.

The plotted data reveals that the maximum value of wheel-rail overlap is 2.3 mm. Specifically, it varies within the range of 0.610 mm to 0.905 mm and 2.04 mm to 2.3 mm at irregularity amplitudes of 1.5 mm and 3 mm, respectively, at the mentioned wheel speed.

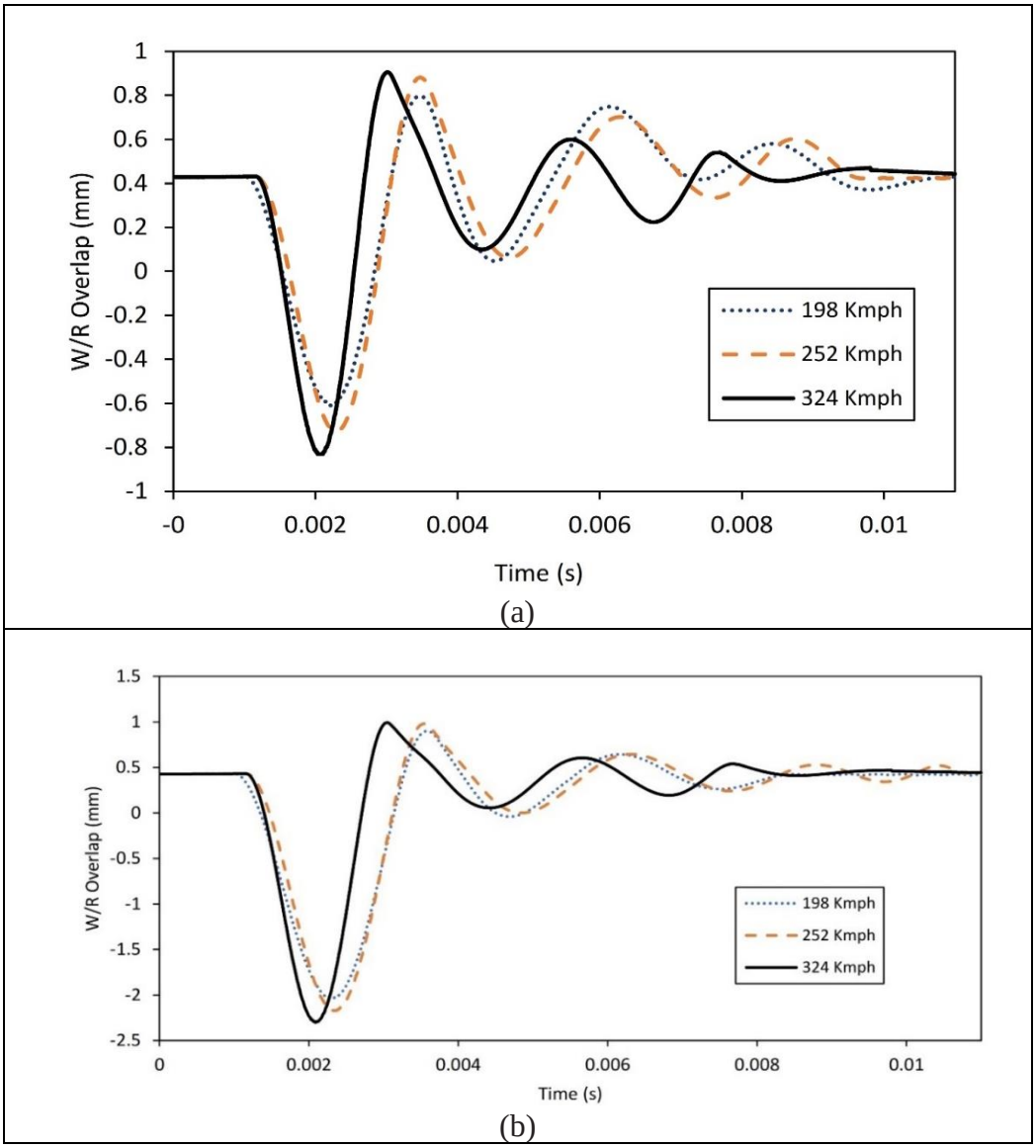

Figure 4.13: Wheel rail overlap response in the speed range of 198 km/h to 324 km/h at the amplitude of the irregularity of (a) 1.5mm (b) 3mm

Time history plots illustrating the wheel-rail overlap response are presented in Figures 4.13 (a) and (b).

4.6.5 Velocity response in rail and concrete slab

Velocity responses in the rail beam (RB) and concrete slab (CRC) are computed in the proximity of 0.65 m, where wheel irregularities impact the rail surface, across six different cases as mentioned earlier. The variation of velocity response in RB and CRC, at a speed

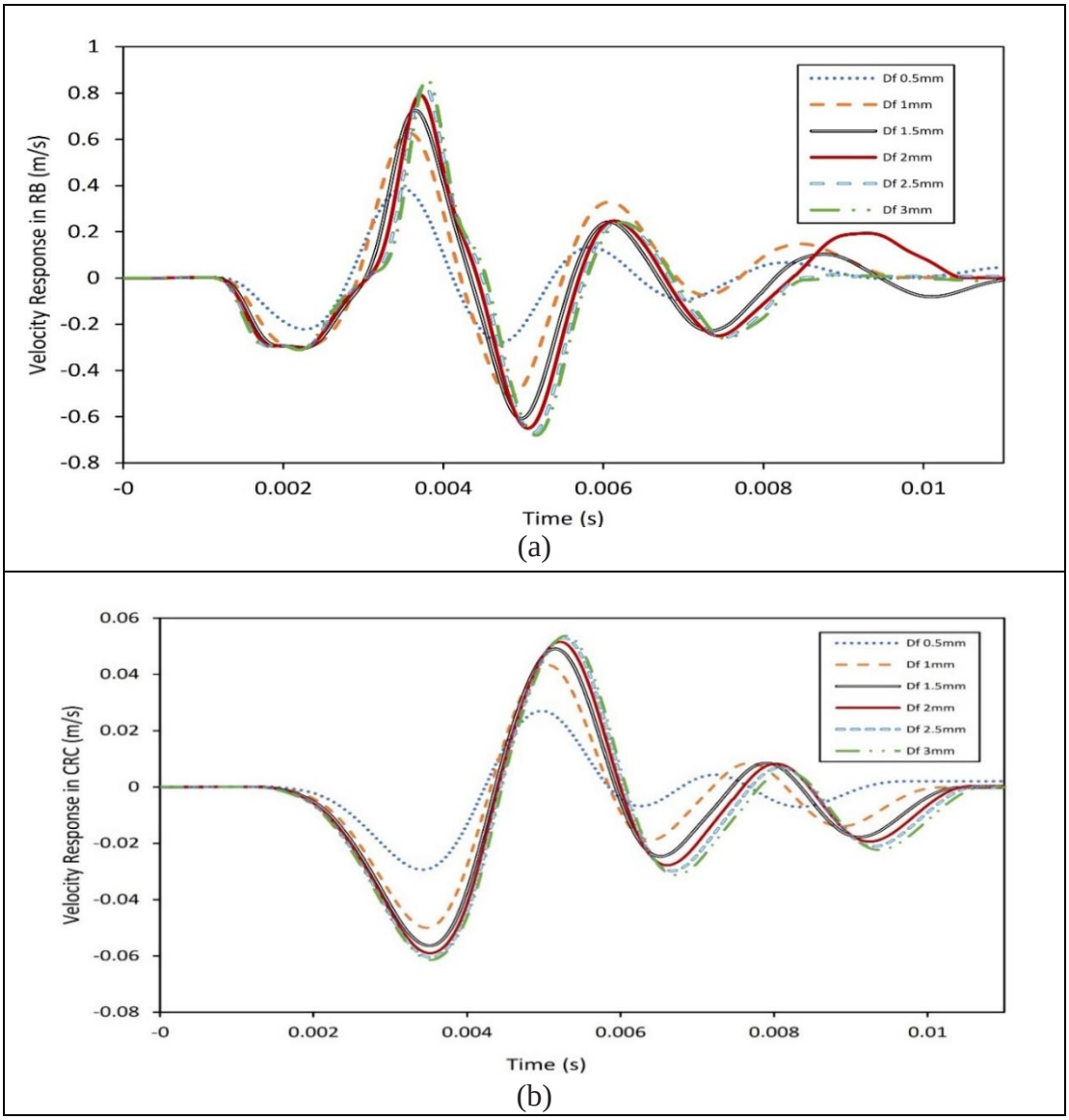

Figure 4.14: Velocity response obtained at speed 198km/h at various D_f in (a) rail (RB) and (b) concrete slab (CRC)

of 198 km/h in the time domain, is depicted in Figure 4.14(a) and (b) respectively.

As the irregularity changes from a smooth to a severe type (with D_f ranging from 0.5 mm to 3.0 mm), the amplitude of velocity responses fluctuates between 0.859 m/s to -0.75 m/s in RB and 0.0536 to -0.06 m/s in CRC at a train speed of 198 km/h. The graph illustrates that velocity responses increase with the augmentation of D_f at a fixed irregularity length and constant train speed, both in RB and CRC. It is evident from the graph that the velocity responses experience a more pronounced increment in the transition region from smooth to moderate type irregularity. This is attributed to the sharp increase in

the maximum contact force induced at the wheel-rail interface when the irregularity type shifts from smooth to moderate.

The velocity responses on the rail exhibit an increase with the train speed, reaching a maximum in the speed range of 260 to 275 km/h. Subsequently, the velocity starts gradually decreasing with further increases in speed, as indicated by the graph in Figure 4.15(a). The amplitude of velocity responses in the right-of-way barrier (RB) varies between 0.9899 m/s and -1.09 m/s, spanning from medium speed to high speed (180 km/h to 378 km/h) and with a change in the severity of irregularity from smooth to severe (0.5 mm to 3 mm), as illustrated in the findings.

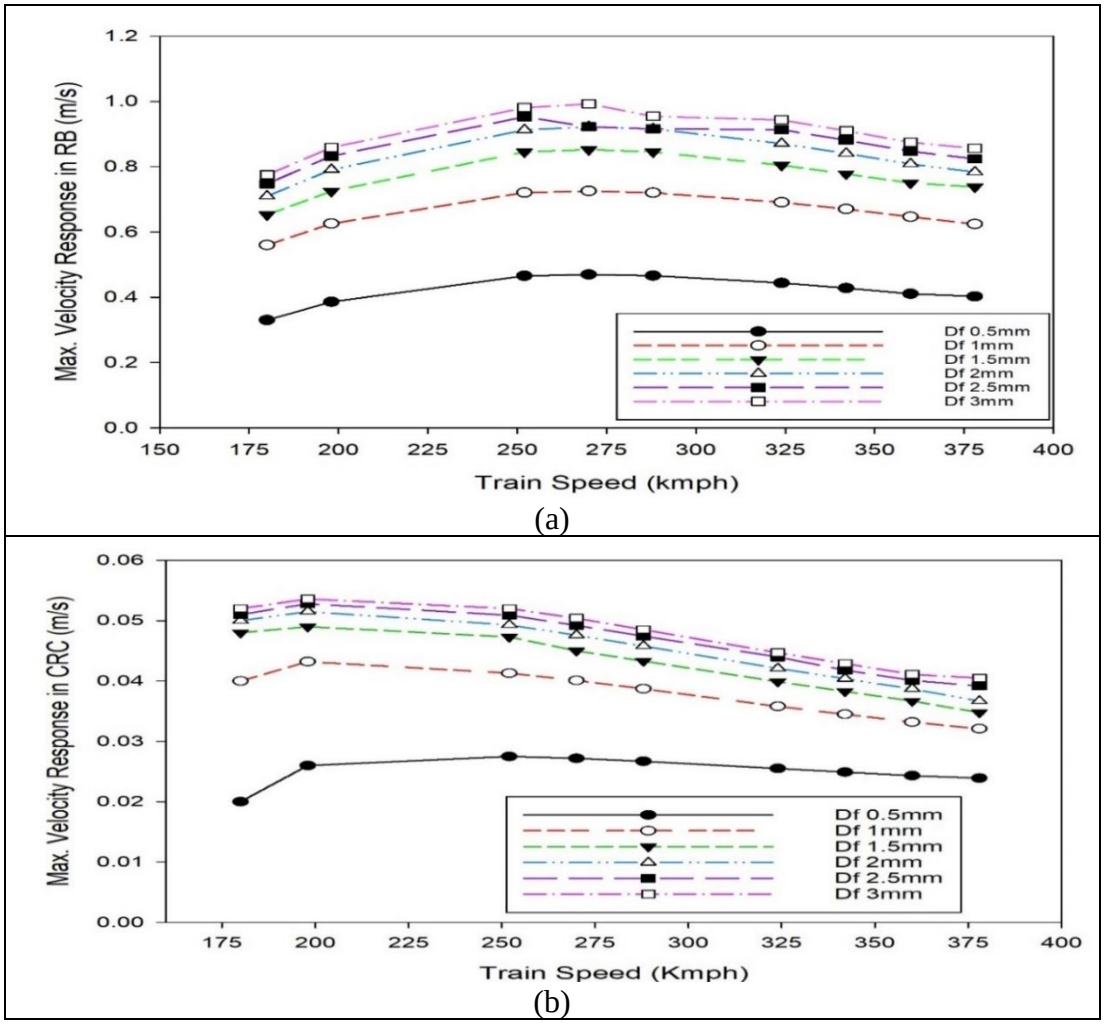

Figure 4.15: Variation of maximum velocity response with train speed at different D_f in (a) RB, (b) Concrete Slab (CRC)

An intriguing observation from Figure 4.15(b) reveals that, for every scenario, the maximum velocity response in the concrete slab structure (CRC) occurs at a speed of 198 km/h. With further increases in speed, the velocity responses start to decrease, although the rate of decrement is minimal. Notably, the maximum velocity response in CRC increases when the irregularity type changes from smooth to severe, all at the same train speed. The velocity responses experience rapid attenuation when transitioning from the rail surface to the concrete slab structure. Additionally, the response values are smaller at higher speeds compared to lower speeds due to the elastic and damping properties of the concrete slab structure and its distance from the point where the irregularity impacts the rail surface. This phenomenon is attributed to the swift passage of the portion of irregularity on the wheel at high train speeds, resulting in a lesser impact force on the velocity response in the concrete slab structure.

4.6.6 Comparison of impact forces at the wheel-rail interface for slab track and ballasted track

In this section, a simulation study of 9 DOF HSRV model, running over slab track and ballasted track, has been presented. Wheel irregularity has been present in the leading wheelset.

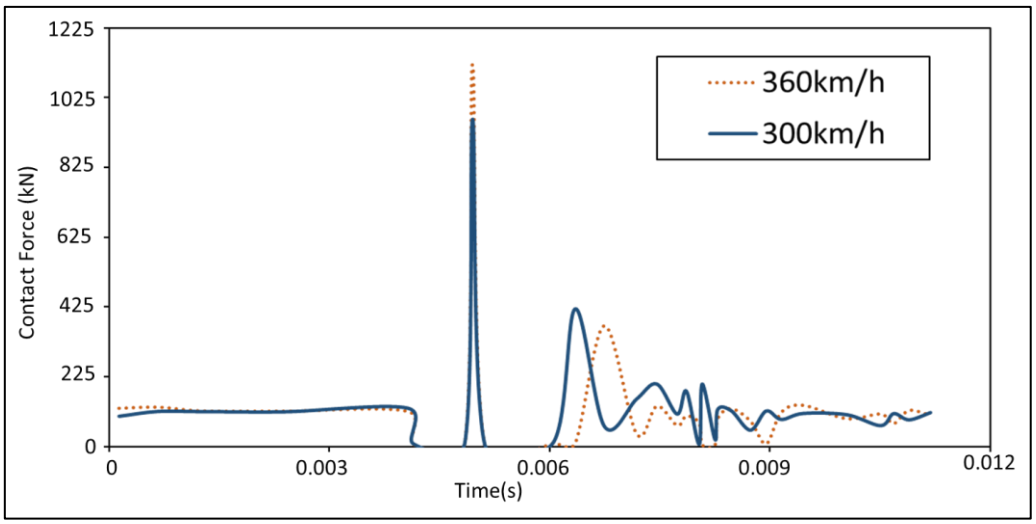

Figure 4.16: Variation of contact force with speed on the slab track

Figure 4.16 shows the variation of contact force at the wheel rail interface when a 9 DOF railway vehicle model moves on the slab track for different speeds.

The plot indicates that when wheel irregularities reach the wheel-rail interface, the induced forces at the interface reduce to zero due to momentary loss of wheel-rail contact. Over time, the wheel again came in contact with the rail, generating impact forces with a magnitude approximately 8 times greater than the static axle load at a vehicle speed of 300 km/h. Following sudden contact with the rail, the wheel experiences bouncing and subsequently loses contact, a phenomenon known as wheel jumping. The plot illustrates that the second peak of the impact force, reaching a magnitude 2 to 3 times larger than the static axle load, is visible. Subsequently, the contact forces gradually weaken over simulation time, eventually reducing to the static value of the contact force. Additionally, it is observed from the plot that the impact forces at the wheel-rail interface increase with the vehicle's speed.

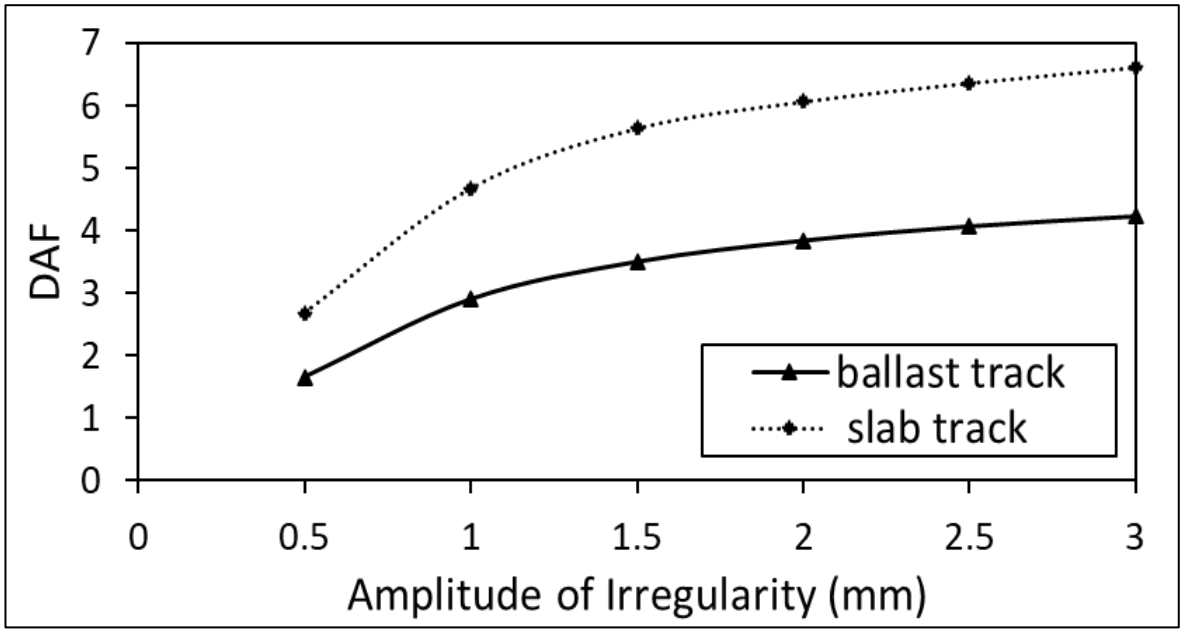

Figure 4.17: Comparison of dynamic amplification factor (DAF) For ballasted track and slab track

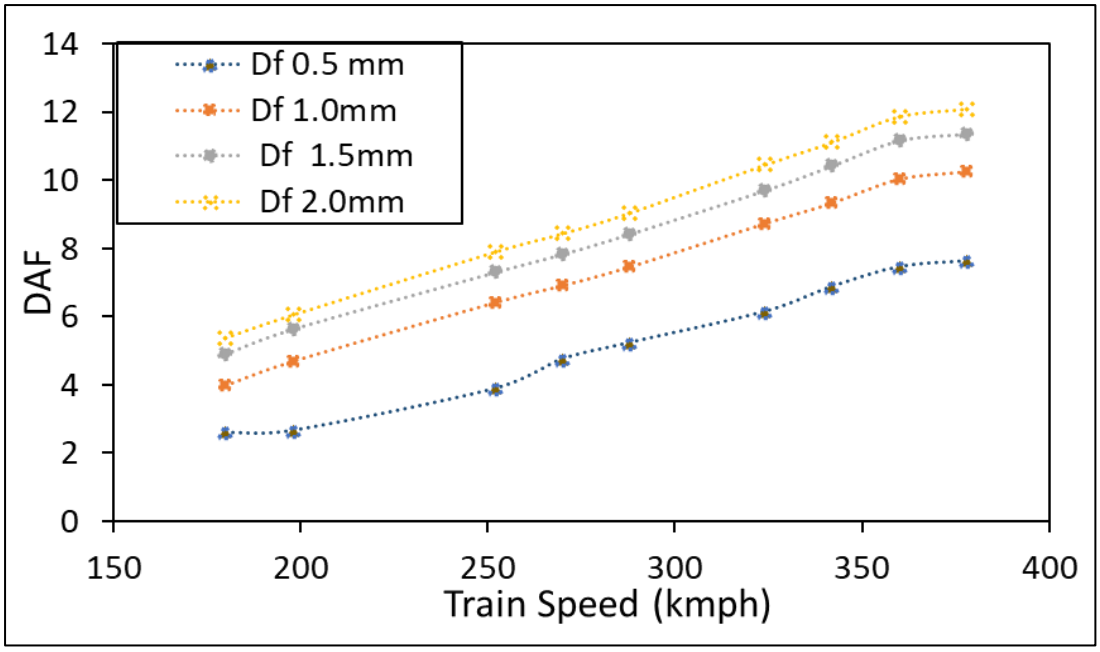

Figure 4.18: Variation of DAF with train speed amplitude of irregularity at different D_f

In Figure 4.17, a comparison is presented for the dynamic amplification factor (DAF) concerning the amplitude of irregularity for a High-Speed Railway Vehicle (HSRV) moving on both ballasted track and slab track. The observation reveals that when the vehicle is on a slab track, the DAF is 2 to 3 times greater than that when the vehicle is on a ballasted track, attributed to the effective damping ability of ballast that mitigates vibrations.

Figure 4.18 illustrates the variation of DAF with the vehicle's speed when the HSRV is moving on a slab track. The graph depicts an increase in DAF with the rise in the amplitude of irregularity. Notably, there is a sudden increment in DAF as the vehicle speed increases from 198 km/h to 250 km/h, followed by a gradual increment in DAF within the speed range of 250 to 300 km/h. Beyond 300 km/h, the DAF rapidly increases with higher speeds.

4.7 Summary

In conclusion, this study employed a conjugated train wheel-slab track dynamic model to investigate the dynamic behaviour of a high-speed train under various running speeds and

irregularity sizes on the wheel. The analysis explored the impact of different train speeds (180 to 378 km/h) on wheel-rail responses, considering fixed irregularity length and static axle load. Results indicated a peak saturation force in the speed range of 100–130 km/h, followed by a decrease in peak contact force beyond 135 km/h. The wheel-rail overlap, induced contact force, and acceleration response were studied for various irregularity types.

The dynamic amplification factor (DAF) was established, indicating variations from 1.96 to 3.55 within the speed range of 180 to 398 km/h. Higher DAF values could induce significant vibrations in the wheel and track system, emphasizing the need for regular track maintenance. The acceleration response exhibited substantial increases in irregularity amplitude and speed. The wheel-rail overlap varied within the range of 0.610 mm to 0.905 mm and 2.04 mm to 2.3 mm for irregularity amplitudes of 1.5 mm and 3 mm, respectively.

Velocity responses in the rail beam and concrete slab increased with irregularity amplitude and train speed, with the maximum velocity response occurring at 198 km/h in the concrete slab. A comparison between slab and ballasted tracks revealed higher dynamic amplification factors (DAF) on slab tracks.

In summary, this comprehensive study provides valuable insights into the complex dynamics of high-speed trains, considering irregularities, speed variations, and track types. The findings contribute to enhance the understanding of dynamic behaviour and aid in the development of strategies for maintaining safety and integrity in high-speed rail systems.

CHAPTER 5

Lateral Dynamics Investigation of High-Speed Trains on Irregular Track

This chapter presents a detailed examination of bond graph formulation applied to high-speed railway vehicles to analyze the lateral dynamic, hunting behaviour and derailment analysis of railway vehicles. The investigation encompasses a comprehensive study focused on the lateral dynamics of a 31 DOF HSRV. The chapter begins by elucidating the fundamental principles governing the dynamics of railway vehicles running on a transition track i.e., vehicle moving from a straight track to a curved track. The impact of short-wave track irregularities on the lateral dynamic behaviour of railway vehicles is thoroughly explored. Track irregularities were introduced just before the transition zone. Additionally, the critical velocities are determined through the simulation of the bond graph model, varying the vehicle's running speeds to provide insights into its dynamic response.

5.1 Introduction

Railway vehicles are often subjected to lateral forces due to braking and traction. These forces affect the dynamics of the vehicle in a complex manner. Thus, the study of railway dynamics as a function of the lateral force is important to avoid hunting and derailment. Being one of the largest modes of transportation, there is a continuous demand for improvements to avoid accidents. Moreover, most of the accidents take place due to irregularities present on the track, which are mainly responsible for the unstable behaviour of the vehicle leading to the derailment. Therefore, from a safety and comfort point of view

effect of irregularities on lateral dynamics of the system needs to be investigated thoroughly to avoid such accidents.

In this research, we examine the roll angle of wheelsets during the development of a 31 DOF model. This approach allows for a precise assessment of the derailment quotient. The model is generated using the bond graph simulation technique, offering the advantage of inherently incorporating suspension forces as suspension elements in the model. Specifically designed for analyzing the derailment behaviour of a high-speed railway vehicle, the 31 DOF model takes into account pitch motion, lateral, vertical, yaw, and roll motion for the vehicle body and two bogies. However, while investigating the derailment quotient, only pitch motion is excluded, while all other motions are considered for the four identical wheelsets. The Derailment quotient was investigated under the condition when the railway vehicle was running on the curved track with speeds varying from 150 km/h to 600 km/h. This 31 DOF model uses the heuristic nonlinear creep model to evaluate the derailment quotient while considering both nonlinear creep forces and moments. This study helps to get the complete behaviour of a high-speed railway vehicle running on a curved track. The benefits of using the presented model are that it can provide accurate values of derailment quotient, and safe speed of vehicle running on the curved tracks.

5.1.1 Concept of Creep

The most important factor in the modelling of the wheel-rail interaction problem is the creep phenomenon. Creep may be defined as a combination of elastic and frictional behaviour of an elastic body that rolls over the surface of another elastic body. Consider a wheelset in motion along a rail, wherein both the wheel and the rail undergo elastic deformation, causing a departure from the ideal rolling motion. These departures are referred to as creepages. Creep, or creepage, is a dimensionless term, except for spin

creepage which is characterized by the deviation of the actual rolling state from pure rolling combined with sliding.

When a wheelset traverses the rails, creepage is specified in both the longitudinal and lateral directions relative to the common normal at the contact patch (spin). The creepages are defined mathematically in terms of velocity difference and are given by Eqs. (5.1-5.3).

$$\xi_x = \frac{v_x - v_x^*}{v_x^*} \tag{5.1}$$

$$\xi_y = \frac{v_y - v_y^*}{v_x^*} \tag{5.2}$$

$$\xi_{sp} = \frac{\omega_w - \omega_r}{v_x^*} \tag{5.3}$$

where, ξ_x , ξ_y and ξ_{sp} represent the longitudinal, lateral, and spin creepages, respectively. It is crucial to emphasize that the longitudinal and lateral creepages lack dimensions, while the spin creepage is dimensioned as L^{-1}. These creepages give rise to creep forces and moments. The equations describing the creep forces (moment) at the contact surface can be found in Eq. (5.4) [4].

$$Creep\ force\ (moment) = Creep\ coefficient\ \times Creepages \tag{5.4}$$

The longitudinal creep force generally acts in the wheelset's forward direction of motion and lateral creep force acts perpendicularly to it in the lateral creep direction, whereas spin creep moment acts in the normal load direction, orthogonal to the creep force components and hence to the plane of contact region.

5.1.2 Critical speed and hunting

The behaviour of railway vehicles is primarily influenced by lateral motion, commonly known as hunting. Vehicle stability during operation, or hunting, is linked to the presence of conically shaped wheels. These wheels offer lateral guidance or centering, compelling the wheels to stay within the tread region when the wheelset deviates laterally from the

centre. The friction or creep forces between the wheel and rail are dependent on the speed of the vehicle. As the speed increases, there's a threshold where the vehicle rail system experiences zero effective damping, leading to a sustained periodic oscillation known as hunting. The speed at which this phenomenon occurs is termed the critical speed. A rail-wheel system is deemed stable around the equilibrium position if its motion, triggered by a small initial disturbance, does not amplify over time [155].

5.1.3 Concept of derailment

The derailment of a railway vehicle is a significant concern for many researchers, as it is directly influenced by the dynamic behaviour of the vehicle during its running operations. To assess operational safety, researchers often calculate and observe a quotient known as the Derailment Quotient (DQ). This quotient is determined by the ratio of lateral and vertical forces acting between the wheels and rails.

The Derailment Quotient (DQ) serves as a critical indicator, with a limiting value of 0.8 when the wheel flange makes contact with the face of a rail [156]. Additionally, during quasi-static testing, the maximum permissible limit of DQ is set at 1.2 [157]. Monitoring and assessing the Derailment Quotient plays a crucial role in ensuring the safety and stability of railway vehicles during their operational activities.

The wheel unloading rate serves as a crucial metric in assessing the potential risk of derailment due to a significant decrease in wheel loads. This parameter provides valuable insights into the dynamic behaviour of railway vehicles and plays a vital role in ensuring their safety and stability during operation [56]. When a wheel unloading rate is calculated, it essentially measures the rate at which the load on a wheel diminishes. This reduction in wheel load may occur under various conditions, such as during braking, acceleration, or dynamic events. Excessive or rapid unloading of the wheels can lead to a range of issues,

including compromised traction, increased lateral forces, and a heightened risk of derailment.

5.2 Modelling of Lateral Dynamics of 31 DOF Railway Vehicle Running on Curved Track

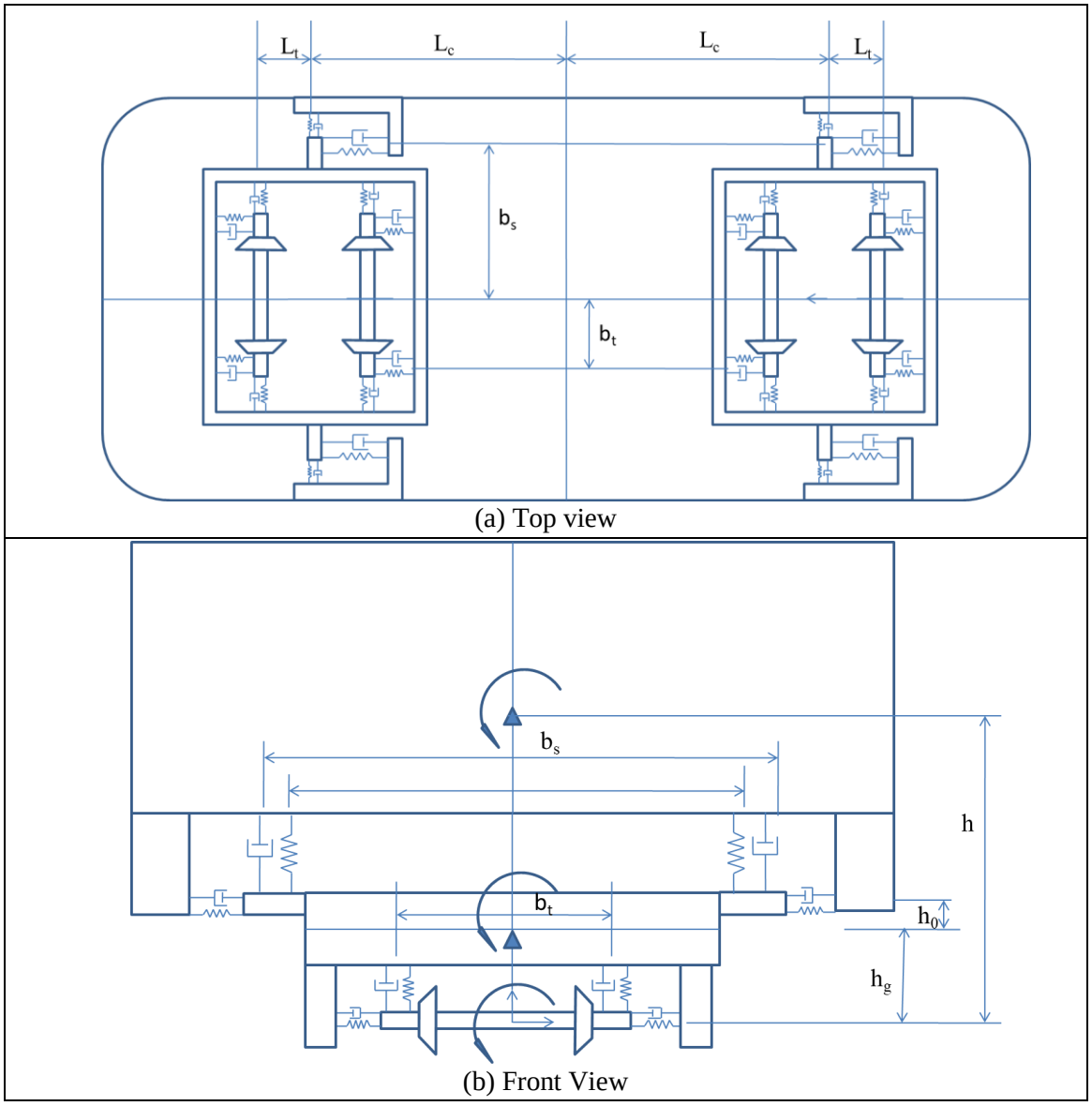

Figure 5.1: Schematic diagram of a high-speed railway vehicle (a) top view (b) front view

A railway vehicle is an integration of various subparts; a vehicle car body structure, truck frame and 2-selfsame wheelsets for each truck frame. These parts of a railway vehicle are interconnected through a suspension system in vertical, lateral and longitudinal directions.

A primary suspension system is incorporated between a bogey and 2-selfsame wheelsets whereas a secondary suspension system is incorporated between a bogie and vehicle car body. The comprehensive suspension system is designed by incorporating springs and damping elements capable of motion along all three coordinate axes. With consideration for all potential movements, the envisioned system exhibits a total of 31 DOF. The model is constructed using the Building Block approach, wherein each component is individually modelled before being seamlessly integrated to form the complete system. Figure 5.1 illustrates the railway vehicle model.

5.2.1 Bond graph modelling of a car body sub-system

The bond graph model exhibited in Figure 5.2, is the sub-model of a vehicle car body of a railway vehicle system. A 0-junction in the model is the joint between the parts connected to each other and represents the force shared between them. The 1-junction in the model represents the velocity shared between all the connected parts at the 1-junction. The TF symbol represents the Transformer module. It represents the relation between flow in-flow out and force in-force out. The symbol C with a complete arrow represents the signal bond. The primary role of the "C" symbol involves the retention of potential energy resulting from specific displacements. Within the bond graph, the symbol "SE" denotes the origin of effort. Positioned at the 1-junction of the bond graph, it serves to amalgamate the gravitational force and centrifugal force exerted by the car body's centre of gravity along the vertical (z) and lateral (y) axes. In the Bond graph modelling technique, the force of the suspension system is the interior part of the model and hence there is no need to represent suspension forces separately in a bond graph model.

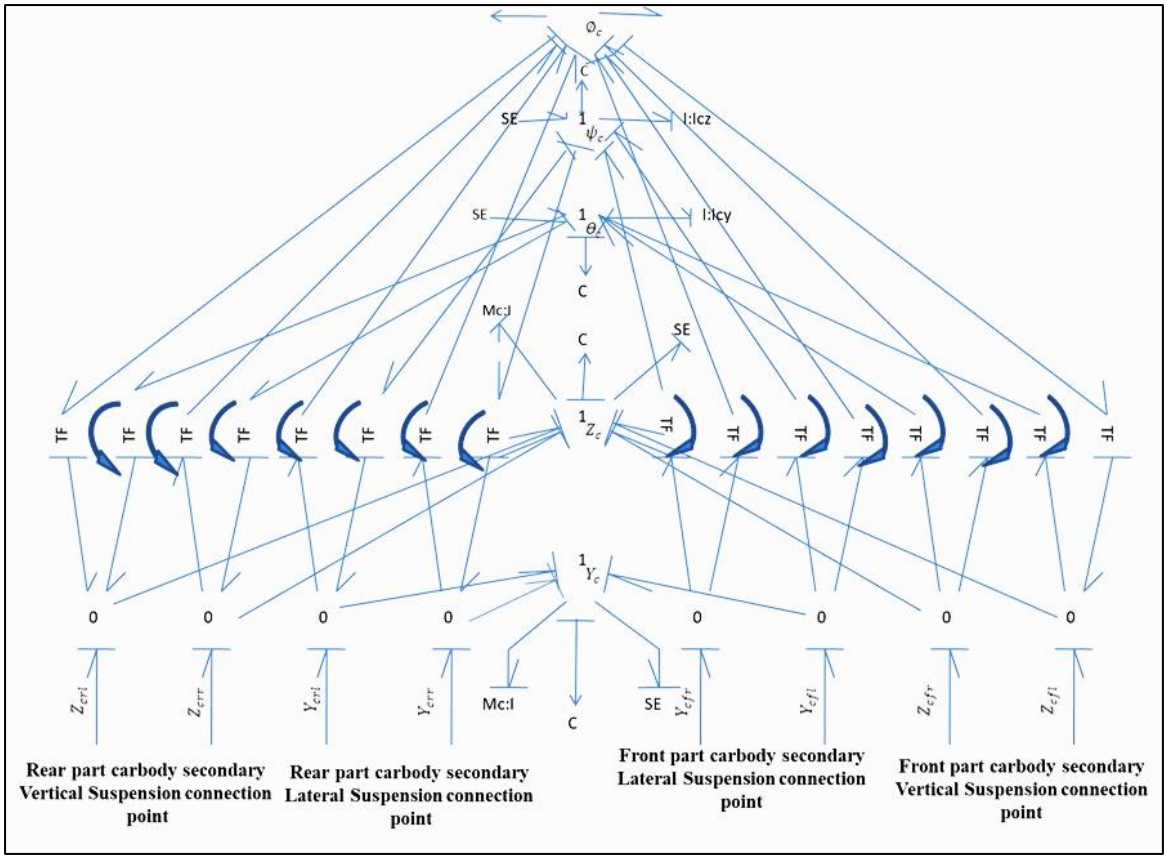

Figure 5.2: Bond graph model of Carbody

The vehicle car body is considered a rigid element. It is linked with the bogie via secondary suspension system at different locations. A kinematic connection is established between the centre of mass and the rotational velocity component to articulate the speeds at various positions on the body of a vehicle. These kinematic relations are expressed in Eqs. (5.5-5.12).

$$\dot{Z}_{cfl} = \dot{Z}_c + l_c\dot{\phi}_c + l_s\dot{\theta}_c \tag{5.5}$$

$$\dot{Y}_{cfl} = \dot{Y}_c + H_1\dot{\phi}_c + l_s\dot{\theta}_c \tag{5.6}$$

$$\dot{Z}_{cfr} = \dot{Z}_c + l_c\dot{\phi}_c - l_s\dot{\theta}_c \tag{5.7}$$

$$\dot{Y}_{cfr} = \dot{Y}_c + H_1\dot{\phi}_c + l_s\dot{\theta}_c 5. \tag{5.8}$$

$$\dot{Z}_{crl} = \dot{Z}_c - l_c\dot{\phi}_c - l_s\dot{\theta}_c \tag{5.9}$$

$$\dot{Y}_{crl} = \dot{Y}_c + H_1\dot{\phi}_c - l_s\dot{\theta}_c \tag{5.10}$$

$$\dot{Z}_{crr} = \dot{Z}_c + l_c\dot{\phi}_c - l_s\dot{\theta}_c \tag{5.11}$$

$$\dot{Y}_{crr} = \dot{Y}_c + H_1\dot{\phi}_c - l_s\dot{\theta}_c \quad (5.12)$$

$$m_c\ddot{z}_c = F_{sfcz} - m_c g - \frac{m_c V^2 \phi_{se}}{R_r} \quad (5.13)$$

$$m_c\ddot{y}_c = F_{sfcy} + \frac{m_c V^2}{R_r} - m_c g\phi_{se} \quad (5.14)$$

$$I_{cz}\ddot{\Psi}_c = M_{scz} \quad (5.15)$$

$$I_{cy}\ddot{\theta}_c = M_{scy} \quad (5.16)$$

$$I_{cx}\ddot{\phi}_c = M_{scx} \quad (5.17)$$

Where φ_{se} is the angle of super elevation, R_r is a curved radius. F_{sfcz}, F_{sfcy}, M_{scz}, M_{scy}, *and* M_{scx} are the suspension force and moment in the respective direction. Mathematical Eqs. (5.13 to 5.17) are the governing equations of a car body in a differential form. These equations of motion are determined in vertical and lateral directions for roll, yaw and pitch motions.

5.2.2 Bond graph modelling of bogie sub-system

The Bogie serves as an integral component within the railway vehicle system. The truck frame connects to the car body through a secondary suspension system at various points and is also linked to the same wheelsets through a primary suspension system, as illustrated in Figure 5.1. The kinematic relations are shown in Eqs. (5.18 to 5.29) are employed to derive the velocity components in the x, y and z directions at different connected locations. The bond graph model of the bogie is shown in Figure 5.3.

$$\dot{Z}_{bl} = \dot{Z}_b - l_p\dot{\phi}_b \quad (5.18)$$

$$\dot{Y}_{bl} = \dot{Y}_b - h_0\dot{\phi}_b \quad (5.19)$$

$$\dot{Z}_{br} = \dot{Z}_b + l_p\dot{\phi}_b \quad (5.20)$$

$$\dot{Y}_{br} = \dot{Y}_b - h_0\dot{\phi}_b \quad (5.21)$$

$$\dot{Z}_{bfl} = \dot{Z}_b - l_p\dot{\phi}_b + l_t\dot{\theta}_b \quad (5.22)$$

$$\dot{Y}_{bfl} = \dot{Y}_b - h_0\dot{\phi}_b + l_t\dot{\psi}_b \quad (5.23)$$

$$\dot{Z}_{bfr} = \dot{Z}_b + l_p\dot{\phi}_b + l_t\dot{\theta}_b \quad (5.24)$$

$$\dot{Y}_{bfr} = \dot{Y}_b + h_g\dot{\phi}_b + l_t\dot{\psi}_b \tag{5.25}$$

$$\dot{Z}_{brl} = \dot{Z}_b - l_p\dot{\phi}_b - l_t\dot{\theta}_b \tag{5.26}$$

$$\dot{Y}_{brl} = \dot{Y}_b + h_g\dot{\phi}_b - l_t\dot{\psi}_b \tag{5.27}$$

$$\dot{Z}_{brr} = \dot{Z}_b - l_p\dot{\phi}_b + l_t\dot{\theta}_b \tag{5.28}$$

$$\dot{Y}_{brr} = \dot{Y}_b + h_g\dot{\phi}_b - l_t\dot{\psi}_b \tag{5.29}$$

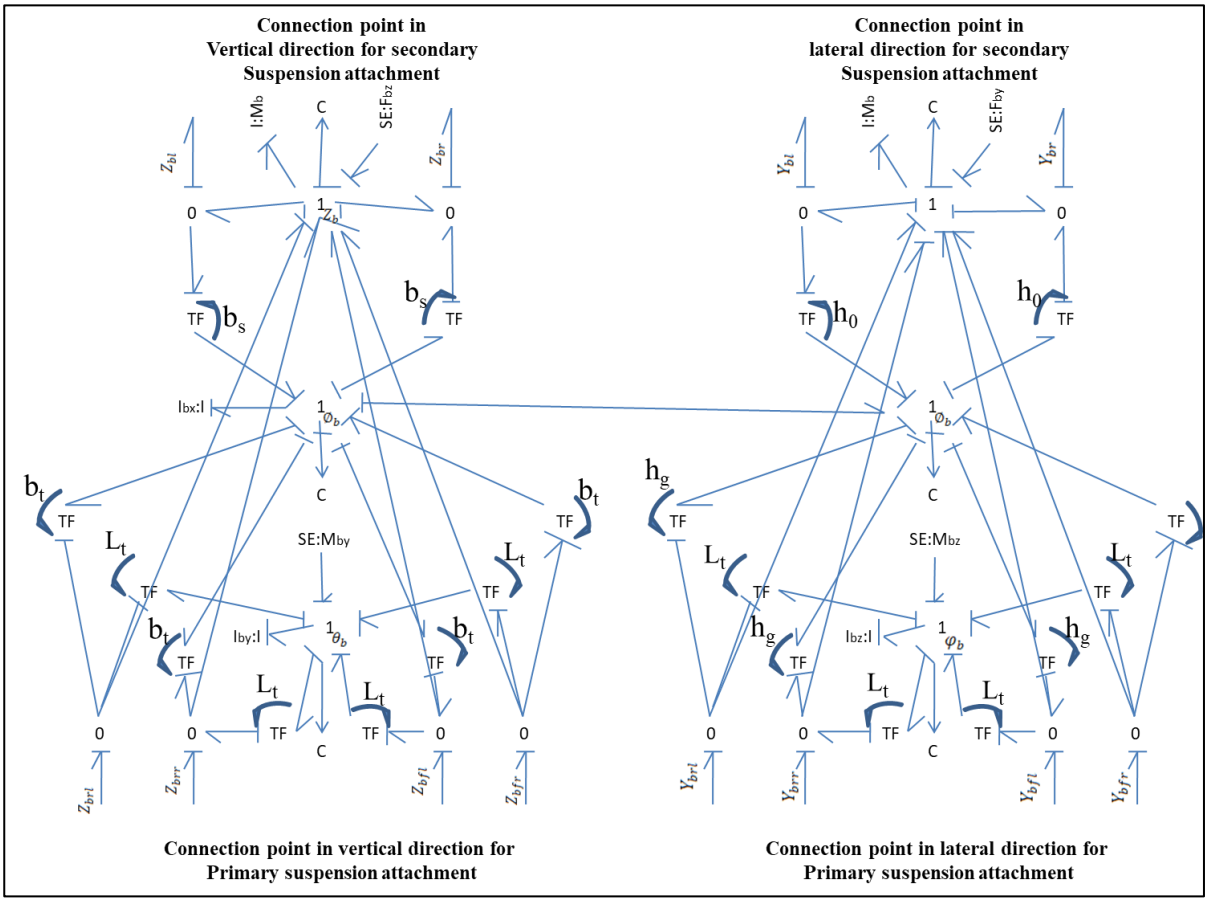

Figure 5.3: Bond graph model of Bogie

Mathematical equation terms mentioned in Eq. (5.30-5.34) are the governing equations of motion of a bogie in a differential form.

$$m_t\ddot{y}_t = F_{sfty} + \frac{m_tV^2}{R_r} - m_tg\Phi_{se} \tag{5.30}$$

$$m_t\ddot{z}_t = F_{sftz} - m_tg - \frac{m_tV^2\Phi_{se}}{R_r} \tag{5.31}$$

$$I_{tz}\ddot{\Psi}_t = M_{stz} \tag{5.32}$$

$$I_{ty}\ddot{\theta}_t = M_{sty} \tag{5.33}$$

$$I_{tx}\ddot{\phi}_t = M_{stx} \tag{5.34}$$

5.2.3 Bond graph modelling of wheelset sub-system

The wheel set is a component of the railway vehicle system which provides support to the complete vehicle. A rigid wheelset in contact with the flexible Knife edged rail is considered for the present research work. The selfsame wheelsets were interconnected to the bogie through a primary suspension system.

5.2.3.1 Kinematic relationship of wheelset

The linkage between the bogie frame and the wheelset comprises two main suspensions. Kinematic relations, grounded in flow variables, delineate the velocity components at these connection points, aligning them in specific directions. To derive the transformer moduli necessary for constructing the bond graph of the wheelset subsystem, the kinematic relations specified in Eqs. (5.35-5.38) is employed. These constraints are incorporated into the bond graph of the wheelset subsystem, illustrated in Figure 5.4, through a 0-junction.

$$\dot{Z}_{wl} = \dot{Z}_w + \dot{\psi}_c l_p \tag{5.35}$$

$$\dot{Y}_{wl} = \dot{Y}_w + l_p \dot{\phi}_c \tag{5.36}$$

$$\dot{Z}_{wr} = \dot{Z}_w + \dot{\psi}_c l_p \tag{5.37}$$

$$\dot{Y}_{wr} = \dot{Y}_w + \dot{\phi}_c \dot{Y}_w \tag{5.38}$$

where, $\dot{Y}_{wl}, \dot{Y}_{wr}$ are lateral and $\dot{Z}_{wl}, \dot{Z}_{wr}$ are vertical components of the velocity of points, where the front left and right suspensions connect with the wheelset respectively. The bondgraph model of the identical wheelset is exhibited in Figure 5.4. Mathematical equation terms mentioned in Eqs. (5.39-5.42) are the governing equations of a wheelset in a differential form.

$$m_w \ddot{y}_w = \frac{m_w V^2}{R_r} - m_w g \Phi_{se} + F^n_{wLy} + F^n_{wRy} + N^L_{wy} + N^R_{wy} + F_{sfwy} - F_{wfc} \tag{5.39}$$

$$I_{wz} \ddot{\Psi}_w = -I_{wy} \frac{V}{R_0} \dot{\Phi}_w + R^R_{x,} F^n_{wRy} - R^R_y F^n_{wRx} + R^L_x F^n_{wLy} - R^L_y F^n_{wLx} + R^R_x N^R_{wy} + R^L_x N^L_{wy} + M^n_{wLz} + M^n_{wRz} + M_{smwz} \tag{5.40}$$

$$m_w\ddot{z}_w = -\frac{m_w V^2 \Phi_{se}}{R_r} - m_w g + F^n_{wLz} + F^n_{wLz} + N^L_{wz} + N^R_{wz} + F_{sfwz} \tag{5.41}$$

$$I_{wx}\ddot{\Phi}_w = -\frac{I_{wy}V\left(\frac{V}{R_r} - \dot{\Psi}_w\right)}{R_0} + R^R_y F^n_{wRz} - R^R_z F^n_{wRy} + R^L_y F^n_{wLz} - R^L_z F^n_{wLy} + R^L_y N^L_{wz} + R^R_y N^R_{wz} - R^L_z N^L_{wy} - R^R_z N^R_{wy} + M^L_{wx} + M^R_{wx} + M_{smwx} \tag{5.42}$$

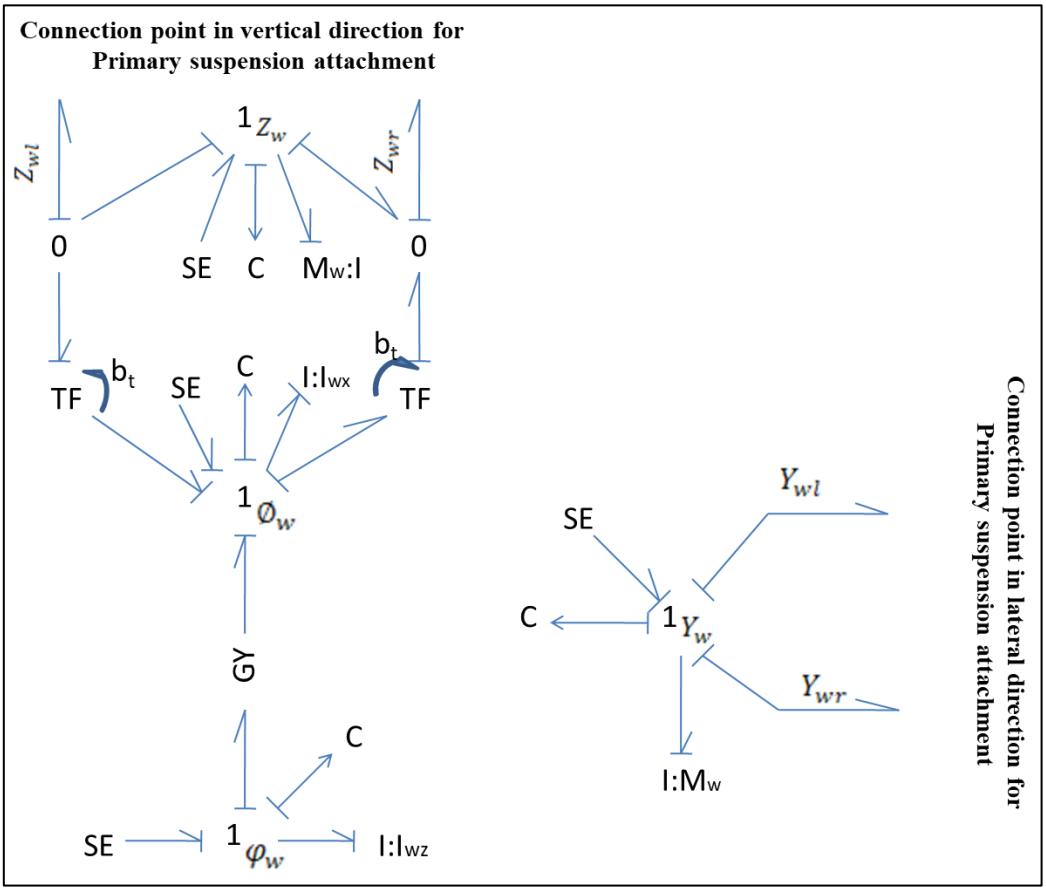

Figure 5.4: Complete bond graph model of wheelset

$F_{sfwz}, F_{sfwy}, M_{smwz}$ *and* M_{smwy} are suspension forces and suspension moment of the wheelset in corresponding directions. F^n_{wLz}, F^n_{wLy}, F^n_{wLx} , M^L_{wx}, $M^L_{wz}$are the nonlinear creep forces and moment at the contact point on the left sided wheel-rail in the corresponding direction. F^n_{wRz}, F^n_{wRy}, F^n_{wRx} , M^R_{wx}, M^R_{wz} are the nonlinear creep forces and moment at the contact point on the right sided wheel-rail in the corresponding direction.N^L_{wy},N^L_{wz}, N^R_{wy}, N^R_{wz} are the normal force components on the left and right wheel-rail contact points. R^L_z,

R_y^L, $R_x^L R_z^R$, R_y^R, R_x^R are the position vectors on the left and right contact points in the respective direction. F_{wfc} is the flange contact force, x indicates longitudinal direction, y indicates lateral direction and z indicates vertical direction.

5.2.3.2 Wheel rail contact modelling

Garg and Dukkipati [158] gave formulas for various linear creep forces and moments after translating them from the contact plane to the equilibrium coordinate system for both the left and right wheels, taking into account the minor roll and yaw angles of each wheelset.

$$F^L{}_{crx} = F_{crx}^{L*} - F_{cry}^{L*}\psi_w \tag{5.43}$$

$$F^L{}_{cry} = F_{cry}^{L*} + F_{crx}^{L*}\psi_w \tag{5.44}$$

$$F^L{}_{crz} = F_{cry}^{L*}(\delta_L + \psi_w) \tag{5.45}$$

$$M^L{}_{crx} = M_{crz}^{L*}(\delta_L + \phi_w)\psi_w \tag{5.46}$$

$$M^L{}_{crz} = M_{crz}^{L*} \tag{5.47}$$

$$F^R{}_{crx} = F_{crx}^{R*} - F_{cry}^{R*}\psi_w \tag{5.48}$$

$$F^R{}_{cry} = F_{cry}^{R*} + F_{crx}^{R*}\psi_w \tag{5.49}$$

$$F^R{}_{crz} = -F_{cry}^{R*}(\delta_R - \psi_w) \tag{5.50}$$

$$M^R{}_{crx} = -M_{crz}^{R*}(\delta_R - \phi_w)\psi_w \tag{5.51}$$

$$M^R{}_{crz} = M_{crz}^{R*} \tag{5.52}$$

Here,δ_L, δ_R are contact angles at the left and right wheels respectively. When a railway vehicle is moving on a curved track, creep forces acting at the left wheel and right wheel are given by Kalker's linear theory [159] and are presented in Eq. (5.53-5.58).

$$F_{crx}^{L*} = -\frac{f_{33}}{V}\left[V\left(1 + \frac{d_p}{R_t} - \frac{r_L}{r_0}\right) - a\dot{\psi}_w\right] \tag{5.53}$$

$$F_{cry}^{L*} = -\frac{f_{11}}{V}\left(\dot{y}_w + r_L\dot{\phi}_w - V\psi_w\right) - \frac{f_{12}}{V}\left(\dot{\psi}_w - \frac{V}{R_t} - \frac{V}{r_0}\delta_L\right) \tag{5.54}$$

$$M_{crz}^{L*} = \frac{f_{12}}{V}\left(\dot{y}_w + r_L\dot{\phi}_w - V\psi_w\right) - \frac{f_{22}}{V}\left(\dot{\psi}_w - \frac{V}{R_t} - \frac{V}{r_0}\delta_L\right) \tag{5.55}$$

$$F_{crx}^{R*} = -\frac{f_{33}}{V}\left[V\left(1 - \frac{d_p}{R_t} - \frac{r_R}{r_0}\right) + a\dot{\psi}_w\right] \tag{5.56}$$

$$F_{cry}^{R*} = -\frac{f_{11}}{V}\left(\dot{y}_w + r_R\dot{\phi}_w - V\psi_w\right) - \frac{f_{12}}{V}\left(\dot{\psi}_w - \frac{V}{R_t} + \frac{V}{r_0}\delta_R\right) \tag{5.57}$$

$$M_{crz}^{R*} = \frac{f_{12}}{V}\left(\dot{y}_w + r_R\dot{\phi}_w - V\psi_w\right) - \frac{f_{22}}{V}\left(\dot{\psi}_w - \frac{V}{R_t} + \frac{V}{r_0}\delta_R\right) \tag{5.58}$$

where $F_{crx}^{L*}, F_{cry}^{L*}, F_{crx}^{R*}, F_{cry}^{R*}$ are linear creep forces and M_{crz}^{L*}, M_{crz}^{R*} are linear creep moments acting at the left and right wheels.

The component of the normal force in the lateral and vertical direction at the left and right wheels is expressed by Eqs. (5.59-5.62).

$$N_{Lz} = -K_{rz}(z_w - \lambda y_w + d_p\phi_w) \tag{5.59}$$

$$N_{Lz} = -K_{rz}(z_w + \lambda y_w - d_p\phi_w) \tag{5.60}$$

$$N_{Ly} = -N_{Lz}\ tan\ tan\ (\delta_L + \phi_w) \tag{5.61}$$

$$N_{Ry} = N_{Lz}\ tan\ tan\ (\delta_L - \phi_w) \tag{5.62}$$

The flange contact force at the secondary contact point due to flange contact is given by [144] as

$$F_{fc} = \begin{cases} K_{ry}(y_w - \delta) & y_w > \delta \\ 0 & -\delta \le \delta \le \delta \\ K_{ry}(y_w - \delta) & y_w > \delta \end{cases} \tag{5.63}$$

Where δ is flange clearance and K_{ry} is the lateral stiffness of the rail.

Assuming that the lateral displacements Δ_L and Δ_R of the contact point are small from their equilibrium state, the geometric arrangement of the wheelset provides position vectors for the contact points as expressed by the following Eq. (5.64-5.69).

$$L_{Rx} = -d_p\psi_w \tag{5.64}$$

$$R_{Ly} = d_p + r_L\psi_w \tag{5.65}$$

$$R_{Lz} = d_p\phi_w - r_L \tag{5.66}$$

$$R_{Rx} = d_p\psi_w \tag{5.67}$$

$$R_{Ry} = -d_p + r_R\psi_w \tag{5.68}$$

$$R_{Rz} = -d_p\phi_w + r_R \tag{5.69}$$

where d_p is the half-track gauge.

In the present study, conical wheels and knife edge rails are assumed and thus the constraint function becomes linear [158]. Therefore, the wheel-rail geometry can be expressed by the following relationship.

$$\frac{1}{2}(r_L - r_R) = \lambda y_w \tag{5.70}$$

$$\frac{1}{2}(r_L + r_R) = r_0 \tag{5.71}$$

$$\frac{1}{2}(\delta_L + \delta_R) = 0 \tag{5.72}$$

$$\frac{1}{2}(\delta_L + \delta_R) = \lambda \tag{5.73}$$

Where λ is the conicity angle

5.2.4 Heuristic nonlinear creep model

In the present work, a Heuristic nonlinear creep model is utilized to form the contact forces between rails and wheels. The heuristic non-linear creep model is a combination of Kalker's linear creep theory and creep force saturation. The nonlinear creep forces and nonlinear creep moments are resulted by multiplying the saturation factor by the corresponding linear creep force and linear creep moment as shown in Eqs. (5.74-5.79).

$$F_{wLx}^{n} = \alpha_{ij} F_{wlx}^{L} \tag{5.74}$$

$$F_{wRx}^{n} = \alpha_{ij} F_{wrx}^{R} \tag{5.75}$$

$$F_{wLy}^{n} = \alpha_{ij} F_{wly}^{L} \tag{5.76}$$

$$F_{wRy}^{n} = \alpha_{ij} F_{wry}^{R} \tag{5.77}$$

$$M_{wLz}^{n} = \alpha_{ij} M_{wlz}^{L} \tag{5.78}$$

$$M_{wRz}^{n} = \alpha_{ij} M_{wrz}^{R} \tag{5.79}$$

Where F_{wlx}^{L}, F_{wly}^{L}, M_{wlz}^{L}, F_{wrx}^{R}, F_{wry}^{R}, M_{wrz}^{R} are linear creep forces and moments on left and right wheels in respective directions. α_{ij} represent the saturation constant in the heuristic creep model obtained from Johnson's approach [158] as given in Eq. (5.80).

$$\alpha_{ij} = \begin{cases} \frac{1}{\beta_{ij}}\left(\beta_{ij} - \frac{1}{3}\beta_{ij}^2 + \frac{1}{27}\beta_{ij}^3\right) => \beta_{ij} \leq 3 \\ \frac{1}{\beta_{ij}} => \beta_{ij} \geq 3 \end{cases} \quad (5.80)$$

Where β_{ij} is the non-linearity factor in the heuristic creep model and it is calculated for vehicles under quasi-static motion over the curved track.

5.2.5 Effect of track irregularities on lateral dynamics of HSRV

A train's operating behaviour and safety depend on a number of variables, including track shape, track stiffness, speed, and vehicle characteristics. Curving tracks usually result in

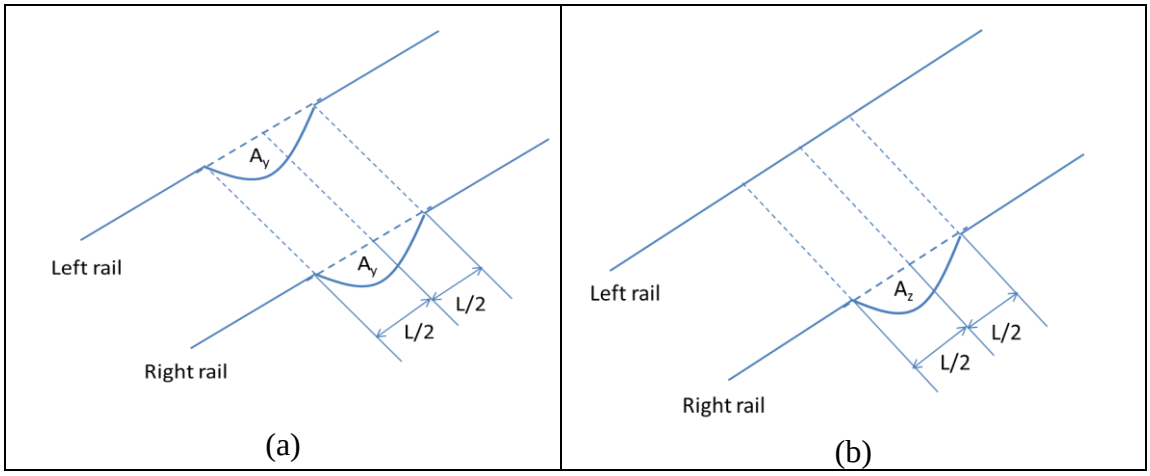

Figure 5.5: Types of irregularity (a) Alignment (b) Cross Level

lower safety standards and performance degradation in comparison to straight tracks. It is difficult to analyse how track irregularities affect running behaviour and safety in simulations when curves are taken into account at the same time. Furthermore, the position of track imperfections on curves has a big impact on how the vehicle responds. Therefore, in the present work transition track has been considered and shown in Figure 5.6. Also, the track irregularities have been introduced at the end of the straight track i.e. in front of the curved track to examine how track abnormalities affect vehicle responses. The length of the straight track and the curved track is 1000 and 3000 m respectively. Alignment and cross level type track irregularities have been introduced are shown in Figure 5.5 and presented as half- sine-wave shaped is given in Eq. (5.81). Different wavelengths and

amplitudes of irregularities are taken into account in the simulations in order to study the effect of track abnormalities. The variation of amplitude and wavelength are tabulated in Table 5.1.

Table 5.1: Variation of different types of irregularity

S. No	Types of irregularity	Wavelength (m)	Amplitude of irregularity (A) (mm)
1	Alignment Irregularity (AL)	3, 5, 10, 20, 40	15
2	Cross Level (CL)	3, 5, 10, 20, 40	15

$$Z_0(t) = \frac{1}{2} A\left(1 - cos\frac{2\pi vt}{L}\right),\ 0 \le t \le \frac{L}{v} \tag{5.81}$$

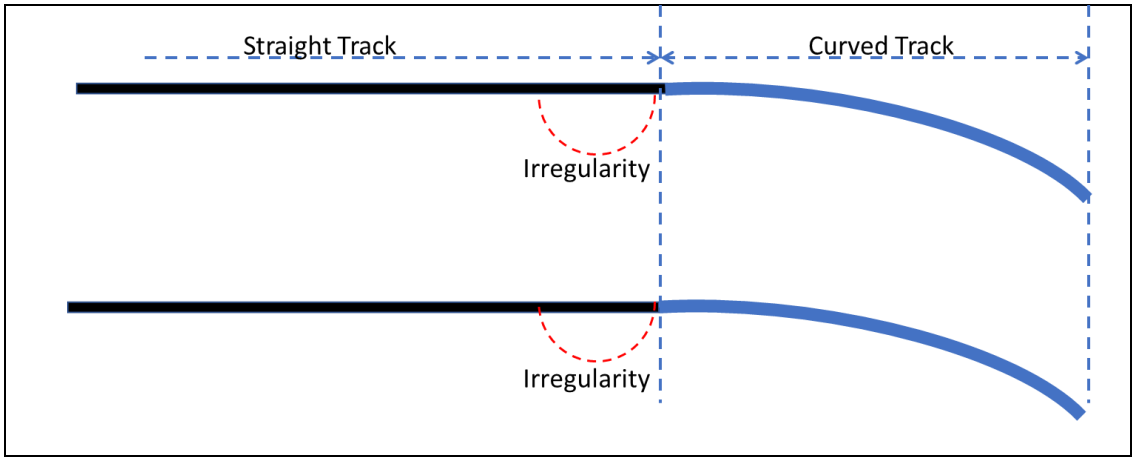

Figure 5.6: Transition from straight track to curved track

5.2.6 Integrated bond graph model of 31 DOF railway vehicle

The comprehensive bond graph representation of a 31-degree-of-freedom (DOF) railway vehicle, as depicted in Figure 3.22, is constructed by consolidating individual bond graph models for the car body (LCB), bogies (LB), and wheelsets (LW) [67]. The symbols LB and LW in Figure 5.7 incorporate subscripts 'f' and 'r,' denoting the front and rear bogie/wheelset, respectively. Each subsystem model employs a 1-junction to portray linear and rotational motion variables, each appropriately labelled with subscripts. Signal bonds

with full arrows are employed within these subsystem models to enable the monitoring of displacement variable values.

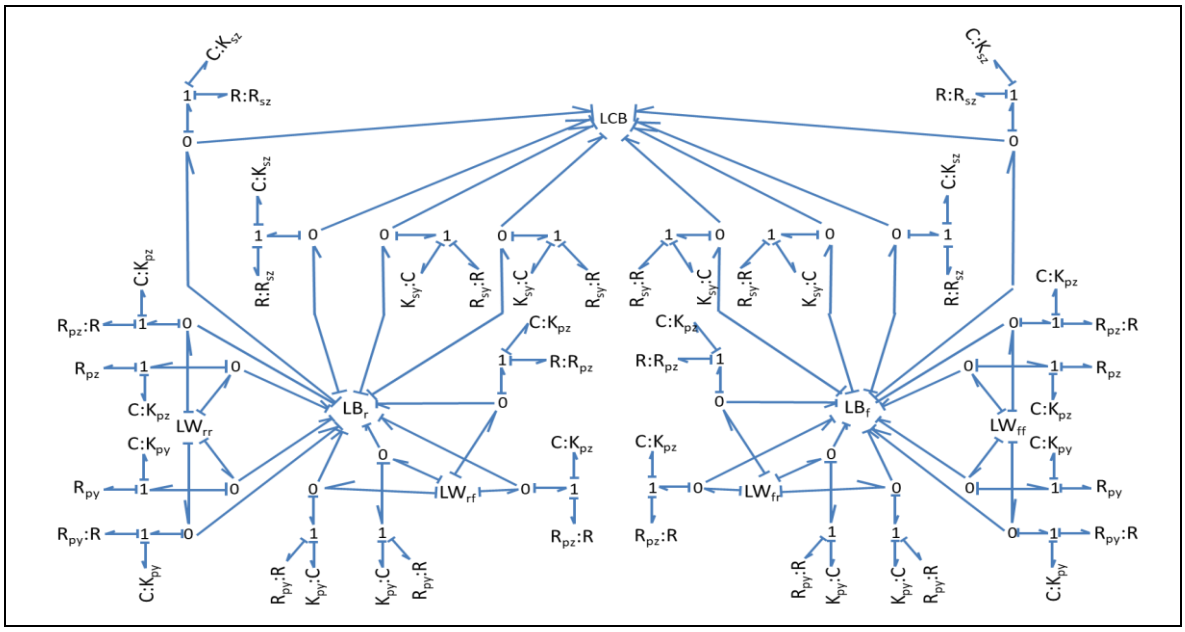

Figure 5.7: Integrated bond graph model of 31 DOF railway vehicle

5.3 Results and Discussions

The simulation of a 31-degree-of-freedom (DOF) railway vehicle's integrated bond graph model is conducted under conditions of flexible track, utilizing the nominal geometrical and inertial parameters outlined in Table 3.2, along with suspension parameters specified in Table 3.3. This analysis aims to explore the lateral dynamics of HSRV running on the transition track and the hunting behaviour of the HSRV moving on the curved track. The simulation has been performed using 'Symbol Shakti' to investigate the lateral dynamic behaviour of HSRV due to track irregularity while moving on the transition track. The investigation was carried out with the parameters mentioned by Kim et al. [144] in their research work. While conducting the simulation, the impact of nonlinearities i.e. flanges contact and heuristic nonlinear creep model, were considered.

This section has been divided into two parts: stability analysis and the effect of track irregularities on the lateral dynamics of HSRV.

5.3.1 Stability analysis

In this study, the critical speed of 31 DOF HSRV has been evaluated and compared using Polach non-linear creep and heuristic nonlinear creep models at different running speeds. Figure 5.8 illustrates the phase portrait diagram of the initial leading wheelset, depicting its lateral displacement within stable, critical, and unstable regions. The diagram is based on a heuristic nonlinear creep model, considering a radius of curvature of 3000 meters. The analysis assumes an initial wheel displacement of 3 mm from the centre of the rail tread.

The findings indicate that, while the vehicle is operating at a speed of 216 km/h, the wheels tend to reposition themselves toward the centre of the rail tread over time. Simulation results reveal that the critical speed for the HSRV under the specified conditions is 257.4 km/h. At this critical speed, the wheelset experiences self-sustained lateral oscillation, leading to hunting motion. Beyond this critical speed, the trajectory of the wheelsets deviates from the centre of the rail tread, and the amplitude of vibration surpasses the flange clearance, as depicted in Figure 5.8 (c) and a rising trend in the vibration characteristics of the wheelset was evident.

Figure 5.9 shows the phase trajectory diagram of the front leading wheelset using the Polach nonlinear creep model. It is evident from Figure 5.9 (a) that the amplitude of vibration is diminishing with time as the vehicle speed is 252 km/h and shows the stable behaviour of the vehicle. At a speed of 288 km/h, the wheelset shows a self-sustained oscillation motion, and it oscillates about the equilibrium position with an amplitude less than the flange clearance. Above the critical speed, lateral displacement of the wheelset increases with time and approaches to the flange clearance as observed in Figure 5.9(c).

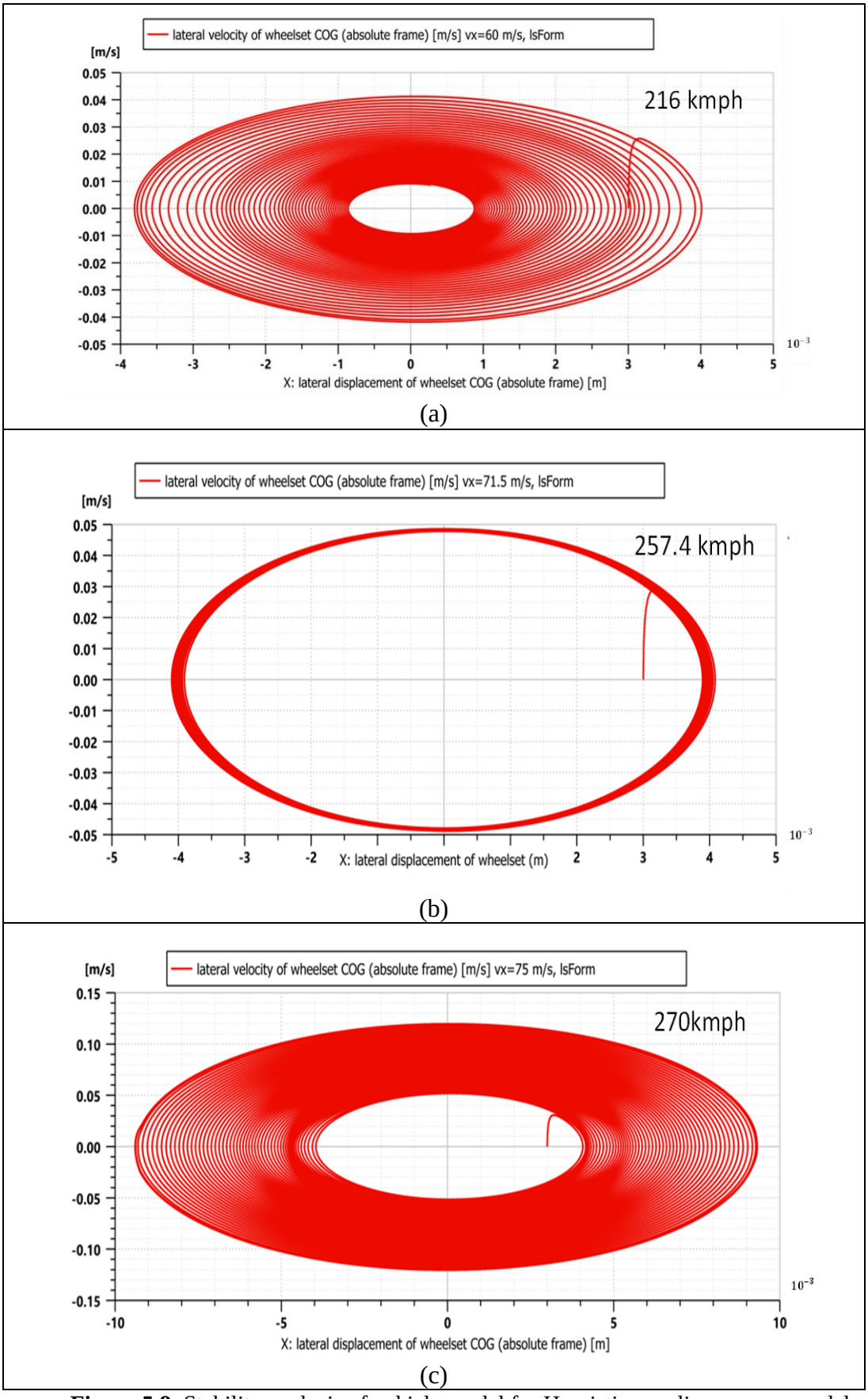

Figure 5.8: Stability analysis of vehicle model for Heuristic non-linear creep model

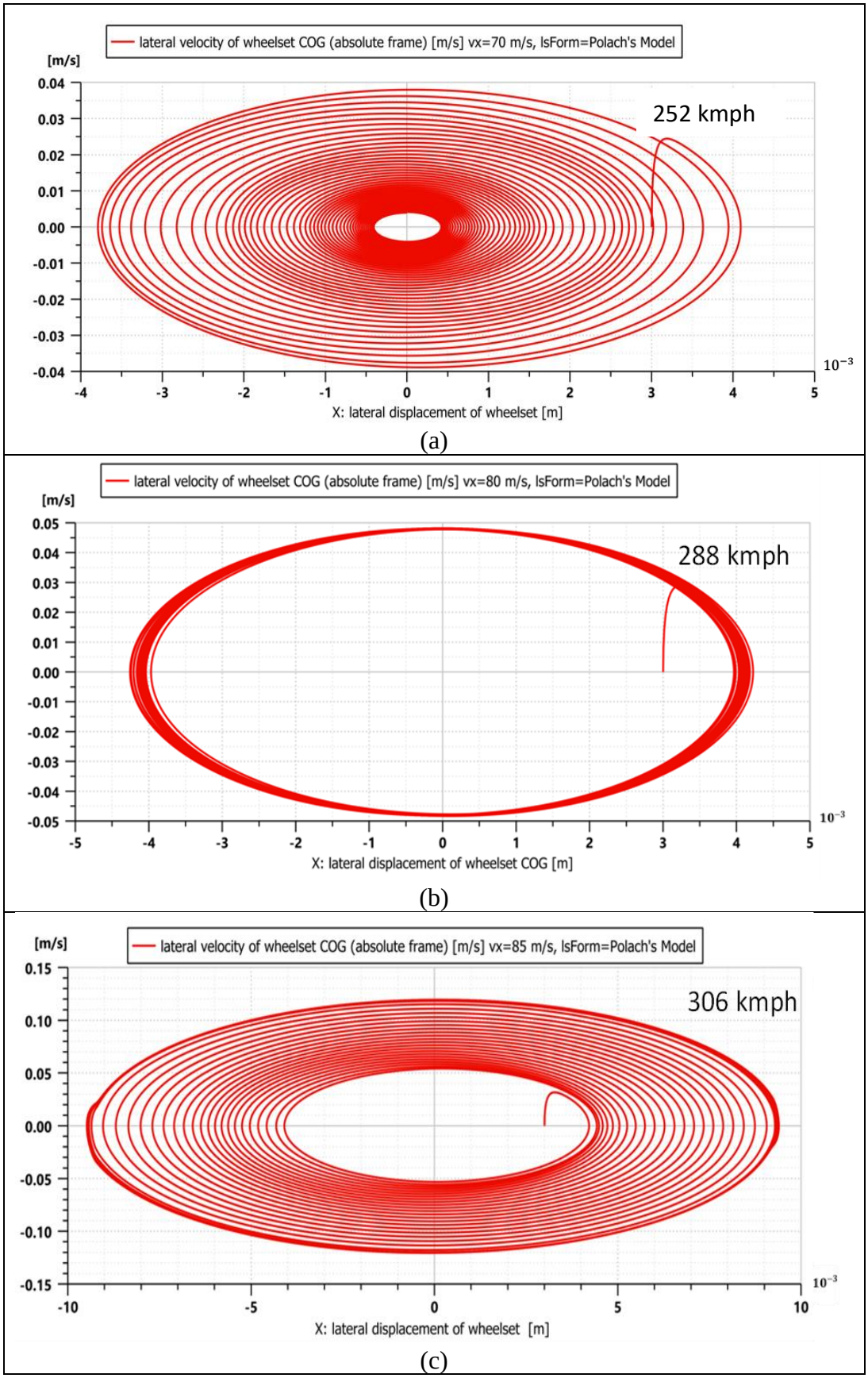

Figure 5.9: Stability analysis of vehicle model for Polach contact model

Stability analysis has been compared for the heuristic nonlinear creep model and Polach model as shown in Figure 5.7 and 5.8 respectively. The critical speed of Polach's model is greater than the critical speed obtained from Kalker's model. When compared to Polach's technique, Kalker's method—which is used to simulate the non-linear dynamic behaviour of the railway vehicle—is more accurate and sophisticated.

5.3.2 Effect of different track irregularities

Track irregularities exert distinct effects on the dynamic performance of high-speed railway vehicles. In the present research work, the focus is on examining the impact of preceding irregularities categorized as alignment irregularity (AL) and cross level irregularity (CL). Simulations are conducted considering wavelengths of 3 m, 5 m, 10 m, 20 m, and 40 m, with amplitudes set at 15 mm for both AL and CL.

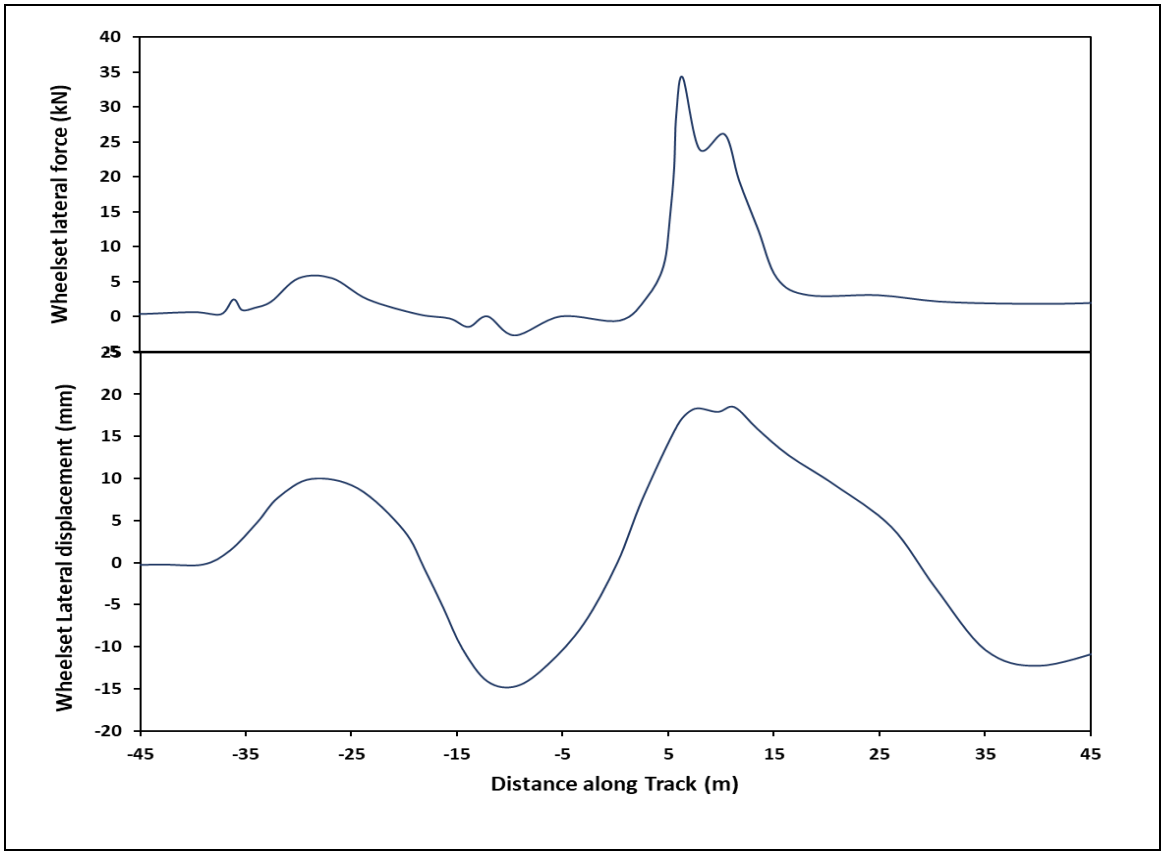

Figure 5.10: Comparison of the wheelset lateral force and wheelset lateral displacement along with the length of track at 40 mm wavelength of AL irregularity

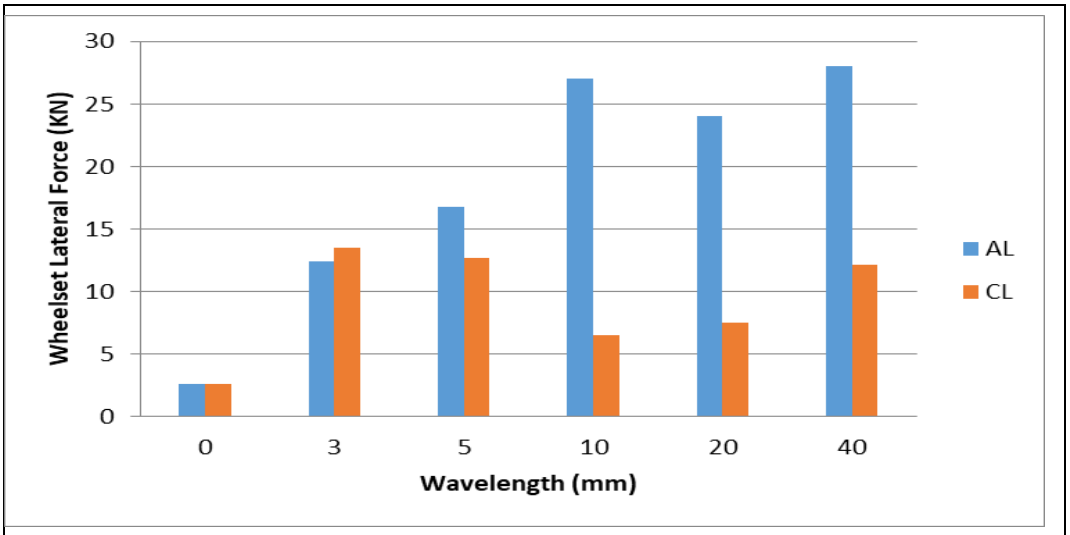
Wheelset Lateral Force (KN)
30
25
20
15
10
5
0
0
3
5
10
20
40
Wavelength (mm)
AL
CL

(a)

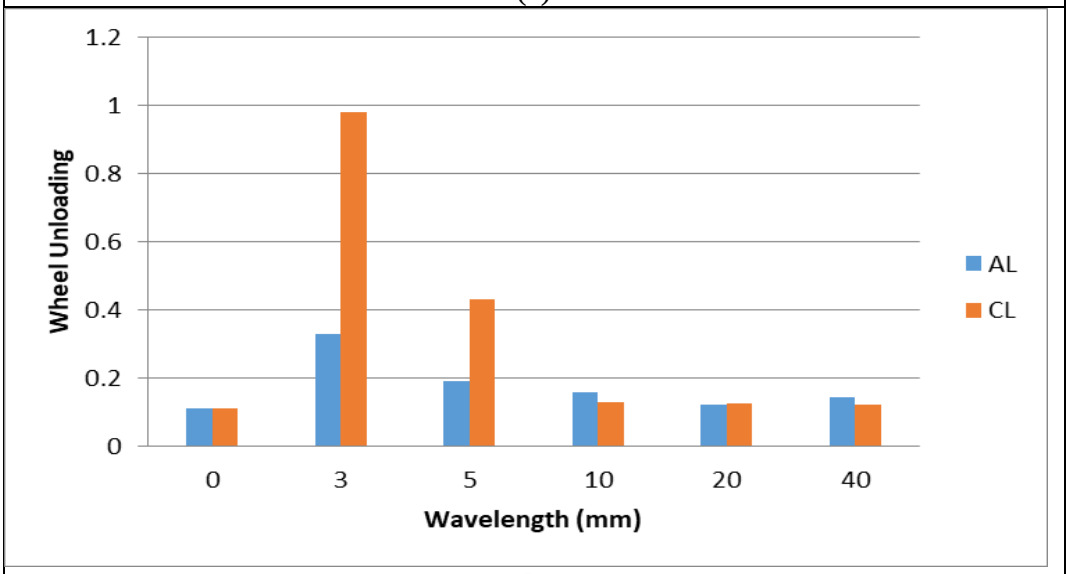
Wheel Unloading
1.2
1
0.8
0.6
0.4
0.2
0
0
3
5
10
20
40
Wavelength (mm)
AL
CL

(b)

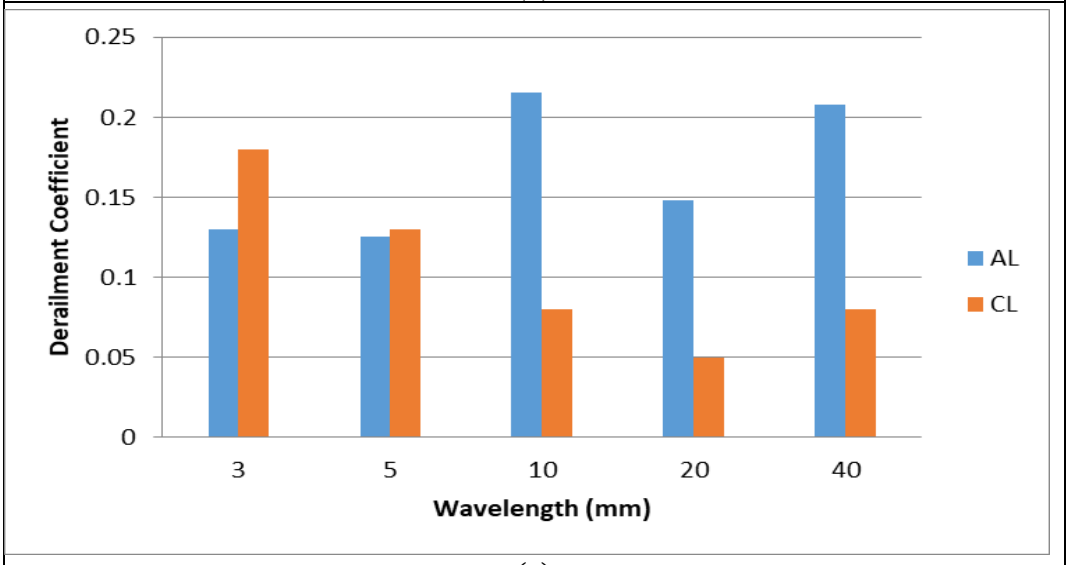
Derailment Coefficient
0.25
0.2
0.15
0.1
0.05
0
3
5
10
20
40
Wavelength (mm)
AL
CL

(c)

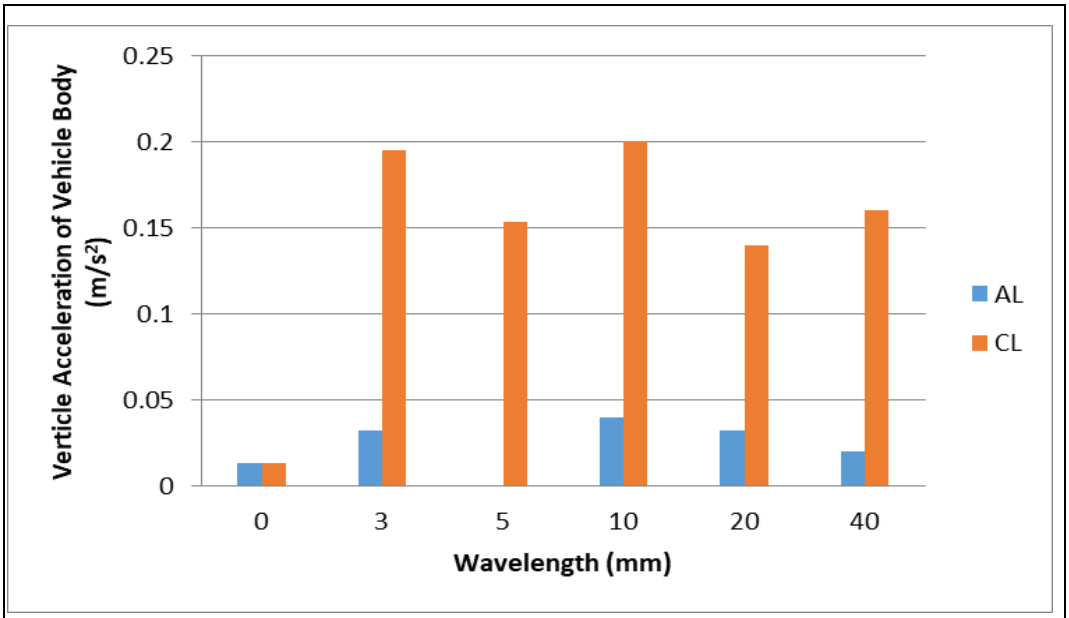

(d)

Figure 5.11: (a) Wheelset lateral force; (b) Wheel unloading rate; (c) Derailment coefficient; (d) Vertical acceleration of the vehicle body.

Figure 5.10 depicts the variation of lateral displacements and wheelset lateral force due to the presence of alignment track irregularity preceding the transition track. The amplitude of AL is 15 mm and the wavelength is 40 mm. Long wavelength track irregularity in front of the transition track leads to the lateral displacement of the wheelset in a simple harmonic waveform in a straight track. When the vehicle follows the track depicted in Figure 5.10 and drives from the straight track to the transition track, the lateral displacement of the wheelset shifts to the extreme right, bringing the wheel flange closer to the rail web. As there is AL present preceding the transition zone, the wheel flange abruptly makes contact with the rail web, leading to a sudden increase in wheelset lateral forces. The presence of AL induces random vibrations in the lateral direction, causing maximum displacement and resulting in maximum lateral forces. Figure 5.11 shows the effect of CL and AL positioned in front of the transition track, on wheelset lateral force, wheel unloading rate, derailment coefficient and vertical acceleration of the HSRV.

From the Figure, it can be inferred that AL has a major impact on the wheelset lateral force and derailment coefficient whereas CL has a major impact on vertical acceleration of the wheelset. In Figure 5.11(c), a comparison of the derailment coefficient due to AL and CL is presented. The analysis indicates that for shorter wavelengths of irregularity, CL has a more pronounced effect on the derailment coefficient compared to AL. However, as the irregularity wavelength increases to medium and longer ranges (5mm to 40 mm), the influence of AL on the derailment coefficient becomes more dominant than CL. The results reveal that the derailment quotient remains below 0.8 for all conditions, signifying that the vehicle is within a safe zone, and there is no risk of wheel climb-up derailment.

Figure 5.11(b) displays a comparative graph of the wheel unloading ratio in the presence of AL and CL. For irregularities across all wavelengths, AL and CL exhibit minimal impact on the wheel unloading ratio, except under specific conditions. Notably, the graph illustrates that, in the presence of CL for a 3mm wavelength, the wheel unloading ratio is approximately close to 1. This condition raises concerns as it may lead to roll-over derailment. In such instances, the reduction in wheel load is approximately equal to the average static wheel load, potentially resulting in the wheel rolling over from the rail head. This emphasizes the importance of considering irregularity wavelengths and the influence of AL and CL in assessing the wheel unloading ratio and potential derailment risks. In Figure 5.11(d), a comparison of the vertical acceleration of the wheelset in the presence of AL and CL is presented. The graph suggests that CL has a significant impact on the vertical acceleration of the railway vehicle, directly influencing passenger ride comfort.

5.4 Conclusions

In conclusion, the simulation study involving a 31 DOF railway vehicle's integrated bond graph model under flexible track conditions has provided valuable insights into its lateral

dynamics. Utilizing nominal geometrical and inertial parameters, along with suspension parameters, the analysis focused on investigating the lateral dynamics during transitions on the track and the hunting behaviour on curved tracks.

The stability analysis revealed critical speeds for the HSRV using both Polach's non-linear creep and heuristic non-linear creep models. The critical speed obtained from Polach's model was found to be greater than that from Kalker's model, indicating the latter's enhanced accuracy and sophistication in simulating non-linear dynamic behaviour.

Examining the impact of different track irregularities, specifically alignment irregularities (AL) and cross level irregularities (CL), the simulations considered various wavelengths and amplitudes. AL was observed to have a significant influence on wheelset lateral force and derailment coefficient, while CL had a pronounced effect on the vertical acceleration of the wheelset, directly affecting passenger ride comfort.

The study also highlighted the importance of considering irregularity wavelengths, as evident in the analysis of the wheel unloading ratio. Notably, a 3 mm wavelength with CL showed a concerning wheel unloading ratio close to 1, potentially leading to roll-over derailment due to a reduction in wheel load.

In summary, the research provides a comprehensive understanding of the lateral dynamics and stability of the HSRV under different track irregularities, emphasizing the critical role of accurate modelling and analysis in ensuring the safety and performance of high-speed railway vehicles.

Table 5.2: Geometric and inertial parameters for 31 DOF railway vehicle model [144]

S.No.	Parameter	Nomenclature	Values
1.	Mass of car body	M_c	34000 kg
2.	Mass of bogie	M_b	3000 kg
3.	Mass of wheelset	M_w	1400 kg
4.	Moment of inertia of car body about X-axis	I_{cx}	75.06 x 10^3 Kg-m^2
5.	Moment of inertia of car body about Y-axis	I_{cy}	2.08 x10^6 Kg-m^2
6.	Moment of inertia of car body about Z-axis	I_{cz}	2.08 x10^6 Kg-m^2
7.	Moment of inertia of bogie about X-axis	I_{bx}	2260 Kg-m^2
8.	Moment of inertia of bogie about Y-axis	I_{by}	2710 Kg-m^2
9.	Moment of inertia of bogie about Z-axis	I_{bz}	3160 Kg-m^2
10.	Moment of inertia of wheelset about X-axis	I_{wx}	915 Kg-m^2
11.	Moment of inertia of wheelset about Y-axis	I_{wy}	140 Kg-m^2
12.	Moment of inertia of wheelset about Z-axis	I_{wz}	915 Kg-m^2
13.	Wheel conicity	λ	0.045 rad
14.	Wheel radius	r_0	0.4575
15.	Half of the primary longitudinal and vertical suspension arm	l_t	0.978 m
16.	Half of the secondary lateral suspension arm	l_c	1.21 m
17.	Half of the primary lateral suspension arm	l_p	0.978 m
18.	Distance between the vehicle body and bogie frame mass centre	l_s	9 m
19.	Height of the vehicle body CG above Wheelset CG	h	1.4 m
20.	Height of the secondary suspension above bogie CG	h_0	0.03 m
21.	Height of bogie CG above wheelset CG	h_g	0.44 m
22.	Radius of Track	R_t	6000m
23.	Lateral creep coefficient	f_{11}	10.2 x 10^6 N
24.	Forward creep coefficient	f_{33}	15 x 10^7 N
25.	Spin creep coefficient	f_{22}	16 N
26.	Lateral/Spin Creep coefficient	f_{12}	3120 N
27.	Track Gauge	d_p	0.7465 m
28.	Cant angle	ϕ_{se}	0.0873 rad
29.	Coefficient of Friction	μ	0.2

Table 5.3: Suspension parameters for 31 DOF railway vehicle model [144]

S.No.	**Parameter**	**Nomenclature**	**Values**
1.	Primary longitudinal stiffness	K_{px}	10000 kN/m
2.	Primary lateral stiffness	K_{py}	5000 kN/m
3.	Primary vertical stiffness	K_{pz}	750 kN/m
4.	Primary longitudinal damping	R_{px}	12 kNs/m
5.	Primary lateral damping	R_{py}	12 kNs/m
6.	Primary vertical damping	R_{pz}	450 kNs/m
7.	Secondary longitudinal stiffness	K_{sx}	150 kN/m
8.	Secondary lateral stiffness	K_{sy}	150 kN/m
9.	Secondary vertical stiffness	K_{sz}	400 kN/m
10.	Secondary longitudinal damping	R_{sx}	10 kNs/m
11.	Secondary lateral damping	R_{sy}	10 kNs/m
12.	Secondary vertical damping	R_{sz}	88 kNs/m
13.	Vertical rail stiffness	K_{rz}	62×10^6 N/m
14.	Vertical rail stiffness	K_{ry}	16.17×10^6 N/m

CHAPTER 6

Simulation-Based Analysis of Passenger Ride Comfort under Different Track Conditions

In the previous chapter, modelling and simulation for the investigation of lateral dynamics and hunting behaviour of a railway vehicle have been presented. This chapter discussed the ride comfort analysis of 50 DOF HSRV model. Modelling and simulation of HSRV have been done in SIMPACK.

6.1 Introduction

With the advancement in technology, railway vehicles are not only achieving new heights but can now run at very high speeds and attain a great extent of comfort. Previous studies exhibit those vibrations are the main source of passenger discomfort. Hence to improve the ride quality, it is required to reduce the vibration. Track irregularities (due to sudden braking of trains, irregular track maintenance, irregular running speed), geometric irregularities (improper design, wear), and material non-linearities are reasons for vibration generation in railway vehicles.

These vibrations are transferred to various components (wheelsets, bogie, car body) of railway vehicles during operations. Vibration responses from the car body are further transferred to the human body through supporting components like the car floor and seats. Once the frequency of two systems becomes nearly equal, a resonance phenomenon arises, which causes a high amplitude of vibration, further resulting in higher discomfort to passengers [63]. These vibration responses are recorded in terms of acceleration signals.

Experimental results show that the human body is more susceptible to vertical acceleration response near 5Hz and less susceptible below the 2Hz frequency range [68, 69]. It is crucial to determine the modes of vibration of the car body near the natural frequency of the human body so that necessary steps can be taken to eradicate that mode. Earlier research shows that rigid car body mode transpired in the frequency range of 0.3 Hz to 8 Hz, and flexible modes take place from 7 Hz to 20 Hz [70].

Passenger comfort while riding a train depends on the intensity of vibrations, direction, frequency and exposure time. These vibrations can prevent passengers from performing any sitting activity and also affect passengers' health. Train vibrations are considered a prime factor in passengers' ride comfort [71, 72]. It becomes necessary to develop a method which assesses a passenger's ride comfort while riding a railway vehicle [73, 74]. However, it becomes impossible to develop a general method acceptable to all the countries and their rail standards as every country has different vibrational characteristics [75]. In the mid-20th century, a researcher named Sperling proposed an advanced method called the ride Index method (W_z) to determine the ride comfort of a passenger [76–78]. Based on the ISO 2631 standards, the International Union of Railways (UIC), the European Committee of Standardization (CEN) and the International Standard Organization (ISO) have firmed the standards of ride comfort of railway vehicles [79, 80]. These methods were known as UIC 513R leaflet [81], EN 12299 [82] and ISO 10056 [83], respectively.

Above mentioned ride comfort evaluation method used different articulation techniques to evaluate the acceleration signal. As a result, establishing an unmediated link between various evaluation methodologies is challenging. However, various researchers tried to establish a correlation between these methods. Kim et al. determined the ride comfort indices using Sperling's method, ISO 2631 and UIC 513 recommended method and tried to establish the relationship between them. Similarly, many researchers compared the ride

comfort indices using Sperling's method, EN12299 continuous comfort and mean comfort method. The comfort index at sitting and standing positions is also calculated and examined by Munawir et al. [87]. Dumitriu et al. evaluated passenger comfort using the mean comfort method and Sperling's method and found that different assessment methods will show different results under identical boundary conditions [88].

Furthermore, Kumar et al. developed a biodynamic model to calculate passenger ride comfort using Sperling's index [89]. Jiang et al. explore the merits and demerits of EN12299 and Sperling's method [90]. Further, experimental data was recorded by Haladin et al. on the in-service tramway to compare different ride comfort evaluation techniques such as the Sperling's Ride index method, EN12299 comfort method and equivalent level of vibrations method [91].

Various numerical simulation tools are designed to predict the dynamic behaviour of the railway vehicle. These numerical tools predict the dynamical performance of a railway vehicle at the designing phase and also examine the issues arising during usage as effectively as possible. Numerical simulations allow the investigation of a railway vehicle's dynamic behaviour under extreme parameters that cannot be noticed during real testing situations [92]. The development of advanced computer systems and Finite-element numerical methods has magnified the search for numerical calculation methods for vehicular vibration. Many researchers have developed a 3D dynamic model of high-speed trains to predict the vibration response and compare the results with those obtained from field monitoring [93–95]. There are different commercially available simulation software like ANSYS, SIMPACK, and LS-DYNA to perform such analysis in various ways.

In previous research work influence of track irregularity on ride comfort assessment has been considered. Very limited research has been found that simulates the passenger ride comfort when track irregularity is introduced on the single rail only. In this article, the

irregularities are introduced on the left rail only. This thesis aims to compare the high-speed railway vehicle ride index under different track conditions at different car positions. For this purpose, a complete 50 Degree of Freedom high-speed railway vehicle is designed in SIMPACK software. Three different track conditions have been generated by incorporating a combination of random track irregularities well described by their power spectral densities. This analysis aims to identify the solutions by which the car body's vertical and lateral acceleration can be minimized, thus giving the vehicle the best dynamic performance in terms of ride quality.

6.2 Modelling and Methodology

There are three main components of a conventional multibody vehicle: bogies, wheelset and coach or car body. In the present study, a multibody vehicle model has been created to conduct the computational simulation. The presented model consists of 2-FIAT bogies, 4-wheelsets and an LBH passenger coach. A dual suspension system has been employed in the presented model. First, a primary suspension system is incorporated between the 4-wheelsets and 2-bogies in three mutually perpendicular directions, i.e., vertical, lateral and longitudinal. Secondly, a secondary suspension system is incorporated between 2-bogies and a passenger coach in mutually perpendicular directions. A 3-dimensional FIAT bogie-wheelset model is shown in Figure 6.1.

The dual suspension system is depicted by a combination of series, parallel and shear springs and nonlinear dampers. The nonlinear dynamic system incorporates dampers in vertical and lateral directions, an Anti-Roll bar, and Anti-yaw dampers. These dampers are the shock absorbers used to dampen the vibrations arising from track irregularities. An anti-roll bar reduces lateral acceleration by applying opposite torque when the vehicle moves on the curved track. Anti-yaw dampers are the secondary suspension element used to

stabilize the hunting phenomenon, favourably improving the ride quality. Additional force elements like bump stops and traction rods are also included in the model. A bumpstop is used to limit the lateral displacement of the car body. The track rod is modelled as a linear spring-damper element to dampen vibration in a longitudinal direction during traction and braking of the train. Force-velocity characteristics of primary and secondary dampers are referred from RDSO [160], as shown in Figure 6.2.

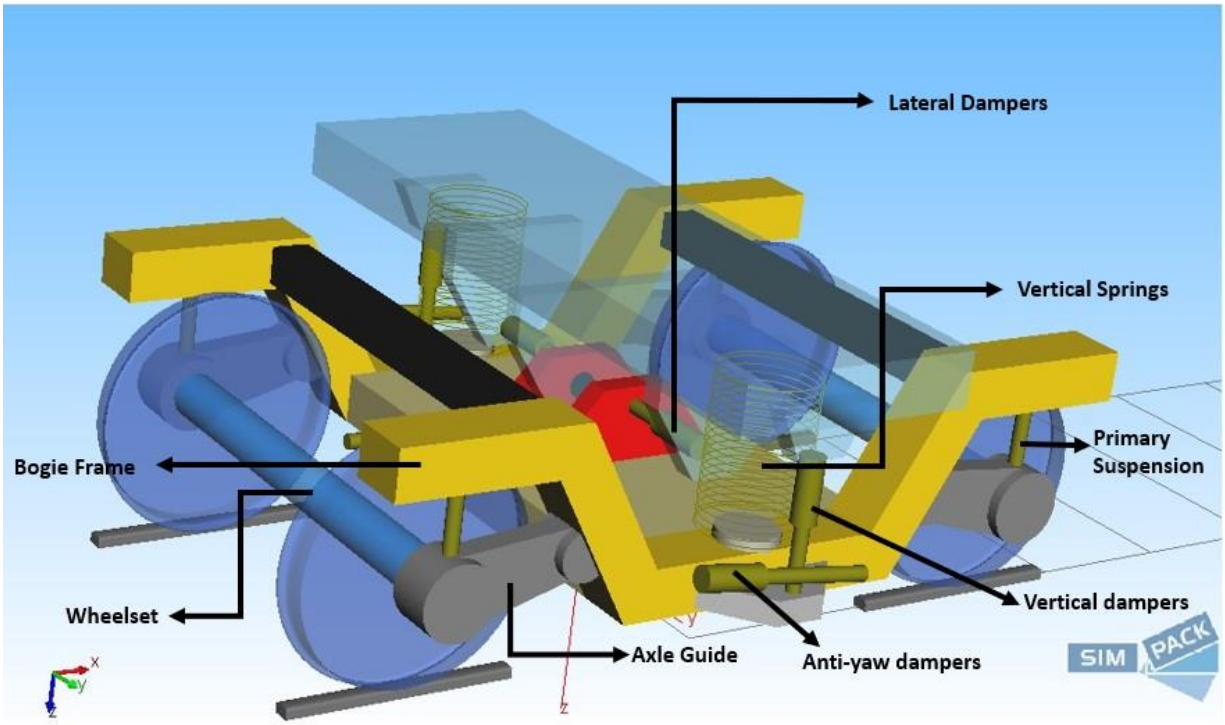

Figure 6.1: 3-D spring Damper model of Dual suspension system

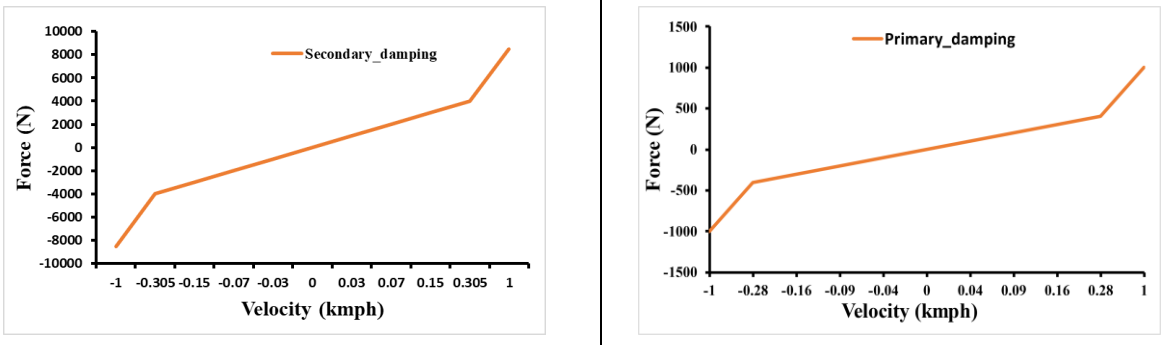

(a) (b)

Figure 6.2: Damping curve in the vertical direction (Force vs Velocity) (a) Primary Suspension Damping (b)Secondary Suspension Damping

The presented multibody model has 50 Degrees of Freedom. It is utilized to compare the comfort of a railway vehicle under diverse track conditions and at different car positions. A multibody software package called 'SIMPACK' which is used to simulate the nonlinear motion of large and complicated multibody systems, is adopted to create a multibody model. The presented model is formed of rigid bodies interconnected by massless spring-damper elements shown in Figure 6.3.

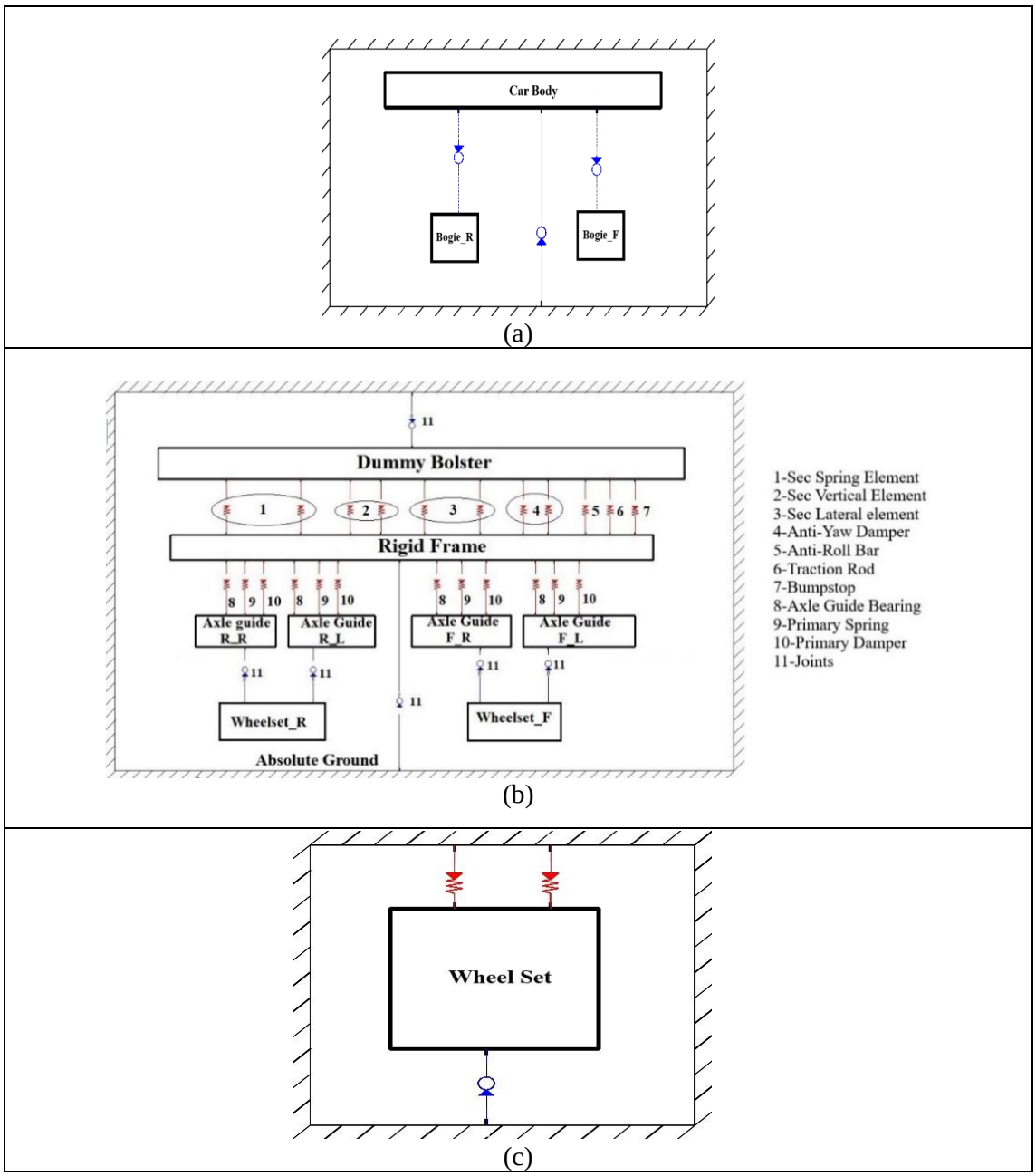

Figure 6.3: Schematic diagram of the model (a) Car body-bogie connection (b) Full bogie model (c) Wheelset model

6.2.1 Power spectral density (PSD) based track irregularities

Track imperfection is the major cause of external excitation for a rolling stock system. As per EN13848, track irregularities are broadly classified as Vertical track irregularities, lateral track irregularities, cross level track irregularities and track gauge irregularities. These track imperfections have a large impact on the dynamic response of a railway vehicle. But, the connection between what occurs at the track level and how the vehicle reacts is not always clear. In terms of correlation, there is often a considerable variation between different vehicles and situations, as seen in many research projects. In this research work, vertical, lateral and combined vertical-lateral track irregularities are incorporated on the left rail to study the effects of track irregularity on ride comfort. The American sixth-grade track spectrum has been used to simulate the track irregularities, which act as random

Table 6.1: Parameter of track irregularity

Parameter	Parameter Value for 6-Level
A_v/cm^2 rad/m)	0.0339
A_l/(cm^2 rad/m)	0.0339
w_s/(rad/m)	0.4380
w_c /(rad/m)	0.8245

excitations to the vehicle. These excitations are introduced as PSD signals derived from the given equations. The vertical and lateral track irregularities in terms of PSD are given in equations 6.1 and 6.2 [149]. In SIMPACK, these PSD signals are converted into distance domain excitation, which can be directly applied to the track.

$$S_v(w) = \frac{kA_v w_c^2}{(w^2 + w_c^2)w^2} \tag{6.1}$$

$$S_l(w) = \frac{kA_l w_c^2}{(w^2 + w_c^2)w^2} \tag{6.2}$$

Where *S(w)* represents the track irregularity in terms of PSD function (cm2/rad/m), *w* is the spatial frequency (rad/m), w_c depicts the cutoff frequency (rad/m), A_v and A_l represent the roughness coefficients (cm2 rad/m), for a particular line level. *k* is generally taken as 0.25. Table 6.1 shows the parameter values for the 6^{th} line level.

6.2.2 Ride comfort assessment

The Mean Comfort standard technique was presented in both UIC-513 and EN-12299 standards and has been used by most countries for ride quality evaluation. The 95th percentile from the five-minute frequency weighted *RMS* values of the individual x,y, and z acceleration signals are considered in the Mean Comfort index (N_{mv}) calculation. Acceleration response in the vertical direction (*Z*-axis) has been shifted by a factor of 9.81 to remove the additional gravitational effect.

For each direction, a particular segment, i.e., sixty continuous five-second weighted *RMS* values, are considered over specific track conditions. From these sixty RMS values, 95th percentiles of the weighted accelerations in three directions are chosen and united with a root-sum-square calculation, as shown in equation (6.3).

$$N_{MV} = 6 * \sqrt{(a_{XP95}^{W_d})^2 + (a_{YP95}^{W_c})^2 + (a_{ZP95}^{W_b})^2} \tag{6.3}$$

Where N_{mv} indicates the Mean Comfort index; *P* denotes the floor level; *X*, *Y* and *Z* represent the longitudinal, lateral and vertical directions, respectively. W_d indicates the frequency-weighted value in longitudinal and lateral directions, while W_b indicates the frequency-weighted value in the vertical direction. Figure 6.4 shows the detailed steps to determine frequency-weighted R.M.S accelerations in three directions. Standard passenger comfort reactions based on the N_{mv} index are given in Table 6.2 [161].

Table 6.2: Comfort reactions based on N_{mv}

EN12299 Index (N_{mv})	**Likely reaction of passengers**
N_{mv}<1.5	Very comfortable
1.5≤N_{mv}<2.5	Comfortable
2.5≤N_{mv}<3.5	Acceptable comfort
3.5≤N_{mv}<4.5	Uncomfortable
N_{mv}≥4.5	Very uncomfortable

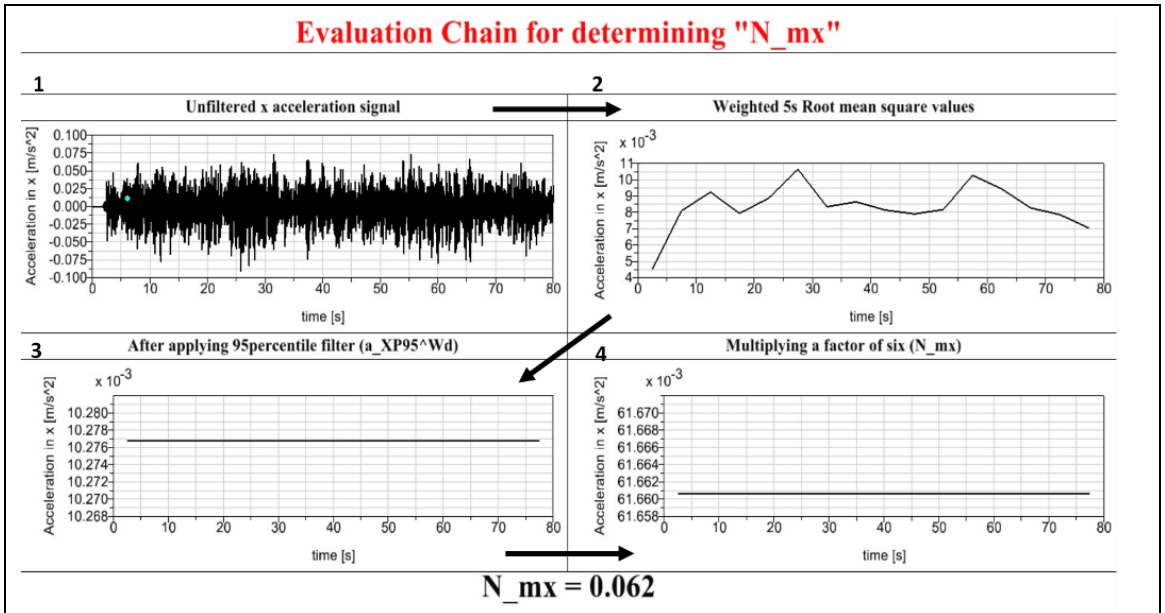

(a)

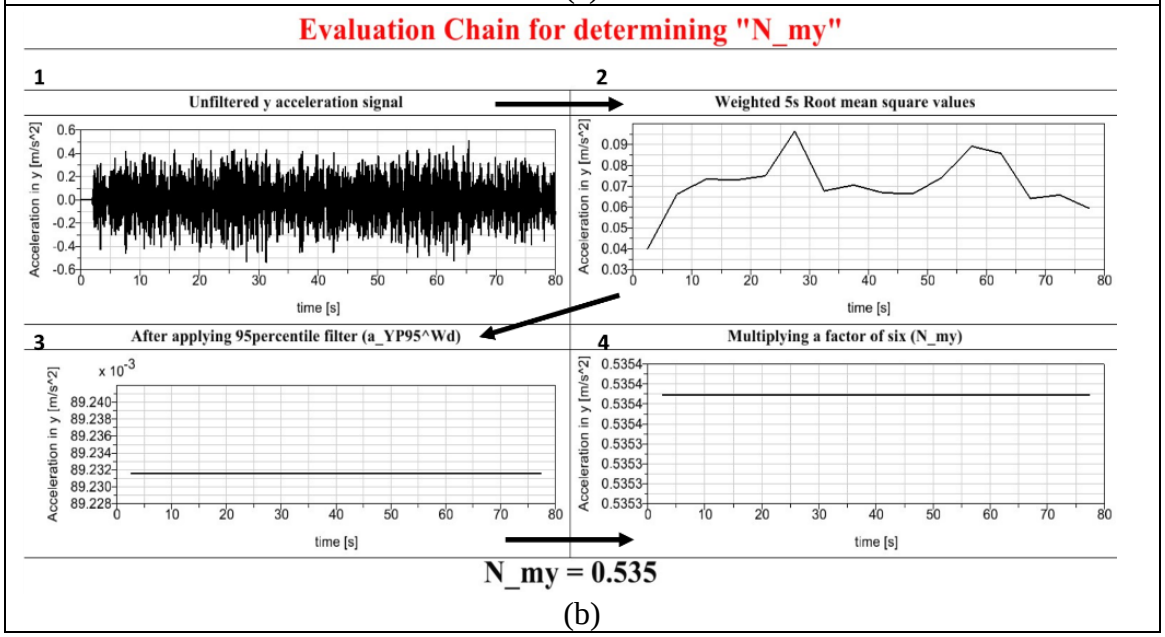

(b)

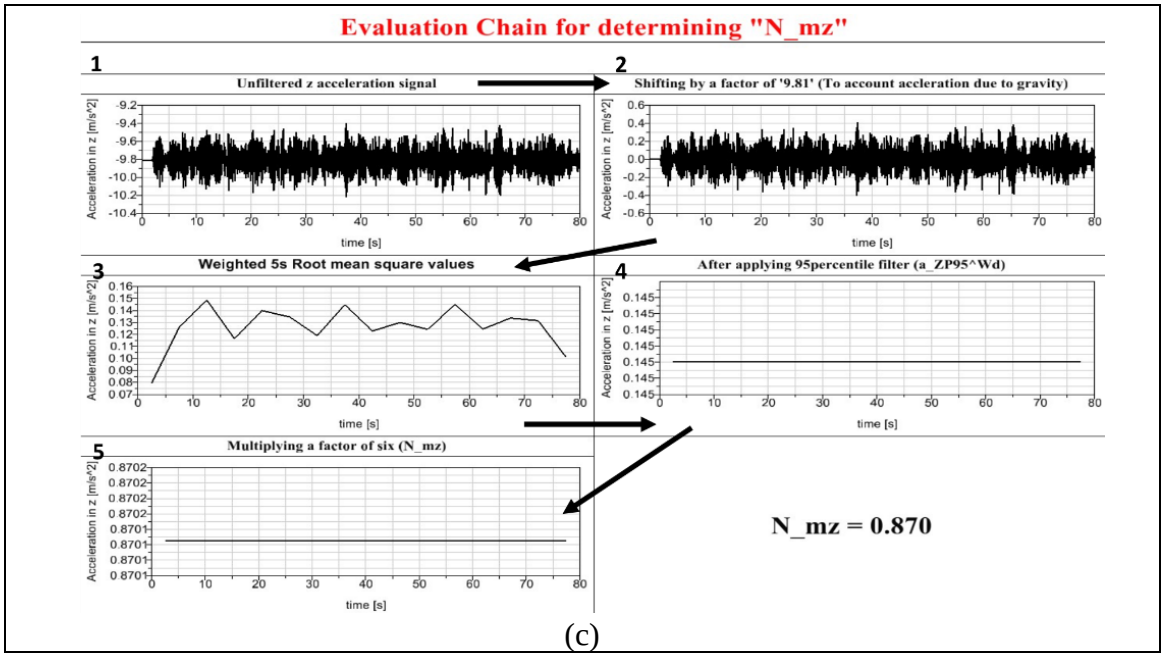

(c)

Figure 6.4: Post-processing steps to calculate acceleration response in the direction of (a) X-axis (b) Y-axis (c) Z-axis

6.2.3 Validation and post-processing

In SIMPACK software, there are different ways to ensure that the model is correct and will run as it should in real-life conditions. One fundamental way to check is by looking at the graphical model and ensuring that all bodies(parts), force elements, joints etc., are in their correct positions. The 'Test call' feature in SIMPACK is the most reliable validation method. This feature gives a detailed description of body position, velocity, acceleration, constraint forces and torques, joint state acceleration etc. If the model setup has been done correctly, all joint state accelerations should be nearly zero, as shown in Figure 6.5.

```
================================================================================
Joint Accelerations:
================================================================================

joint.st.acc($S_Model.$S_Bogie_B.$S_WS_B.$J_WS   ) =   7.9373756E-08  2.2187987E-06  1.4063152E-09 -1.8231157E-06 -1.5472206E-07  7.4727718E-07
joint.st.acc($S_Model.$S_Bogie_B.$S_WS_F.$J_WS   ) =  -7.9067109E-08 -2.2037847E-06  1.4008365E-09  1.8212695E-06  1.2495946E-08 -7.4439021E-07
joint.st.acc($S_Model.$S_Bogie_B.$J_BogieFrame   ) =   2.9577063E-15  2.5351769E-15  5.5647859E-15 -4.2252948E-15  0.0000000E+00  4.9295106E-15
joint.st.acc($S_Model.$S_Bogie_F.$S_WS_B.$J_WS   ) =   2.4879587E-10  6.9792233E-09  2.0024965E-12 -5.7346225E-09 -4.8667279E-10  2.3426998E-09
joint.st.acc($S_Model.$S_Bogie_F.$S_WS_F.$J_WS   ) =  -5.5077634E-10 -1.5498841E-08  7.5317611E-12  1.2808698E-08  8.7884520E-11 -5.1878125E-09
joint.st.acc($S_Model.$S_Bogie_F.$J_BogieFrame   ) =  -1.2783801E-12  2.5351769E-15  0.0000000E+00 -4.2252948E-15  0.0000000E+00  7.4504931E-13
joint.st.acc($S_Model.$J_CB                      ) =   5.2295642E-14  0.0000000E+00  0.0000000E+00  0.0000000E+00  0.0000000E+00 -9.4304979E-14
joint.st.acc($S_Model.$S_Bogie_B.$J_AxleGuide_B_R) =  -4.4615445E-06
joint.st.acc($S_Model.$S_Bogie_B.$J_AxleGuide_B_L) =   3.0393175E-06
joint.st.acc($S_Model.$S_Bogie_B.$J_AxleGuide_F_R) =  -3.1081875E-06
joint.st.acc($S_Model.$S_Bogie_B.$J_AxleGuide_F_L) =   4.5249203E-06
joint.st.acc($S_Model.$S_Bogie_F.$J_AxleGuide_B_R) =  -1.4031388E-08
joint.st.acc($S_Model.$S_Bogie_F.$J_AxleGuide_B_L) =   9.5626286E-09
joint.st.acc($S_Model.$S_Bogie_F.$J_AxleGuide_F_R) =  -2.1900011E-08
joint.st.acc($S_Model.$S_Bogie_F.$J_AxleGuide_F_L) =   3.1782420E-08
joint.st.acc($S_Model.$S_Bogie_F.$J_DummyBolster ) =
joint.st.acc($S_Model.$S_Bogie_B.$J_DummyBolster ) =
```

Figure 6.5: Test call output

Another method to double-check the model is to investigate preload values calculated by the software for attaining equilibrium. Due to symmetry, a similar preload value should come up for similar force elements. Additionally, it is recommended that the maximum residual acceleration should be less than 0.1. Figure 6.6 and Figure 6.7 show the value of calculated preload values and maximum residual acceleration, respectively.

The validity of the presented model has been examined with Wu et al. rigid model in the presence of 5th American track [149] spectra for a vehicle running speed of 200km/h to 350 km/h. Simulation results in terms of equivalent acceleration are compared with Wu et al., shown in Figure 6.8. It can be observed from the graph simulation results

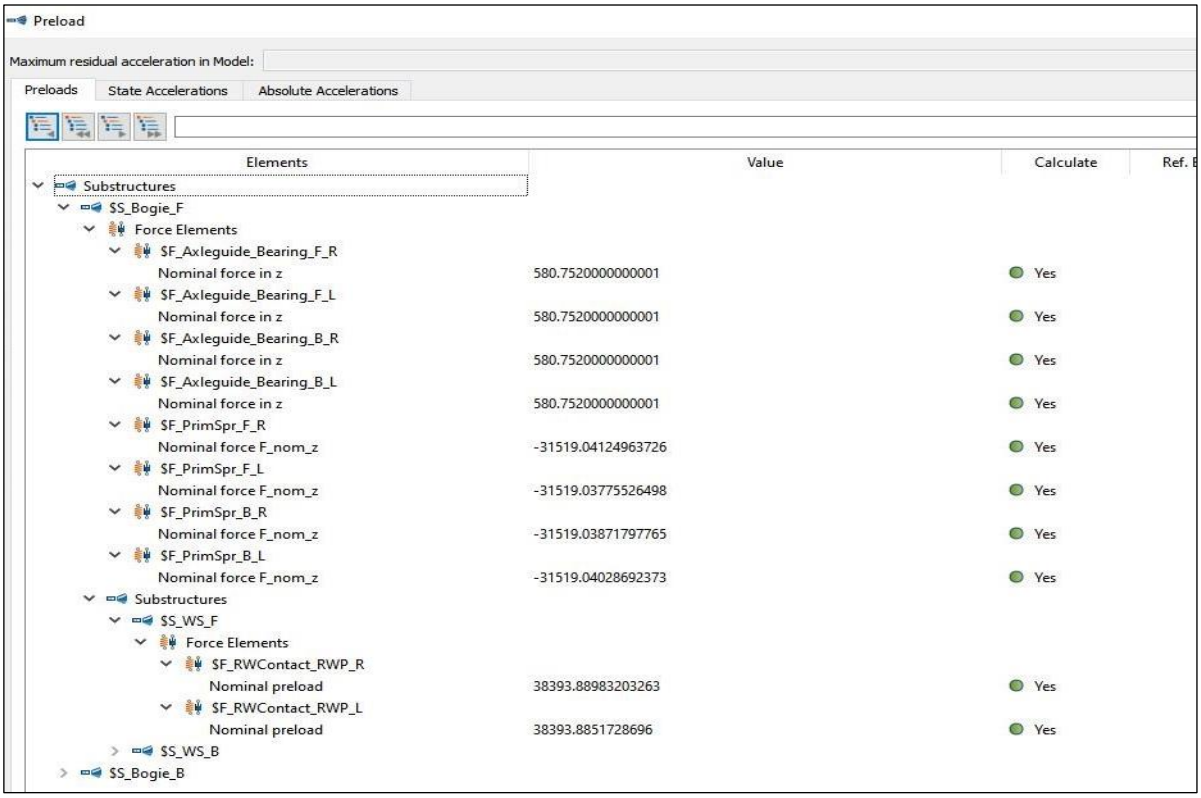

Figure 6.6: Calculated Preload values for attaining equilibrium

Figure 6.7: Maximum residual acceleration in the model

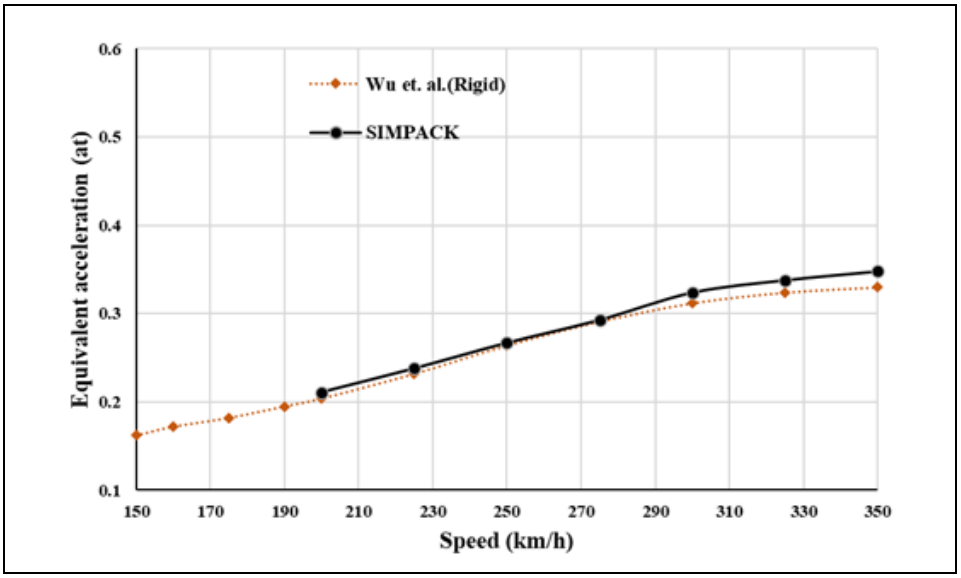

Figure 6.8: Comparison of equivalent acceleration at the centre of rail car floor

obtained from the rigid model show good agreement with the rigid model of Wu et al. up to a speed of 280 km/h. However, given that non-linearities in the suspension element have been taken into account by the SIMPACK model, minimal variance with similar patterns in the data may be seen above 280 km/h. From the acceleration PSD results of Wu et al., It has been found that the rigid model shows similar behaviour to the flexible model below 7.5 Hz; hence rigid model can be used for the comfort analysis if the excitation frequency is less than 7.5 Hz.

6.3 Results and Discussion

Vibration response in the Railway vehicle is influenced by various parameters such as track irregularity, vehicle speed, non-linearity in suspension elements etc. These vibration responses directly affect the moving train's running safety and passenger comfort. As passenger comfort varies from location to location on the car floor surface, a detailed analysis is required to evaluate the passenger ride comfort at different car floor locations by varying the type of track irregularity and running speed.

The first part of this section computes the PSD of acceleration at different rail car floor locations for the different running velocities of railway vehicles. Ride comfort assessment has been done in the second part. To measure the passenger ride comfort, the Authors calculated the N_{mv} index using the EN12299 evaluation method at different locations on the rail-car floor. To evaluate the N_{mv} index, the authors evaluated the acceleration signal by placing the accelerometer sensor at a different position. The accelerometer sensors were placed at Front-left, Front-Right, Rear-Left, Rear-Right, Center-left and Center-Right of the rail-car floor.

6.3.1 PSD of acceleration at different car floor positions

The PSD of the acceleration at various car-floor positions is the cumulative sum of the PSDs under various track irregularity excitations. Vertical, Lateral and combined vertical-lateral track irregularities have been introduced on the left rail only. The contribution of

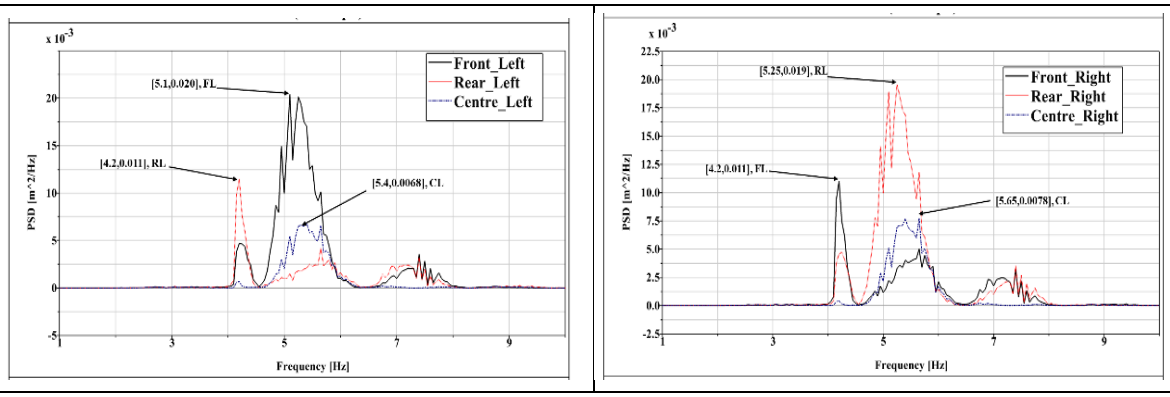

Figure 6.9: PSD curves for Vertical lateral track irregularity_200km/h Left Position, PSD curves for Vertical lateral track irregularity_200km/h Right Position

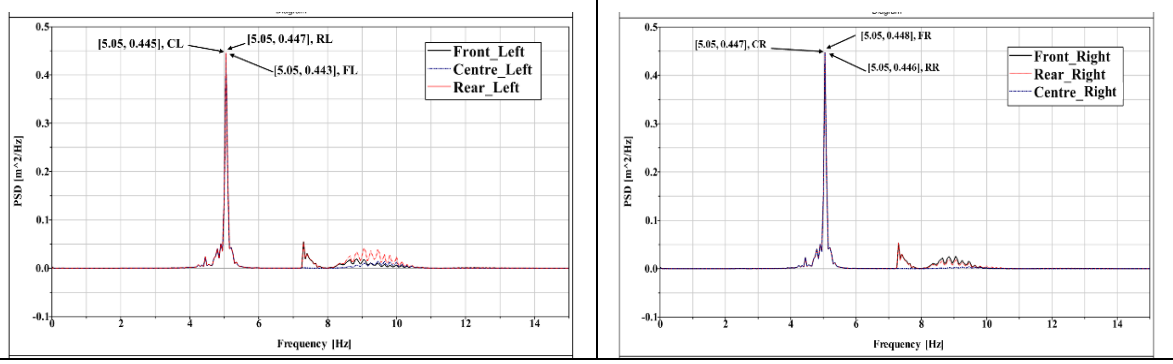

Figure 6.10: PSD curves for Vertical lateral track irregularity_350km/h Left Position, PSD curves for Vertical lateral track irregularity 350km/h Right Position

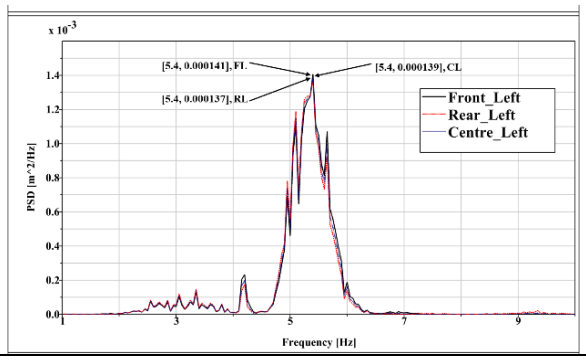

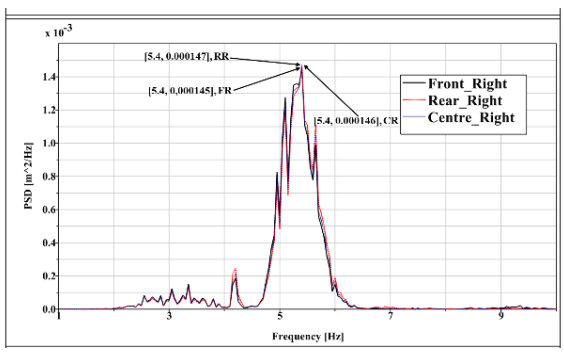

Figure 6.11: PSD curves for Lateral track irregularity_200km/h Left Position, PSD curves for Lateral track irregularity_200km/h Right Position

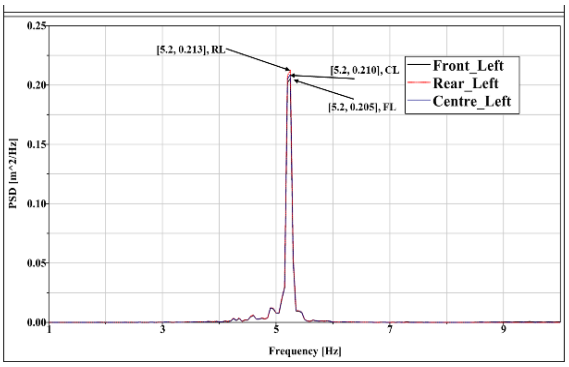

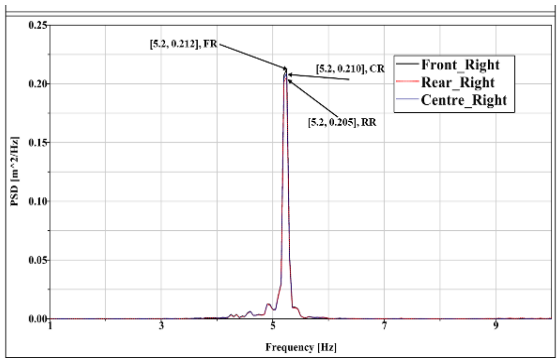

Figure 6.12: PSD curves for Lateral track irregularity_350 km/h Left Position, PSD curves for Lateral track irregularity_350 km/h Right Position

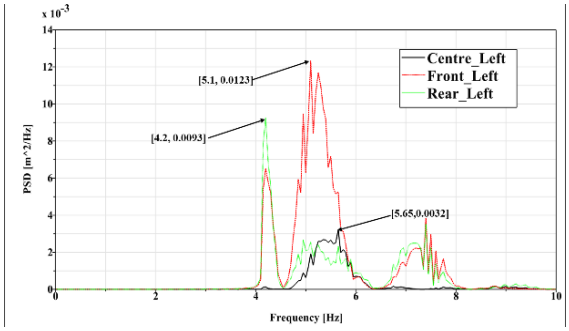

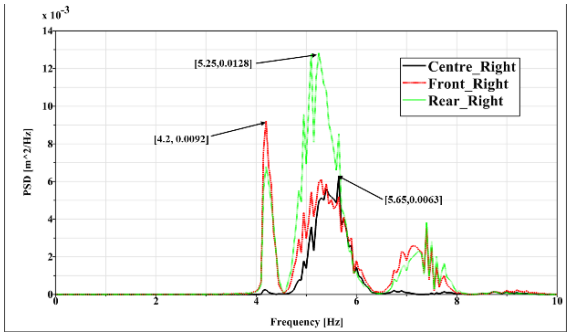

Figure 6.13: PSD curves for Vertical track irregularity_200km/h Left Position, PSD curves for vertical-lateral track irregularity_200km/h Right Position

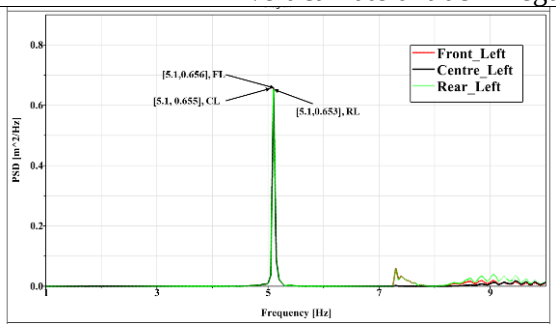

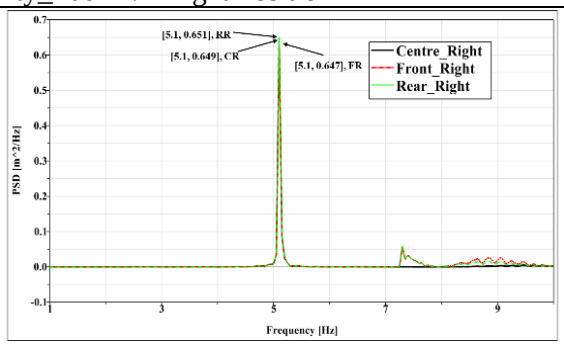

Figure 6.14: PSD curves for Vertical track irregularity_350km/h Left Position, PSD curves for Vertical track irregularity_350km/h Right Position

these irregularities in PSD of acceleration at different floor positions have been examined and illustrated in Figures 6.9-6.14. As irregularities are introduced only on the left rail their influence is felt on the complete rail-car floor, thoroughly investigated in this section.

The effect of combined track irregularities on PSD of acceleration at a different location on the rail car floor at a speed of 200 and 350 km/h has been observed and illustrated in Figures 6.9 & 6.10, respectively. The peak of PSD acceleration has been seen approximately at 5 Hz, possibly due to the mode shape contribution of the car body and bogie. At low speeds, the peak value for PSD acceleration was observed at different frequency values nearby to 5 Hz for different car floor locations, but at high speed, all the peaks were seen at the same frequency value. Lateral irregularity has little influence on the PSD of absolute acceleration, illustrated in Figures 6.11 & 6.12; also, the maximum PSD value is observed at the same frequency value for all car-floor positions at a given speed.

Figures 6.13 and 6.14 show the effect of vertical track irregularity on the PSD of acceleration at different floor positions at a speed of 200 and 350 km/h, respectively. Results show that vertical track irregularity has a prominent effect on PSD of acceleration compared to lateral track irregularity. However, the effect of lateral track irregularity can't be neglected on the curved track. The irregularity introduced on the left rail excites random vibration transferred to the whole car body. Maximum PSD of acceleration obtained at the front left and rear right location of the car floor. Some fluctuation in the results has also been noticed due to the vehicle's geometric filter effect [162]. Also, it is important to note that different rail-car model behaves differently under different track surface conditions.

6.3.2 EN1229-based ride comfort assessment

Case 1:

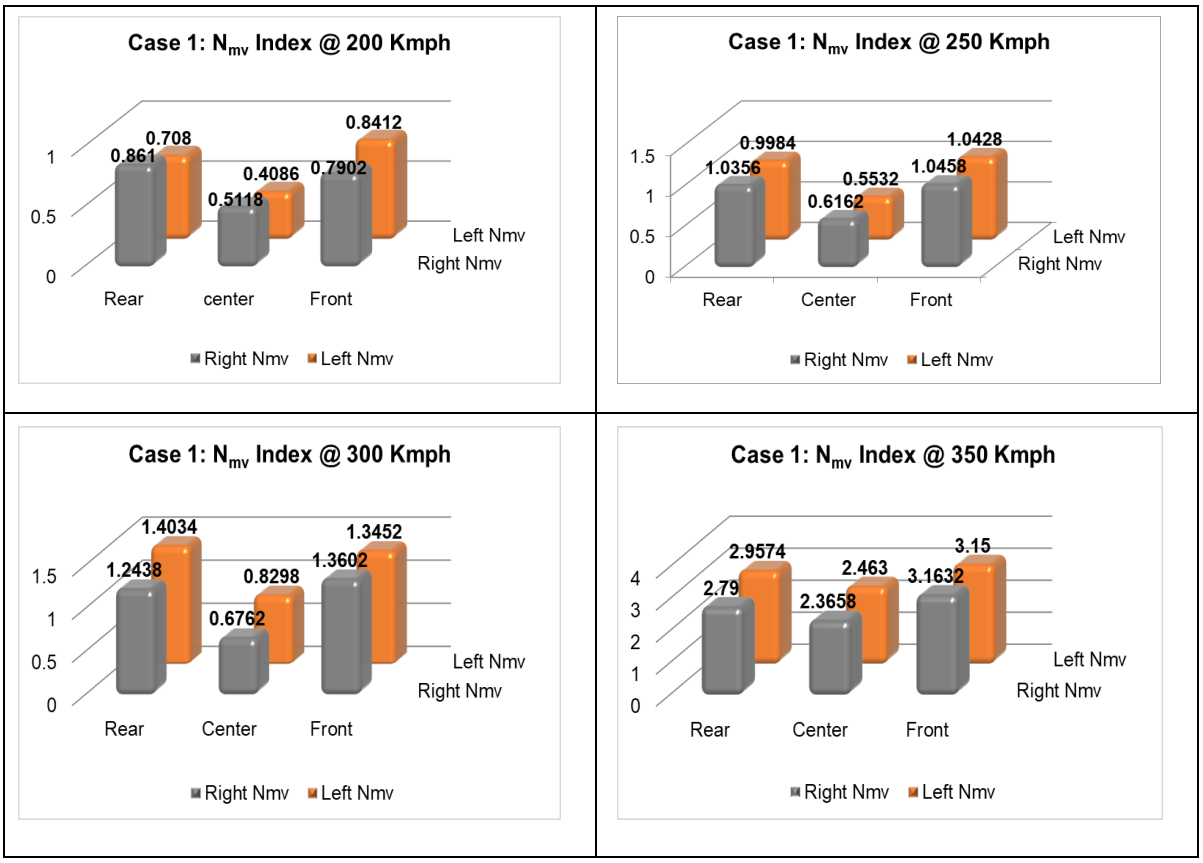

Figure 6.15: The distribution of the N_{mv} index due to vertical track irregularity for different running speed

Figure 6.15 shows the distribution of N_{mv} index at different car floor positions at different operating speeds. As per case 1, vertical track irregularity has been inculcated on the left rail up to 8000m. The figure shows that the left side of the car floor surface has a higher N_{mv} index than the right side due to vertical irregularities on the left rail. A similar type of behaviour has been deduced at all the operating speeds. From the calculated data of N_{mv} Index, it can be observed that the vibrational effects generated from irregularity, introduced on the left side, were transferred to the whole car body. For an operating speed of 200 Km/h, the highest value of N_{mv} index is at the front left and right rear.

Similarly, for an operating speed of 250 km/h, the highest value of N_{mv} index is on the right front side of the vehicle. For operating speed above 300 km/h, the Highest value of

N_{mv} index is at the left rear side of the vehicle. The maximum value of N_{mv} index is always found on the rear and front location of the car floor. However the position of peak N_{mv} may shift from left to right, and vice-versa may be due to the effect of geometry filter or non-linearity in the suspension parameter.

Case 2:

Figure 6.16 shows the distribution of N_{mv} index at various locations on the car floor due to lateral track irregularity. These N_{mv} index data are much lower than the 1.5 limit value up to 300 km/h and close to 1.5 limit value at 350 km/h. At these values of the N_{mv} index, the rider will feel 'very comfortable' as shown in Table 6.2 up to 300 km/h. The index value increases with increasing speed, and at a given speed, it shows the same index value for both the left and right sides of the front, rear and centre position of the car floor. The index value shows less influence of lateral irregularities on the ride comfort when the vehicle moves on a straight track.

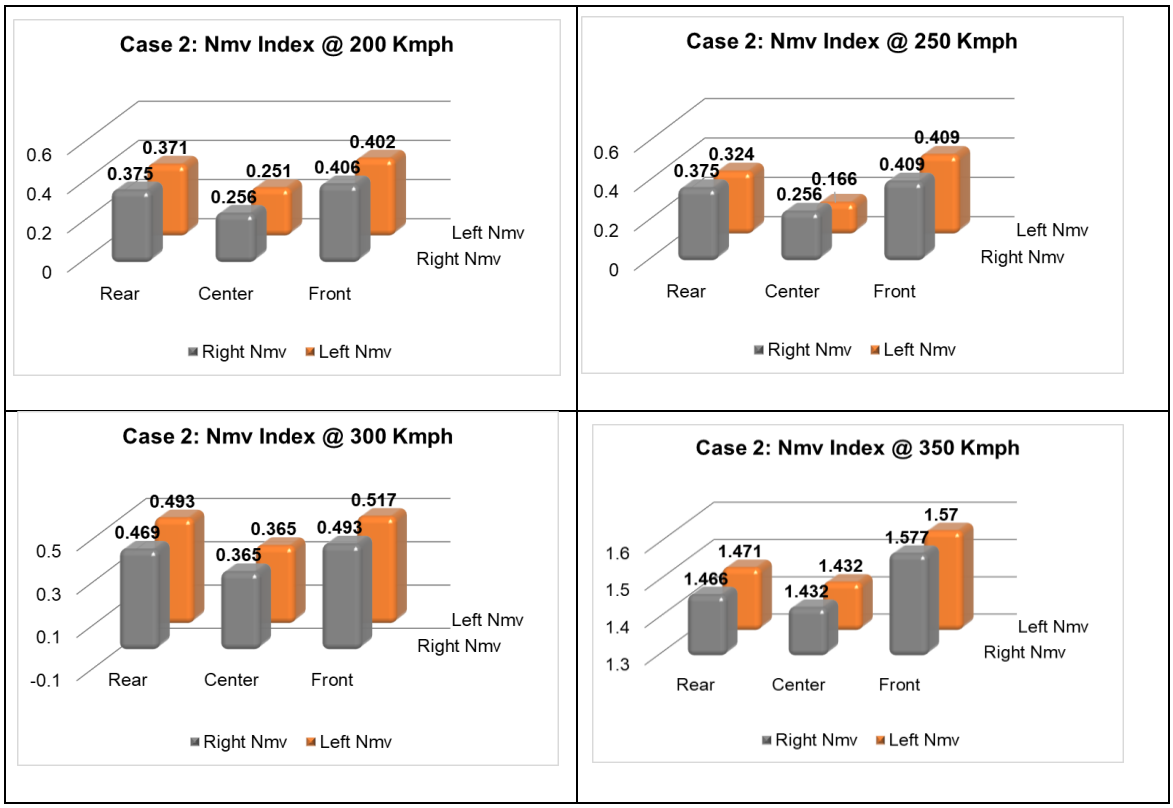

Figure 6.16: The distribution of the N_{mv} index due to lateral track irregularity for different running speed

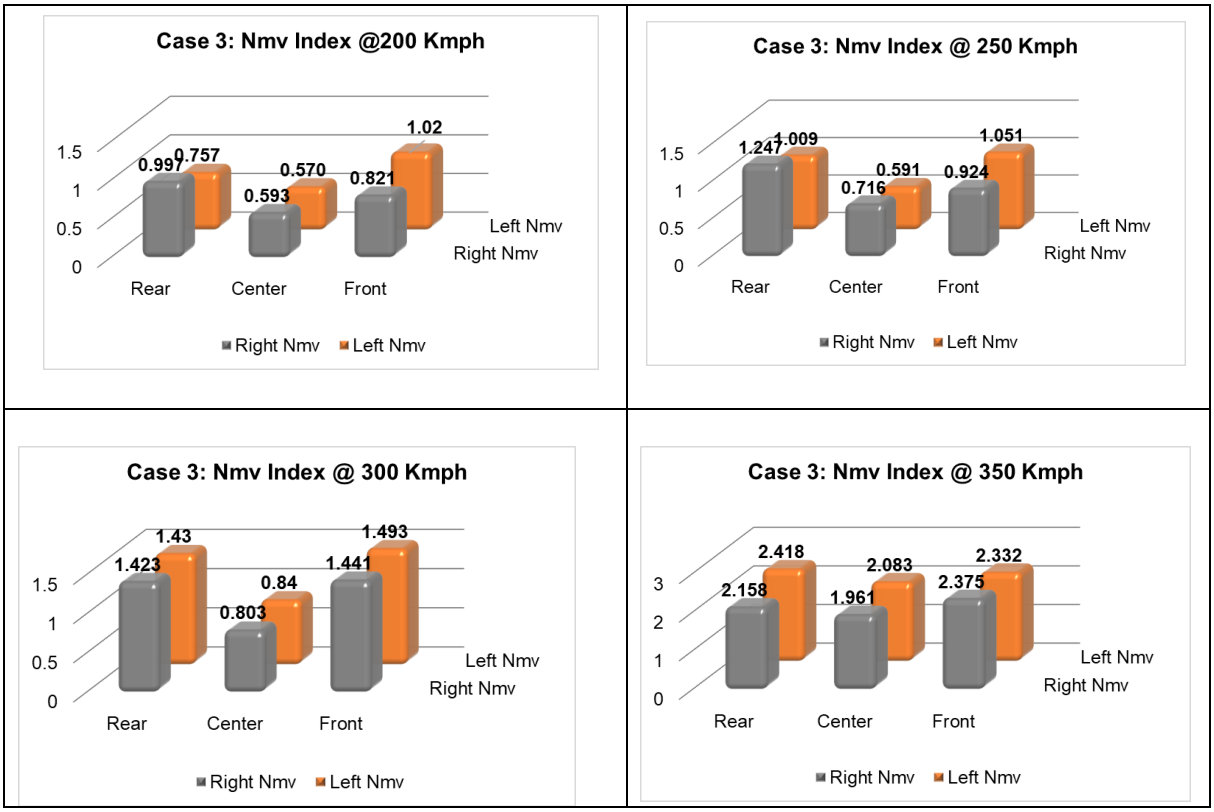

Figure 6.17: The distribution of the N_{mv} index due to combined vertical-lateral track irregularity for different running speed

Case 3:

The distribution of N_{mv} index under the influence of combined track irregularity is shown in Figure 6.17. Index results show that passengers will be in a comfortable zone, even though the comfort index increases with increasing operational speed. Since the track irregularities are introduced on the left rail, the maximum N_{mv} index should be positioned on the left side of the car floor. But from the graph shown in Figure 6.17, it is inferred that critical location (i.e., the position of the highest N_{mv} index) changes with increasing speed. The change in critical position may be due to the cross-wheel momentum transferred at the rail-wheel interface.

6.4 Summary

For various track irregularity conditions, the PSD of acceleration and N_{mv} index have been estimated in this study at various car floor positions at speeds ranging from 200 km/h to

350 km/h. SIMPACK MBS is a very reliable software for developing the 50 DOF high-speed railway vehicle model. The peak value of PSD of absolute acceleration has been obtained approximately at 5Hz, possibly due to the mode shape of the rail car body and bogie.

As irregularity has been introduced only on the left rail, maximum PSD of acceleration and N_{mv} index are found at the front left position in most cases. Still, with increasing speed, the peak values shifted to the right side of the car floor, possibly due to cross-wheel momentum transfer.

N_{mv} index was calculated at different car floor locations at different running speeds and track irregularities. From the simulation results, it has been found that for N_{mv} index less than 1.5 and between 1.5 to 2.5 value, passengers feel 'very comfortable' and 'comfortable', respectively, up to the speed of 300 km/h for a given track irregularity. Still, beyond 300 km/h the N_{mv} value is between 2.5 and 3, which is an 'Acceptable comfort' condition. The results also observed that the maximum value of N_{mv} index was found on the Front-Left location for the speed range of 200-300km/h. But at 350 km/h maximum value of the N_{mv} index was obtained at the Rear-Right and Front-Right locations instead of the front, and the minimum N_{mv} index was obtained at the centre of floor locations.

This study provides a deeper understanding of passenger ride comfort at six car-floor positions and under various track conditions. The same model can be used to determine and analyze passenger comfort in the event of vehicle hunting instability, which has recently received less consideration when assessing ride comfort.

CHAPTER 7

Conclusions and Future Scopes of Study

This chapter presents an overview of the conclusions drawn from the research study on "Dynamic analysis wheel-track interactions for the high train through bond graph" and gives directions that can be carried out in future research.

7.1 Conclusions

The research focused on the characteristics of a railway vehicle, utilizing simulated results obtained through bond graph methodology and SIMPACK Multi-Body Simulation software. Various models were developed, including a single degree of freedom wheel model, a nine degree of freedom high-speed railway vehicle (HSRV) model, a thirty-one degree of freedom HSRV model, and a fifty-degree of freedom HSRV model, to investigate different aspects of railway vehicles. To understand the wheel track interaction dynamics, a two-layer slab track structure and three layer ballasted track structure has also been developed in bond graph. The rail and slab have been developed as an Euler-Bernoulli beams. The rail pad/fasteners, ballast and subgrade were considered as massless spring damping element. The sleepers were modelled as lumped mass elements discretely supported on ballasts. In the presented research work, the wheel-rail contact is given by the nonlinear Hertzian contact theory commonly used in the vertical dynamics of wheel-rail interaction analysis. To calculate the tangential contact forces at wheel-rail interface, Heuristics nonlinear creep model and Polach non linear creep theory has been utilised. Although comparing bond graph methodology with other approaches posed challenges, several distinct advantages of the presented methodologies emerged. The findings provide

a deeper understanding of railway dynamics. The conclusions drawn from the present research are presented below:

- Theoretical modelling of ballasted track and slab track has been developed to study wheel/track interaction and it has been found that for the normal contact problem, Hertzian nonlinear theory is found to be efficient. However, for addressing the non-elliptical contact patch at the wheel-rail interface, non-Hertzian contact theory found more suitable.
- The computational framework of different HSRV model developed through bond graph methodology, provided a valuable insight into the complex dynamics of high-speed trains, aiding in the development of strategies for maintaining safety and integrity in high-speed rail systems. Six distinct cases of wheel irregularity have been examined to investigate how sinusoidal wheel irregularity (with a constant wavelength and varying amplitude) affects the dynamic response at the wheel-rail interface. Additionally, the impact of wheel irregularity on the contact force induced at the wheel-rail interface has been thoroughly investigated.
    - The single degree of freedom wheel model and the nine degree of freedom high-speed railway vehicle model, developed using bondgraph methodology to study the dynamic behavior of high-speed trains under varying speeds and wheel irregularities, have been validated by the results of the Fermer and Nielsen field experiment under low-speed conditions and the SIMPACK simulation results of Wu and Rakheja across the low to high-speed range. The validated results exhibited a strong agreement with both experimental data and SIMPACK simulation within the speed range of 50 km/h to 140 km/h
    - It was observed that between 200 km/h and 250 km/h, the maximum contact force increased rapidly due to rising momentum. However, beyond 250 km/h,

the rate of increase slowed, and the contact force eventually decreased as the wheel speed continued to rise. This change was attributed to the reduced contact time between the wheel irregularity and the rail at higher speeds, which lessened the impact of momentum."

- The dynamic amplification factor (DAF) varied between 1.96 and 3.55 for speeds ranging from 180 km/h to 398 km/h. The higher DAF values could lead to substantial vibrations, underscoring the importance of regular track maintenance.
- Dynamic impact forces at the wheel-rail interface were evaluated and compared for slab and ballasted tracks using a 9-degree-of-freedom railway vehicle model with wheel irregularity on the leading right wheelset. It was found that the dynamic amplification factor (DAF) was 2 to 3 times higher on slab tracks than on ballasted tracks, which is due to the better damping properties of ballasted tracks.

➢ To study the lateral dynamics of HSRV moving on a curved track, a thirty one degree of freedom of HSRV model has been developed using bond graph methodology. Heuristic non-linear creep model and Polach non-linear creep model has been used to study and compare the stability analysis of HSRV model when vehicle is moving on the curve track. Further a transition track has been developed with track irregularity at the end of straight track (i.e. in front of the curve track) to examine the dynamic responses in terms of wheelset lateral force, wheel unloading rate, derailment coefficient and vehicle vertical acceleration. Following points has been summarized from the study.

- The simulation results revealed that the wheelset demonstrated self-sustained oscillatory motion at 257.4 km/h speeds for the heuristic non-linear creep

model and 288 km/h for the Polach non-linear creep model. Stability analysis identified critical speeds for the HSRV using Polach's non-linear creep and Heuristic non-linear creep model. Polach's model indicated a higher critical speed compared to Kalker's model.

- "The research highlighted the effects of alignment irregularity (AL) and cross level irregularity (CL) on the lateral dynamic performance of high-speed railway vehicles. The study examined track irregularities with wavelengths of 3m, 5m, 10m, 20m, and 40m, and amplitudes of 15mm for both types of irregularities. It was found that AL has a significant impact on wheelset lateral force and derailment coefficient, especially for medium to long wavelengths (5m-40m), while CL primarily affects the derailment coefficient at shorter wavelengths and has a lesser impact at longer wavelengths."
- For a 3m wavelength CL, the wheel unloading ratio approached 1, raising concerns about potential roll-over derailment.
- AL has a greater impact on lateral forces and derailment coefficient as the wavelength increases, whereas CL influences vertical acceleration and wheel unloading ratio. This underscores the importance of considering these factors to ensure safety and enhance ride comfort.

➢ Passenger ride comfort becomes a significant concern at high speeds. To address this concern a 50 DOF HSRV model developed and simulated in SIMPACK-multibody simulation software to evaluate the passenger ride comfort under random track irregularity. EN12299-mean comfort standard method has been used to calculate ride comfort under vertical, lateral, and combined track irregularity. From the simulated results following conclusions has been made.

- The power spectral density (PSD) of acceleration and Nmv index has been estimated at various car floor positions for speeds ranging from 200 km/h to 350 km/h using SIMPACK MBS software. Track irregularities introduced on the left rail typically resulted in the highest PSD of acceleration and Nmv index at the front-left position in most cases.
- The peak PSD of absolute acceleration was noted at approximately 5 Hz, likely due to the mode shape of the rail car body and bogie. Since the resonance frequency of the human stomach falls between 4-8 Hz, passengers might experience nausea under these conditions.
- The maximum Nmv index was found at the front-left position for speeds ranging from 200-300km/h. However, at 350 km/h, the highest values shifted to the rear-right and front-right positions, with the lowest values recorded at the centre of the floor. Increasing speed caused the peak values to shift to the right side of the car floor, potentially due to cross-wheel momentum transfer.
- The vertical stiffness of secondary suspension has a greater impact on ride comfort than lateral stiffness. Vertical stiffness of secondary suspension can help to reduce the PSD of acceleration at lower stiffness value (in the range of 10^3 kN/m) thus reducing the N_{mv} index value.
- SIMPACK MBS is a very reliable software for developing the 50 DoF high-speed railway vehicle model.

7.2 Future Scopes of Study

Future research can address the following issues in the field of railway dynamics:

- This thesis presents the effect of wheel irregularity at the wheel rail interface, for a 1-DOF wheel/track model and 9-DOF quarter car model. A 3D full car model could be developed to study the effect of wheel irregularity on passenger ride comfort along with its effect on the lateral dynamics of HSR vehicles including creeping forces and longitudinal creepage.
- The stress analysis can be carried out at the wheel rail interface consisting wheel and track irregularities.
- The presented vehicle model can be used to study the effect of swing motion on passenger ride comfort.
- This research uses Hertzian theory to simulate the interaction between the wheel and track. Researchers frequently employ Hertzian theory, which presupposes single-point contact at the wheel's center, to study the vertical dynamics of railway vehicles at the wheel-rail interface. A non hertzian contact model can be used to simulate the forces that interact between the wheel and the rail, particularly when operating at high speeds.

REFERENCES

LIST OF PUBLICATIONS

REFERENCES

1. Dong RG, Sankar S, Dukkipati R V. (1994) A finite element model of railway track and its application to the wheel flat problem. Proc Inst Mech Eng F J Rail Rapid Transit 208(1):61–72: https://doi.org/10.1243/PIME_PROC_1994_208_234_02.
2. Shabana AA, Zaazaa KE, Sugiyama H. Railroad Vehicle Dynamics. 2007 Jul 23; Available from: http://dx.doi.org/10.1201/9781420045857.
3. Keylin A, Ahmadian M, Taheri M, Tajaddini A (2012). Wheel-Rail Contact Characteristics on a Tangent Track Vs a Roller Rig. ASME 2012 Rail Transportation Division Fall Technical Conference. Oct 16; Available from: http://dx.doi.org/10.1115/rtdf2012-9406.
4. Dukkipati R V., Amyot JR (1988) Computer-aided simulation in railway dynamics. Marcel Dekker, New York.
5. Pacejka HB (1987) Bond graphs in vehicle dynamics. Vehicle System Dynamics. Jan;16(sup1):263–87. Available from: https://doi.org/10.1080/00423118708969178.
6. KARNOPP D (1976). Bond Graphs for Vehicle Dynamics. Vehicle System Dynamics. Oct;5(3):171–84. Available from: http://dx.doi.org/10.1080/00423117608968412.
7. Karnopp DC, Margolis DL, Rosenberg RC (2012). System Dynamics. Feb 8; Available from: http://dx.doi.org/10.1002/9781118152812.
8. A. Mukherjee, R. Karmarkar and A. K. Samantaray (2006). Bondgraph in Modeling Simulation and Fault Identification, I. K. International Publishing House Pvt. Ltd., New Delhi.

9. Correia A, Cunha J, Marcelino J, Caldeira L, Varandas J, Dimitrovová Z, et al (2007). Dynamic analysis of rail track for high-speed trains. 2D approach. Applications of Computational Mechanics in Geotechnical Engineering V. Mar 13; Available from: http://dx.doi.org/10.1201/9781439833414.ch39.

10. Uzzal RUA, Rakheja S, Ahmed W. Dynamic Analysis of Pitch Plane Railway Vehicle-Track Interactions Due to Single and Multiple Wheel Flats. IEEE/ASME/ASCE 2008 Joint Rail Conference. 2008 Jan 1; Available from: http://dx.doi.org/10.1115/jrc2008-63023.

11. Bian J, Gu Y, Murray MH (2013) A dynamic wheel-rail impact analysis of railway track under wheel flat by finite element analysis. Vehicle System Dynamics. https://doi.org/10.1080/00423114.2013.774031.

12. Hou K, Kalousek J, Dong R (2003) A dynamic model for an asymmetrical vehicle/track system. In: Journal of Sound and Vibration.

13. Kumar V, Rastogi V, Pathak PM (2018) Dynamic analysis of vehicle–track interaction due to wheel flat using bond graph. Proceedings of the Institution of Mechanical Engineers, Part K: Journal of Multi-body Dynamics 232:398–412. https://doi.org/10.1177/1464419317739754.

14. Sayeed MdA, Shahin MA (2016). Three-dimensional numerical modelling of ballasted railway track foundations for high-speed trains with special reference to critical speed. Transportation Geotechnics. Mar; 6:55–65. Available from: http://dx.doi.org/10.1016/j.trgeo.2016.01.003.

15. Ling L, Xiao X biao, Xiong J yang, et al (2014) A 3D model for coupling dynamics analysis of high-speed train/track system. Journal of Zhejiang University: Science A 15:964–983. https://doi.org/10.1631/jzus.A1400192.

16. Jin S (2016). Resonance response analysis of the slab track caused by moving vehicle. Journal of Vibroengineering. May 15;18(3):1798–810. Available from: http://dx.doi.org/10.21595/jve.2016.16786.

17. Dai F, Thompson DJ, Zhu Y, Liu X (2014). Vibration properties of slab track installed on a viaduct. Proceedings of the Institution of Mechanical Engineers, Part F: Journal of Rail and Rapid Transit. May 26;230(1):235–52. Available from: http://dx.doi.org/10.1177/0954409714533790.

18. Heydari-Noghabi H, Varandas JN, Esmaeili M, Zakeri J (2017). Investigating the Influence of Auxiliary Rails on Dynamic Behavior of Railway Transition Zone by a 3D Train-Track Interaction Model. Latin American Journal of Solids and Structures.;14(11):2000–18. Available from: http://dx.doi.org/10.1590/1679-78253906.

19. Mazilu T (2009). Interaction between a moving two-mass oscillator and an infinite homogeneous structure: Green's functions method. Archive of Applied Mechanics. Jul 31;80(8):909–27. Available from: http://dx.doi.org/10.1007/s00419-009-0350-x.

20. Hussein MFM, Hunt HEM (2006). Modelling of floating-slab tracks with continuous slabs under oscillating moving loads. Journal of Sound and Vibration. Oct;297(1–2):37–54. Available from: http://dx.doi.org/10.1016/j.jsv.2006.03.026.

21. Feng Q, Lei X, Lian S (2009). Vibration Analysis of High-Speed Railway Slab Track on Soil Subgrade with Geometric Irregularities. International Conference on Transportation Engineering 2009 Jul 29; Available from: http://dx.doi.org/10.1061/41039(345)213.

22. Zhang J, Zhao Y, Zhang Y hui, Jin X song, Zhong W xie, Williams FW, et al (2012). non-stationary random vibration of a coupled vehicle–slab track system using a parallel algorithm based on the pseudo excitation method. Proceedings of the Institution of Mechanical Engineers, Part F: Journal of Rail and Rapid Transit. Aug 29;227(3):203–16. Available from: http://dx.doi.org/10.1177/0954409712458403.

23. Song H, Bian X, Chen Y, Jiang J (2011) An analytical approach for slab track vibration with train-track-ground coupling effect. In: Proceedings of the 8th International Conference on Structural Dynamics, EURODYN 2011.

24. Sadeghi J, Khajehdezfuly A, Esmaeili M, Poorveis D (2016). Dynamic Interaction of Vehicle and Discontinuous Slab Track Considering Nonlinear Hertz Contact Model. Journal of Transportation Engineering. Apr;142(4). Available from: http://dx.doi.org/10.1061/(asce)te.1943-5436.0000823.

25. Cheng YC, Hsu CT (2014). Running Safety and Comfort Analysis of Railway Vehicles Moving on Curved Tracks. International Journal of Structural Stability and Dynamics. Apr 2;14(04):1450004. Available from: http://dx.doi.org/10.1142/s0219455414500047.

26. Cheli F, Corradi R (2011). On rail vehicle vibrations induced by track unevenness: Analysis of the excitation mechanism. Journal of Sound and Vibration. Jul;330(15):3744–65. Available from: http://dx.doi.org/10.1016/j.jsv.2011.02.025.

27. Graa M, Nejlaoui M, Houidi A, Affi Z, Romdhane L (2016). Modelling and Control for Lateral Rail Vehicle Dynamic Vibration with Comfort Evaluation. Advances in Acoustics and Vibration. Sep 2;89–100. Available from: http://dx.doi.org/10.1007/978-3-319-41459-1_9.

28. Farahpour H, Younesian D, Esmailzadeh E (2006). Ride Quality of High-Speed Trains Traveling Over the Corrugated Rails. Rail Transportation. Jan 1; Available from: http://dx.doi.org/10.1115/imece2006-16137.

29. Zhai W, Wang K, Cai C (2009). Fundamentals of vehicle–track coupled dynamics. Vehicle System Dynamics. Oct 14;47(11):1349–76. Available from: http://dx.doi.org/10.1080/00423110802621561.

30. Zhao X, Zhang P, Wen Z (2019). On the coupling of the vertical, lateral and longitudinal wheel-rail interactions at high frequencies and the resulting irregular wear. Wear. Jul;430–431:317–26. Available from: http://dx.doi.org/10.1016/j.wear.2019.05.017.

31. Zhu M, Cheng X, Miao L (2014). Numerical Simulations of Dynamic Responses of High-Speed Trains to Random Track Irregularities. Sustainable Development of Critical Infrastructure. Apr 21; Available from: http://dx.doi.org/10.1061/9780784413470.030.

32. Dižo J, Blatnický M, Steišunas S, Skočilasová B (2018). Assessment of a rail vehicle running with the damaged wheel on a ride comfort for passengers. Vasko M, Handrik M, Jakubovičová L, Kopas P, Blatnický M, Baniari V, et al., editors. MATEC Web of Conferences.;157:03004. Available from: http://dx.doi.org/10.1051/matecconf/201815703004.

33. Rodrigues AF, Dimitrovová Z (2014). Optimization of the behaviour of high-speed railway tracks using a genetic algorithm approach. Proceedings of the Institution of Mechanical Engineers, Part F: Journal of Rail and Rapid Transit. Jun 6;229(4):345–63. Available from: http://dx.doi.org/10.1177/0954409714537252.

34. Dubey SP, Sharma SC, Harsha SP (2018). Finite Element Simulation of Wheel-Rail Interaction: Technical Note. International Journal of Vehicle Structures and Systems. Aug 29;10(3). Available from: http://dx.doi.org/10.4273/ijvss.10.3.13.

35. Zhai W, Wang K (2010). Lateral Hunting Stability of Railway Vehicles Running on Elastic Track Structures. Journal of Computational and Nonlinear Dynamics. Jul 28;5(4). Available from: http://dx.doi.org/10.1115/1.4001908.

36. Mohan A, Ahmadian M (2004). Nonlinear Investigation of the Effect of Primary Suspension on the Hunting Stability of a Rail Wheelset. Joint Rail. Jan 1; Available from: http://dx.doi.org/10.1115/rtd2004-66004.

37. Park JH, Koh HI, Kim NP (2011). Parametric study of lateral stability for a railway vehicle. Journal of Mechanical Science and Technology. Jul;25(7):1657–66. Available from: http://dx.doi.org/10.1007/s12206-011-0421-0.

38. Ahmed AKW, Sankar S (1987). Lateral Stability Behavior of Railway Freight Car System with Elasto-Damper Coupled Wheelset: Part 2—Truck Model. Journal of Mechanisms, Transmissions, and Automation in Design. Dec 1;109(4):500–7. Available from: http://dx.doi.org/10.1115/1.3258828.

39. Polach O (2006). On non-linear methods of bogie stability assessment using computer simulations. Proceedings of the Institution of Mechanical Engineers, Part F: Journal of Rail and Rapid Transit. Jan 1;220(1):13–27. Available from: http://dx.doi.org/10.1243/095440905x33251.

40. Cheng YC, Hsu CT (2011). Hunting stability and derailment analysis of a car model of a railway vehicle system. Proceedings of the Institution of Mechanical Engineers, Part F: Journal of Rail and Rapid Transit. Jul 18;226(2):187–202. Available from: http://dx.doi.org/10.1177/0954409711407658.

41. Lee SY, Cheng YC (2006). Influences of the vertical and the roll motions of frames on the hunting stability of trucks moving on curved tracks. Journal of Sound and Vibration. Jun;294(3):441–53. Available from: http://dx.doi.org/10.1016/j.jsv.2005.10.025.

42. Lee SY, Cheng YC (2005). Hunting stability analysis of high-speed railway vehicle trucks on tangent tracks. Journal of Sound and Vibration. Apr;282(3–5):881–98. Available from: http://dx.doi.org/10.1016/j.jsv.2004.03.050.

43. Wang W, Li GX (2010). Development of a simulation model of a high-speed vehicle for a derailment mechanism. Proceedings of the Institution of Mechanical Engineers, Part F: Journal of Rail and Rapid Transit. Jan 7;224(2):103–13. Available from: http://dx.doi.org/10.1243/09544097jrrt277.

44. Cheng YC, Lee SY, Chen HH (2009). Modeling and nonlinear hunting stability analysis of high-speed railway vehicle moving on curved tracks. Journal of Sound and Vibration. Jul;324(1–2):139–60. Available from: http://dx.doi.org/10.1016/j.jsv.2009.01.053.

45. Nadal FJoseph (1896) Theorie de la stabilite des locomotives. Vve C Dunod et P Vicq.

46. Weinstock H (1984) WHEEL CLIMB DERAILMENT CRITERIA FOR EVALUATION OF RAIL VEHICLE SAFETY. In: American Society of Mechanical Engineers (Paper).

47. Sweet LM, Karmel A, Moy PK (2018). Wheel climb Derailment Criteria Under Steady Rolling and Dynamic Loading Conditions. The Dynamics of Vehicles on roads and on tracks. May 8;496–510. Available from: http://dx.doi.org/10.1201/9780203736845-41.

48. Spinola Barbosa R (2004). A 3D Contact Force Safety Criterion for Flange Climb Derailment of a Railway Wheel. Vehicle System Dynamics. Dec;42(5):289–300. Available from: http://dx.doi.org/10.1080/0042311042000266711.

49. DUKKIPATI RV, NARAYANASWAMY S (2002). Lateral Stability and Steady State Curving Performance of Unconventional Rail Trucks. JSME International Journal Series C.;45(1):176–86. Available from: http://dx.doi.org/10.1299/jsmec.45.176.

50. WICKENS AH (1996). Railway Vehicles with Generic Bogies Capable of Perfect Steering. Vehicle System Dynamics. Jun;25(6):389–412. Available from: http://dx.doi.org/10.1080/00423119608968973.

51. Wang W, Li G xian (2012). Development of high-speed railway vehicle derailment simulation – Part II: Exploring the derailment mechanism. Engineering Failure Analysis. Sep; 24:93–111. Available from: http://dx.doi.org/10.1016/j.engfailanal.2012.02.001.

52. Zboinski K, Dusza M (2010). Extended study of railway vehicle lateral stability in a curved track. Vehicle System Dynamics. Oct 14;49(5):789–810. Available from: http://dx.doi.org/10.1080/00423111003770447.

53. ZENG J, WU P (2004). Stability Analysis of High-Speed Railway Vehicles. JSME International Journal Series C.;47(2):464–70. Available from: http://dx.doi.org/10.1299/jsmec.47.464.

54. Polach O (1999). A Fast Wheel-Rail Forces Calculation Computer Code. Vehicle System Dynamics. Jan 1;33(sup1):728–39. Available from: http://dx.doi.org/10.1080/00423114.1999.12063125.

55. Yung-Chang Cheng; Sen-Yung Lee; Hsing-Hao Chen (2009) Yung-Chang Cheng 2009.pdf. 139–160.

56. Fei Y, Jialin S, Zilong W, Zhou Y, Wahab MA (2022). High-speed train derailment detection under complex track irregularities using a dynamic vehicle-track interaction model. Jun 14; Available from: http://dx.doi.org/10.21203/rs.3.rs-1714659/v1.

57. Choi IIY, Um JH, Lee JS, Choi HH (2012). The influence of track irregularities on the running behavior of high-speed trains. Proceedings of the Institution of Mechanical Engineers, Part F: Journal of Rail and Rapid Transit. Jul 31;227(1):94–102. Available from: http://dx.doi.org/10.1177/0954409712455146.

58. Wickens AH (1965). The dynamic stability of railway vehicle wheelsets and bogies having profiled wheels. International Journal of Solids and Structures. Jul;1(3):319–41. Available from: http://dx.doi.org/10.1016/0020-7683(65)90037-5.

59. Karis T, Berg M, Stichel S (2019). Analysing the correlation between vehicle responses and track irregularities using dynamic simulations and measurements. Proceedings of the Institution of Mechanical Engineers, Part F: Journal of Rail and Rapid Transit. Apr 2;234(2):170–82. Available from: http://dx.doi.org/10.1177/0954409719840450.

60. Karis T, Berg M, Stichel S, Li M, Thomas D, Dirks B (2017). Correlation of track irregularities and vehicle responses based on measured data. Vehicle System Dynamics. Nov 24;56(6):967–81. Available from: http://dx.doi.org/10.1080/00423114.2017.1403634.

61. Cantero D, Basu B (2014). Railway infrastructure damage detection using wavelet transformed acceleration response of traversing vehicle. Structural Control and Health Monitoring [Internet]. Apr 10;22(1):62–70. Available from: http://dx.doi.org/10.1002/stc.1660.

62. Sadeghi J, Rabiee S, Khajehdezfuly A (2019). Effect of Rail Irregularities on Ride Comfort of Train Moving Over Ballast-Less Tracks. International Journal of Structural Stability and Dynamics. Jun;19(06):1950060. Available from:

http://dx.doi.org/10.1142/s0219455419500603.

63. Liu C, Thompson D, Griffin MJ, Entezami M (2019). Effect of train speed and track geometry on the ride comfort in high-speed railways based on ISO 2631-1. Proceedings of the Institution of Mechanical Engineers, Part F: Journal of Rail and Rapid Transit Aug 15;234(7):765–78. Available from: http://dx.doi.org/10.1177/0954409719868050.

64. Youcef K, Sabiha T, El Mostafa D, Ali D, Bachir M (2013). Dynamic analysis of train-bridge system and riding comfort of trains with rail irregularities. Journal of Mechanical Science and Technology. Apr;27(4):951–62. Available from: http://dx.doi.org/10.1007/s12206-013-0206-8.

65. Hung CF, Hsu WL (2017). Influence of long-wavelength track irregularities on the motion of a high-speed train. Vehicle System Dynamics. Jun 30;56(1):95–112. Available from: http://dx.doi.org/10.1080/00423114.2017.1346261.

66. Hung CF, Hsu WL (2017). Influence of long-wavelength track irregularities on the motion of a high-speed train. Vehicle System Dynamics. Jun 30;56(1):95–112. Available from: http://dx.doi.org/10.1080/00423114.2017.1346261.

67. Kumar V, Rastogi V, Pathak P (2018). Modelling and evaluation of the hunting behaviour of a high-speed railway vehicle on curved track. Proceedings of the Institution of Mechanical Engineers, Part F: Journal of Rail and Rapid Transit. Jul 29;233(2):220–36. Available from: http://dx.doi.org/10.1177/0954409718789531.

68. Shoenberger RW, Harris CS (1971). Psychophysical Assessment of Whole-Body Vibration. Human Factors: The Journal of the Human Factors and Ergonomics Society. Feb;13(1):41–50. Available from: http://dx.doi.org/10.1177/001872087101300106.

69. GRIFFIN MJ, WHITHAM EM, PARSONS KC (1982). Vibration and comfort I. Translational seat vibration. Ergonomics. Jul;25(7):603–30. Available from: http://dx.doi.org/10.1080/00140138208925023.

70. Carlbom P, Berg M (2003) Passengers, seats and car body in rail vehicle dynamics. In: Vehicle System Dynamics.

71. Stanica DI, Dumitriu M (2019). Critical points numerical analysis of ride comfort of the flexible railway car body. IOP Conference Series: Materials Science and Engineering. Nov 1;682(1):012004. Available from: http://dx.doi.org/10.1088/1757-899x/682/1/012004.

72. Suzuki H (1998). Effects of the range and frequency of vibrations on the momentary riding comfort evaluation of a railway vehicle. Japanese Psychological Research. Sep;40(3):156–65. Available from: http://dx.doi.org/10.1111/1468-5884.00087.

73. Wei X, Liu Y, Sun Q, Jia L, Wang Y (2013). Rail vehicle ride comfort prediction based on bogie acceleration measurements. 25th Chinese Control and Decision Conference (CCDC). 2013 May; Available from: http://dx.doi.org/10.1109/ccdc.2013.6561613.

74. Kim YG, Kwon HB, Kim SW, Kim CK, Kim TW (2003). Correlation of ride comfort evaluation methods for railway vehicles. Proceedings of the Institution of Mechanical Engineers, Part F: Journal of Rail and Rapid Transit. Mar 1;217(2):73–88. Available from: http://dx.doi.org/10.1243/095440903765762823.

75. Dumitriu M, Leu M (2018). Correlation between Ride Comfort Index and Sperling's Index for Evaluation Ride Comfort in Railway Vehicles. Applied Mechanics and Materials. Mar; 880:201–6. Available from: http://dx.doi.org/10.4028/www.scientific.net/amm.880.201.

76. Loach JC (1958). A New Method of Assessing the Riding of Vehicles and Some Results Obtained. Journal of the Institution of Locomotive Engineers. Mar;48(262):183–240. Available from: http://dx.doi.org/10.1243/jile_proc_1958_048_028_02.

77. Sperling E BC (1956) Contribution to the evaluation of ride comfort in rail vehicles. Glasers Annalen 80(10):314–317.

78. Dumitriu Madalina GMA (2016) Evaluation of the ride quality and ride comfort in railway vehicles based on the index Wz. International Journal of Engineering 13(3):123–132.

79. (1993) B153/RP21. Application of ISO Standard to Railway Vehicles: Comfort Index Nmv-Comparison with the ISO/SNCF Comfort Note and with the Wz. The Netherlands.

80. (1981) B153/RP1-RP20. Application of ISO Standard to Railway Vehicles. Netherland.

81. (1994) UIC 513R. Guidelines for Evaluating Passenger Comfort in Relation to Vibration in Railway Vehicles. France.

82. Railway applications. Ride comfort for passengers. Measurement and evaluation. Available from: http://dx.doi.org/10.3403/30153019u.

83. Mechanical vibration. Measurement and analysis of whole-body vibration to which passengers and crew are exposed in railway vehicles. Available from: http://dx.doi.org/10.3403/02391233u.

84. Suzuki H (1998). Research trends on riding comfort evaluation in Japan. Proceedings of the Institution of Mechanical Engineers, Part F: Journal of Rail and Rapid Transit. Jan 1;212(1):61–72. Available from: http://dx.doi.org/10.1243/0954409981530689.

85. Gangadharan KV SC and R V. (2004) Experimental and analytical ride comfort evaluation of a railway coach. In: In: A conference & exposition on structural dynamics (SEM ORG IMAC XXII). Society for Experimental Mechanics., Dearborn, Michigan, pp 1–15.

86. Kim YG, Choi S, Kim SW, et al (2009) An experimental study on the ride comfort of the Korean high-speed train. Exp Tech 33:30–37. https://doi.org/10.1111/j.1747-1567.2008.00419.x

87. Munawir TIT, Samah AAA, Rosle MAA, Azlis-Sani J, Hasnan K, Sabri SM, et al (2017). A Comparison Study on the Assessment of Ride Comfort for LRT Passengers. IOP Conference Series: Materials Science and Engineering. Aug; 226:012039. Available from: http://dx.doi.org/10.1088/1757-899x/226/1/012039.

88. Dumitriu M, Stănică DI (2021). Study on the Evaluation Methods of the Vertical Ride Comfort of Railway Vehicle—Mean Comfort Method and Sperling's Method. Applied Sciences. Apr 27;11(9):3953. Available from: http://dx.doi.org/10.3390/app11093953.

89. Kumar V, Rastogi V, Pathak P (2016). Simulation for whole-body vibration to assess ride comfort of a low–medium speed railway vehicle. SIMULATION. Nov 28;93(3):225–36. Available from: http://dx.doi.org/10.1177/0037549716679254.

90. Jiang Y, Chen BK, Thompson C (2019). A comparison study of ride comfort indices between Sperling's method and EN 12299. International Journal of Rail Transportation. May 12;7(4):279–96. Available from: http://dx.doi.org/10.1080/23248378.2019.1616329.

91. Haladin I, Lakusic S, Bobut M (2019) Overview and analysis of methods for assessing ride comfort on tram tracks. Journal of the Croatian Association of Civil Engineers 71:901–921. https://doi.org/10.14256/JCE.2731.2019.

92. Evans J, Berg M (2009). Challenges in simulation of rail vehicle dynamics. Vehicle System Dynamics. Aug;47(8):1023–48. Available from: http://dx.doi.org/10.1080/00423110903071674.

93. Galvín P, Romero A, Domínguez J (2010). Vibrations induced by HST passage on ballast and non-ballast tracks. Soil Dynamics and Earthquake Engineering. Sep;30(9):862–73. Available from: http://dx.doi.org/10.1016/j.soildyn.2010.02.004.

94. Kouroussis G, Verlinden O, Conti C (2011) Free field vibrations caused by high-speed lines: Measurement and time domain simulation. Soil Dynamics and Earthquake Engineering 31: https://doi.org/10.1016/j.soildyn.2010.11.012.

95. Xue FC, Zhang JM (2015) Attenuations of acceleration spectra of high-speed railway embankment subjected to moving loads. Yantu Lixue/Rock and Soil Mechanics 36:445–451. https://doi.org/10.16285/j.rsm.2015.S1.077.

96. Paynter Henry M. (1961) Analysis and design of engineering systems. Cambridge, Mass.: M.I.T. Press.

97. Banerjee N, Karmakar R (2007). Bond Graph Modeling of Rail Wheelset on Curved Track. SIMULATION. Oct;83(10):695–706. Available from: http://dx.doi.org/10.1177/0037549707084489.

98. Saha* AK, Karmakar R, Bhattacharyya R (2007). Lateral Dynamics of a Railway Truck on Flexible Tangent Track. Vibration Problems ICOVP. 339–45. Available from: http://dx.doi.org/10.1007/978-1-4020-9100-1_35.

99. Banerjee N, Saha AK, Karmakar R, Bhattacharyya R (2009). Bond graph modelling of a railway truck on curved track. Simulation Modelling Practice and Theory. Jan;17(1):22–34. Available from: http://dx.doi.org/10.1016/j.simpat.2008.02.001.

100. Banerjee N, Karmakar R (2014). Modelling of a free rail wheelset using non-linear creep force. International Journal of Heavy Vehicle Systems.;21(4):310. Available from: http://dx.doi.org/10.1504/ijhvs.2014.068101.

101. Lozano J, Félez J, Mera JM, Sanz J de D (2010). Using Bond-Graph Technique for Modelling and Simulating Railway Drive Systems. 2010 12th International Conference on Computer Modelling and Simulation. Mar; Available from: http://dx.doi.org/10.1109/uksim.2010.88.

102. Margolis D, Shim T (2001). A bond graph model incorporating sensors, actuators, and vehicle dynamics for developing controllers for vehicle safety. Journal of the Franklin Institute. Jan;338(1):21–34. Available from: http://dx.doi.org/10.1016/s0016-0032(00)00068-5.

103. Kumar V, Rastogi V (2009) Investigation of vertical dynamic behaviour and modelling of a typical Indian rail road vehicle through bond graph. World Journal of Modelling and Simulation 5:130–138.

104. Kumar V, Rastogi V (2020) Lateral dynamic analysis of rail road vehicle through bond graph modeling. 14th National Conference on Machines and Mechanisms, NaCoMM 2009 345–352

105. Kumar V, Rastogi V, Pathak P (2017). Dynamic analysis of vehicle–track interaction due to wheel flat using bond graph. Proceedings of the Institution of Mechanical Engineers, Part K: Journal of Multi-body Dynamics. Nov 7;232(3):398–412. Available from: http://dx.doi.org/10.1177/1464419317739754.

106. Patel Y, Rastogi V, Borutzky W (2022). Simulation study on the influence of wheel irregularity on the vertical dynamics of wheel–rail interaction for high-speed railway track using bond graph. SIMULATION. Dec 1;99(6):643–56. Available from: http://dx.doi.org/10.1177/00375497221138943.

107. Wu X, Rakheja S, Ahmed A, Chi M (2017). Influence of a flexible wheelset on the dynamic responses of a high-speed railway car due to a wheel flat. Proceedings of the Institution of Mechanical Engineers, Part F: Journal of Rail and Rapid Transit. May 16;232(4):1033–48. Available from: http://dx.doi.org/10.1177/0954409717708895.

108. Jelila YD, Lemu HG (2021). Study of Wheel-Rail Contacts at Railway Turnout Using Multibody Dynamics Simulation Approach. Advanced Manufacturing and Automation X.;371–9. Available from: http://dx.doi.org/10.1007/978-981-33-6318-2_46

109. Du G, Han F, Fan X, Li Y, Liang T (2021). Dynamic simulation analysis of rail track and track structure based on SIMPACK and ABAQUS. Wang L, Yepes V, editors. E3S Web of Conferences.;248:03007. Available from: http://dx.doi.org/10.1051/e3sconf/202124803007.

110. Bosso N, Zampieri N (2018). A Novel Analytical Method to Calculate Wheel-Rail Tangential Forces and Validation on a Scaled Roller-Rig. Advances in Tribology. Aug 9; 2018:1–11. Available from: http://dx.doi.org/10.1155/2018/7298236.

111. A. Mukherjee (2006) Users Manual of SYMBOLS Shakti. High Tech Consultants, STEP, Indian Institute of Technology, Kharagpur.

112. Montenegro PA, Calçada R (2023). Wheel–rail contact model for railway vehicle–structure interaction applications: development and validation. Railway Engineering Science. Apr 24;31(3):181–206. Available from: http://dx.doi.org/10.1007/s40534-023-00306-4.

113. Michas G (2012) Slab Track Systems for High-Speed Railways. MSc Thesis 95.

114. Wu TX, Thompson DJ (2004) The effects of track non-linearity on wheel/rail impact. Proc Inst Mech Eng F J Rail Rapid Transit 218:1–16. https://doi.org/10.1243/095440904322804394.

115. Hodas S [2014]. Design of Railway Track for Speed and High-speed Railways. Procedia Engineering. 91:256–61. Available from: http://dx.doi.org/10.1016/j.proeng.2014.12.056.

116. Fermér M, Nielsen JCO (1995). Vertical Interaction between Train and Track with Soft and Stiff Railpads—Full-Scale Experiments and Theory. Proceedings of the Institution of Mechanical Engineers, Part F: Journal of Rail and Rapid Transit. Jan;209(1):39–47. Available from: http://dx.doi.org/10.1243/pime_proc_1995_209_253_02.

117. Dukkipati RV, Dong R (1999). Impact Loads due to Wheel Flats and Shells. Vehicle System Dynamics. Jan 1;31(1):1–2. Available from: http://dx.doi.org/10.1076/vesd.31.1.1.2097.

118. Margolis DL (1985). A survey of bond graph modelling for interacting lumped and distributed systems. Journal of the Franklin Institute.Jan;319(1–2):125–35. Available from: http://dx.doi.org/10.1016/0016-0032(85)90069-9.

119. Karnopp DC, Margolis DL, Rosenberg RC (2012). System Dynamics. Feb 8; Available from: http://dx.doi.org/10.1002/9781118152812.

120. Dahlberg T (2006). Track Issues. Handbook of Railway Vehicle Dynamics. May 22;143–79. Available from: http://dx.doi.org/10.1201/9781420004892.ch6.

121. Spiryagin M, Cole C, Sun YQ, McClanachan M, Spiryagin V, McSweeney T (2014). Design and Simulation of Rail Vehicles. CRC Press; Available from: http://dx.doi.org/10.1201/b17029.

122. Zhang W (2020). Dynamic modelling of coupled systems in the high-speed train. Dynamics of Coupled Systems in High-Speed Railways. ;55–181. Available from: http://dx.doi.org/10.1016/b978-0-12-813375-0.00002-9

123. Shi H, Yu Z, Shi H (2016). An improved method for dynamic modelling of a slab track on a high-speed railway. Computers in Railways XV: Railway Engineering Design and Operation. Jul 19; Available from: http://dx.doi.org/10.2495/cr160211.

124. Antolín P, Zhang N, Goicolea JM, Xia H, Astiz MÁ, Oliva J (2013). Consideration of nonlinear wheel–rail contact forces for dynamic vehicle–bridge interaction in high-speed railways. Journal of Sound and Vibration. Mar;332(5):1231–51. Available from: http://dx.doi.org/10.1016/j.jsv.2012.10.022.

125. Gu Q, Liu Y, Guo W, Li W, Yu Z, Jiang L (2019). A Practical Wheel-Rail Interaction Element for Modelling Vehicle-Track-Bridge Systems. International Journal of Structural Stability and Dynamics. Feb;19(02):1950011. Available from: http://dx.doi.org/10.1142/s0219455419500111.

126. Cai Y, Cao Z, Sun H, Xu C (2010). Effects of the dynamic wheel–rail interaction on the ground vibration generated by a moving train. International Journal of Solids and Structures. Aug;47(17):2246–59. Available from: http://dx.doi.org/10.1016/j.ijsolstr.2010.04.013.

127. Pombo JC, Ambrósio JAC. A Hertzian Contact Formulation for the Wheel-Rail Contact Problem in Railway Dynamics. III European Conference on Computational Mechanics. :774–774. Available from: http://dx.doi.org/10.1007/1-4020-5370-3_774.

128. Hertz H (1881) The contact of elastic solids. J Reine Angew, Math 92:156–171

129. Zhang X, Thompson DJ, Li Q, Kostovasilis D, Toward MGR, Squicciarini G, et al (2019). A model of a discretely supported railway track based on a 2.5D finite element approach. Journal of Sound and Vibration. Jan; 438:153–74. Available from: http://dx.doi.org/10.1016/j.jsv.2018.09.026.

130. Ma X, Jing L, Han L (2018). A computational simulation study on the dynamic response of high-speed wheel–rail system in rolling contact. Advances in Mechanical Engineering Nov;10(11): 168781401880921.Available from: http://dx.doi.org/10.1177/1687814018809215.

131. Han L, Jing L, Liu K (2017) A dynamic simulation of the wheel–rail impact caused by a wheel flat using a 3-D rolling contact model. Journal of Modern Transportation 25:124–131. https://doi.org/10.1007/s40534-017-0131-0.

133. Srivastava JP, Sarkar PK, Kiran MR, Ranjan V (2018). A numerical study on effects of friction-induced thermal load for rail under varied wheel slip conditions. SIMULATION. Jul 2;95(4):351–62. Available from: http://dx.doi.org/10.1177/0037549718782629.

133. Srivastava JP, Sarkar PK, Ranjan V (2014). Contact Stress Analysis in Wheel–Rail by Hertzian Method and Finite Element Method. Journal of The Institution of Engineers (India): Series C. Sep 2;95(4):319–25. Available from: http://dx.doi.org/10.1007/s40032-014-0145-x.

134. Han L, Jing L, Zhao L (2017). Finite element analysis of the wheel–rail impact behavior induced by a wheel flat for high-speed trains: The influence of strain rate. Proceedings of the Institution of Mechanical Engineers, Part F: Journal of Rail and Rapid Transit. Apr 18;232(4):990–1004. Available from: http://dx.doi.org/10.1177/0954409717704790.

135. Newton SG, Clark RA (1979). An Investigation into the Dynamic Effects on the Track of Wheel flats on Railway Vehicles. Journal of Mechanical Engineering Science. Aug;21(4):287–97. Available from: http://dx.doi.org/10.1243/jmes_jour_1979_021_046_02.

136. Uzzal M (2012). Analysis of a three-dimensional railway vehicle-track system and development of a smart wheelset. PhD Thesis, Concordia University, Canada, 2012.

137. Enblom R, Berg M (2005). Simulation of railway wheel profile development due to wear—influence of disc braking and contact environment. Wear. Mar;258(7–8):1055–63. Available from: http://dx.doi.org/10.1016/j.wear.2004.03.055.

138. Sun Y, Zhai W, Guo Y (2018). A robust non-Hertzian contact method for wheel–rail normal contact analysis. Vehicle System Dynamics. Feb 21;56(12):1899–921. Available from: http://dx.doi.org/10.1080/00423114.2018.1439587.

139. Sun Y, Ling L (2021). An optimal tangential contact model for wheel-rail non-Hertzian contact analysis and its application in railway vehicle dynamics simulation. Vehicle System Dynamics. Jun 15;60(9):3240–68. Available from: http://dx.doi.org/10.1080/00423114.2021.1942078.

140. Sebès M, Chollet H, Ayasse JB, Chevalier L (2014). A multi-Hertzian contact model considering plasticity. Wear. Jun;314(1–2):118–24. Available from: http://dx.doi.org/10.1016/j.wear.2013.11.036.

141. Kalker JJ, Johnson KL (1993). Three-Dimensional Elastic Bodies in Rolling Contact. Journal of Applied Mechanics. Mar 1;60(1):255–255. Available from: http://dx.doi.org/10.1115/1.2900773.

142. Fang C, Jaafar SA, Zhou W, Yan H, Chen J, Meng X (2023). Wheel-rail contact and friction models: A review of recent advances. Proceedings of the Institution of Mechanical Engineers, Part F: Journal of Rail and Rapid Transit. Feb 9;237(10):1245–59. Available from: http://dx.doi.org/10.1177/09544097231156730.

143. KALKER JJ (1982). A Fast Algorithm for the Simplified Theory of Rolling Contact. Vehicle System Dynamics Feb;11(1):1–13. Available from: http://dx.doi.org/10.1080/00423118208968684.

144. Kim P, Jung J, Seok J (2011). A parametric dynamic study on hunting stability of full dual-bogie railway vehicle. International Journal of Precision Engineering and Manufacturing. Jun;12(3):505–19. Available from: http://dx.doi.org/10.1007/s12541-011-0064-1.

145. DUKKIPATI RV (1998). Dynamics of a Wheelset on Roller Rig. Vehicle System Dynamics. Dec;30(6):409–30. Available from: http://dx.doi.org/10.1080/00423119808969458.

146. Spiryagin M, Polach O, Cole C (2013). Creep force modelling for rail traction vehicles based on the Fastsim algorithm. Vehicle System Dynamics. Nov;51(11):1765–83. Available from: http://dx.doi.org/10.1080/00423114.2013.826370.

147. Lei X (2017). High Speed Railway Track Dynamics. Springer Singapore; Available from: http://dx.doi.org/10.1007/978-981-10-2039-1.

148. Dong R (1994) Vertical Dynamics of Railway Vehicle-Track System. 1–257

149. ANG KK, DAI J, TRAN MT, LUONG VH (2014). ANALYSIS OF HIGH-SPEED RAIL ACCOUNTING FOR JUMPING WHEEL PHENOMENON. International Journal of Computational Methods. Jun;11(03):1343007. Available from: http://dx.doi.org/10.1142/s021987621343007x.

150. Yan W, Fischer FD (2000). Applicability of the Hertz contact theory to rail-wheel contact problems. Archive of Applied Mechanics (Ingenieur Archiv). May 23;70(4):255–68. Available from: http://dx.doi.org/10.1007/s004199900035.

151. Gohar R, Rahnejat H (2017). Fundamentals of Tribology. WORLD SCIENTIFIC (EUROPE); Available from: http://dx.doi.org/10.1142/q0152.

152. Johnson KL (1985) Contact Mechanics. Cambridge University Press, Cambridge.

153. Renger A. Johnson, K. L., Contact Mechanics. Cambridge etc., Cambridge University Press 1985. XII, 452 pp., £ 17.50 P/B. ISBN 0521347963. ZAMM - Journal of Applied Mathematics and Mechanics / Zeitschrift für Angewandte Mathematik und Mechanik. 1989 Jan;69(7):214–214. Available from: http://dx.doi.org/10.1002/zamm.19890690713.

154. Kumar V, Rastogi V, Pathak P (2017). Dynamic analysis of vehicle–track interaction due to wheel flat using bond graph. Proceedings of the Institution of Mechanical Engineers, Part K: Journal of Multi-body Dynamics. Nov 7;232(3):398–412. Available from: http://dx.doi.org/10.1177/1464419317739754

155. Dukkipati R V, Amyot JR (1988) Computer-aided simulation in railway dynamics. Marcel Dekker, New York.

156. ISHIDA H, MATSUO M (1999). Safety Criteria for Evaluation of Railway Vehicle Derailment. Quarterly Report of RTRI.;40(1):18–25. Available from: http://dx.doi.org/10.2219/rtriqr.40.18.

157. Guarro SB (1994). Reliability, availability, maintainability and safety assessment. Reliability Engineering & System Safety. Jan;43(3):331–2. Available from: http://dx.doi.org/10.1016/0951-8320(94) 90038-8.

158. Garg V.K. DRV (2000) Dynamics of Railway Vehicle Systems. Academic Press

159. KALKER JJ (1979). Survey of Wheel—Rail Rolling Contact Theory. Vehicle System Dynamics. Sep;8(4):317–58. Available from: http://dx.doi.org/10.1080/00423117908968610.

160. (2000) (RDSO)-MT-240 Oscillation trails on LHB coach (AC chair car) in Palwal-Mathura section of central railway up to a maximum test speed of 180 KM/H on Rajdhani track main-tined to standards laid down. Lucknow, India.

161. Kouroussis G, Connolly DP, Alexandrou G, Vogiatzis K (2015). The effect of railway local irregularities on ground vibration. Transportation Research Part D: Transport and Environment. Aug; 39:17–30. Available from: http://dx.doi.org/10.1016/j.trd.2015.06.001.

162. Wu J, Qiu Y (2020). Analysis of ride comfort of high-speed train based on a train-seat-human model in the vertical direction. Vehicle System Dynamics. Jul 16;59(12):1867–93. Available from: http://dx.doi.org/10.1080/00423114.2020.1794014.

LIST OF PUBLICATIONS

In Journals

6. Patel Y, Rastogi V, Borutzky W. Simulation study on the influence of wheel irregularity on the vertical dynamics of wheel–rail interaction for high-speed railway track using bond graph. SIMULATION.2023;99(6):643-656. doi:10.1177/00375497221138943. **(SCI-E, IF-1.3)**

7. Patel Y, Rastogi V, Borutzky W. Influence of suspension parameter for derailment analysis of a full railway vehicle model cruising on a curved track. Journal of Engineering research. 2021; 95:95-108. **(SCI-E, IF-0.9)**

8. Patel Y, Singh RC, Borutzky W. Simulation-based analysis of passenger ride comfort under different track conditions. International journal of Heavy Vehicles. 2023. 30(5):609-626. https://doi.org/10.1504/IJHVS.2023.134329 **(SCI-E, IF-0.8)**

9. Patel Y, Singh RC, Borutzky W. Numerical-based dynamic frequency response analysis of rigid rail vehicle model. Journal of vibration engineering and Technologies. **(SCI-E, IF-2.1) (Communicated).**

10. Patel Y, Singh RC, Borutzky W. A Review of Passenger Ride Comfort in Railways: Evaluation and Enhancement Methods. Proc. Inst. of Mech Engg Part K-journal Of Multi-body Dynamics **(SCI-E, IF-1.9) (Communicated).**

International conferences

3. Patel, Y., Rastogi, V., Borutzky, W. (2022). Parametric Investigation of Ballastless Railway Track for High-Speed Railway. EMSME 2020. Lecture Notes in Mechanical Engineering. Springer, Singapore. https://doi.org/10.1007/978-981-16-2794-1_91

4. Patel, Y., Rastogi, V., Borutzky, W. (2022). Effect of Suspension Parameter on Lateral Dynamics Study of High Speed Railway Vehicle. CoMSO 2022. Modelling, Simulation and Optimization. Smart Innovation, Systems and Technologies, vol 292. Springer, Singapore. https://doi.org/10.1007/978-981-19-0836-1_27